Developmental Emergence of Cortical Neurogliaform Cell Diversity

Gomez Teijeiro, Lucia

UNIVERSITÉ DE GENÈVE
FACULTÉ DE PSYCHOLOGIE ET DES SCIENCES DE L'ÉDUCATION

Faculté de Psychologie et des Sciences de L'Éducation

LEMANIC NEURO SCIENCE DOCTORAL SCHOOL

DOCTORAT EN NEUROSCIENCES
des Universités de Genève
et de Lausanne

UNIVERSITÉ DE GENÈVE
UNIL | Université de Lausanne

UNIVERSITÉ DE GENÈVE — FACULTÉ DE PSYCHLOGIE

Professeur Denis Jabaudon, directeur de thèse
Professeure Daphne Bavelier, co-directrice de thèse

TITRE DE LA THÈSE

DEVELOPMENTAL EMERGENCE OF CORTICAL NEUROGLIAFORM CELL DIVERSITY

THÈSE
Présentée à la
Faculté de Psychologie et des Sciences de L'Éducation

de l'Université de Genève

pour obtenir le grade de
Docteure en Neurosciences

par

Lucia GÓMEZ TEIJEIRO

de Espagne

Thèse N° 439

Genève

Editeur ou imprimeur : Université de Genève

2022

Acknowledgements

ShineBright

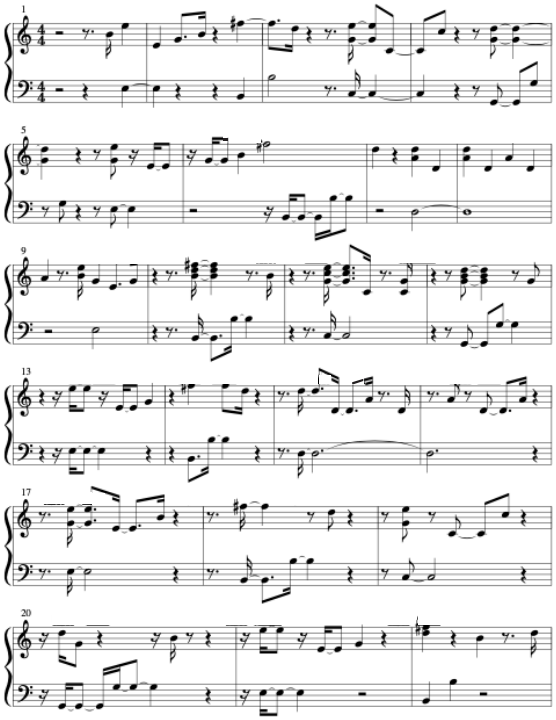

Thank you for who you were,
its thanks of you that I trust I can
thank you for giving me the chance
Shine bright, see you there

I hope you knew it,
its thanks of you that I am here
I hope, you knew it,...
But through your smile you cried...
wish you could come back and shine

Thank you for who you were,
for breaking walls and for joining hands
Thank you cause you always cared
ShineBright, see you there

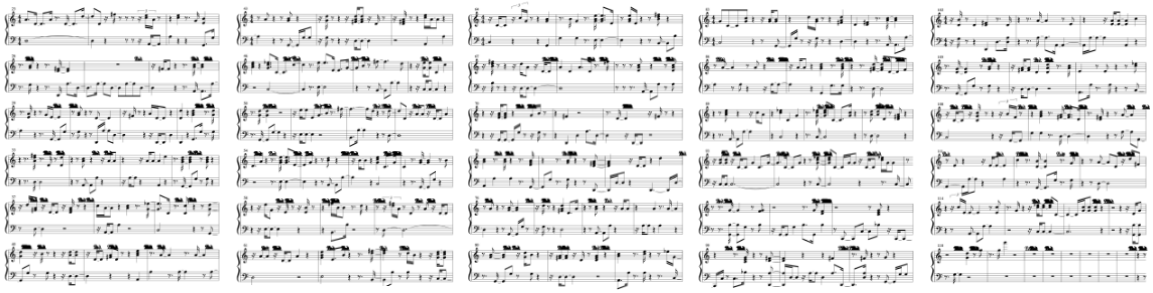

D. addendum:

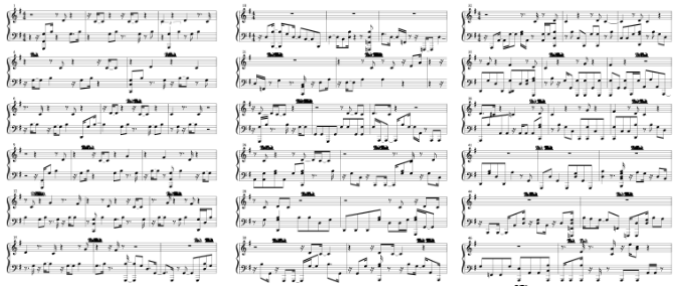

Thank you Alex for seeing the beauty on imperfection, for embracing the difference.

Your imprint is within me and shines brightly every day. I know now that we are all perfect molds and it is the best version of ourselves that we should aspire to become.

The two greatest reasons why this thesis exists are: 1) because you had tons of passion and a brilliant question and 2) because one day you thought to show what neurobiology is about an "atypical profile".

I really, really, really… wish you were here.

I have you here indeed, you are in each of the words of this manuscript, in each of the notes of the previous page, and please allow me give you a summary of what has happened since you left so that we can go through it at the next meeting. Anyways, my intuition tells me that you know this and much more.

There is another crucial reason why this thesis exists, it is D.Addendum, Denis. You thought it was a good idea for the DayLab to continue doing great science under Denis supervision. let me tell you, turned out to be another life lesson of yours, at least for me. You have always pushed me to grow and, in large part, I became the person and professional I am by your side. But the growth continued at an exponential rate thanks to how inspiring Denis is and has been.

Many thanks Denis, thank you for assuming the responsibility of guiding me and all DayLab members, for helping us going through hard times and ensure all would rise up again stronger. From the very first day, one of your characteristics, rare to find as diamonds, inspired me and made me navigate life in a lighter way: you have an art for delegating, for admitting to not have the answers and for multitasking without seemingly taking things so seriously while keeping astonishingly high standards ("*keep the pressure!*"). You appear to go through life smoothly, letting things happen, trusting, and moving elegantly from topic to topic. Thank you so much for mediating the most troublesome project discussions: as you say, "*keep it simple*" (how easier is it that way, hope I'll always keep it simple). Thank you for giving me so much independence for doing research: thanks to that, I am not afraid anymore to think outside the box or to be creative in science. Thank you for organizing and giving me the opportunity to participate in Alex memorial, no words exist to articulate how much that meant to me. Thank you for your words during the January 2022 booster meeting, woke me up from a period of lethargy. Thank you for spreading the passion you have for quality science and for willing to keep on working together even if this PhD journey arrives to an end.

Denis, covered in sweet, told me you left this world, and certainly him and the JabLab team saved my mind in those times (infinite thanks). Christelle and I were sideways that day, as we were most of the time, and we remained an unstoppable team determined to honor your name together with Denis. Until she left, we worked tirelessly to materialize one of the ideas we dreamed about one day, you remember? We deleted Tax2 electroporating the POA. Turns out you were right, let`s cheer for it, because Tax2 means the life for neurogliaform cells.

Thank you Christelle, we grew up together since the day we met, supporting and helping each other to calm down the perfectionist whip inside both of us. Working carefully and rigorously, each day better than the one before. This thesis would not exist without your contributions: at least half of it belongs to you: you've been the biology mind and hands behind for a long time. You are extremely talented and definitely have a gift for animals that emanates from your deep heart, you merit so much were you are right now. More on the personal side, I could write forever: listening to each other in difficult times, celebrating every little and big milestone and pushing each other to achieve our dreams. Thank you infinitely Chris, although our paths have taken different directions, you are also in every word of this manuscript and I will always carry your teachings with me.

A huge part of this thesis, the professional that I am today and the one I will be the rest of my life, has its roots on the infinitely talented data mentor you put next to me: Julien.

None of the lines of code behind this thesis would exist if not for you Julien. Initially I would spend hours seeing you writing code and taking pictures of your screen, slowly I got a grasp on it. The knowledge you gifted allowed me to access to the world of freedom. There are no limits to the language of code: you are remarkable data detective and artist, and an excellent teacher. Thank you so much for sharing your knowledge with me, all I'll ever produce from data will carry your mark; my professional present and future has emerged from your teachings, thank you forever.

Immediately after you left, JabLab people became my shelter. I am extremely thankful for their hugs: now they are tired to know I am a huggy person, but the strength of their hugs those days rescued me and is still alive, I was reborn under them. Let me tell you about the JabLab family, you really made the right decision uh?
As you know, Natalia had previously saved me from one of the hardest struggles of my life. She kept on being my saver every single day, having the right and warm words, the patience and the love.

Thank you Natalia, you are a wonderful person and I am so grateful to live the journey of life by your side. You are extremely talented in so many ways: smart, creative, artistic, sweet, caring… You took me by the hand to start to live

again twice, and that's something. You taught me many things through the PhD years, both personally and professionally. Personally, the self-growth path we share and the thousands of balcony sessions are fundamental building blocks of who I am today. Professionally, oh my goodness thank you so much for teaching me, among other million things, to use baobab. I was so scared even to touch it, and resulted so fundamental for my PhD work, and we ended up deploying the Rstudio server together, wowwww!! Bravo tus ovarios niña, vas a llegar tan lejos en la vida como quieras, eres un coco y un alma como ninguna.

Another person from JabLab played a fundamental role in the rebirth process, Sergi. You never got the chance to meet him but I am sure you would spot at first sight how of a great person he is. He was and is always there ready to know about you, listening with ears of love and speaking as if he knew you, to the point I think that he would recognize your soul if you decide to pass by. He keeps one of your books, it could not be in better hands.

Sergi, I am enormously thankful for your support both personally and professionally. You pictured my thoughts so many times and this way helped me to materialize ideas, shared precious lines of code that afforded me days of work and sent me freshly released papers out of which some became part of this thesis, you told me when to stop with the insatiable perfection (at the end I included the 3rd type, couldn't resist it). Por favor sigue siendo la persona que eres a pesar de lo frustrante que pueda llegar a ser a veces. Dejas una clara huella en la gente, o al menos en mi, tu altruismo inspira a hacer de este mundo un lugar mejor.

Well the JabLab was and is big, composed by many very united people with brilliant minds and deep hearts. I' ll be eternally grateful to each one of them, who like in a herd, transmitted me all their good energy and feeling of belonging. Each of JabLab member became neurogliaform experts and reviewers, the illustrations and storytelling of this thesis belong to them to a large extent.

Adrien (thank you for your wise words, there is definitely a psychotherapist inside of you), Audrey (thank you for organizing everything to perfection and making me feel welcomed. You felt how hard it was for me without me saying a word, it was you who tirelessly made it possible, thanks), Quentin (thank you for all the moments together speaking openly and freely about life, I really feel you like a brother), Moein (thank you for all the frustration-releasing sessions and for always walking one the side of the road), Esther (your strength and audacity to express your ideas are so inspiring, there is a lot of life inside of you and certainly a bright future, thank you for counting on me to team up for Humous and collaborating democratically even in the most critical moments), Theo (thank you for telling me your stories, through them I realized many times I was not alone. Plus, you are the number 1 reviewer of this thesis manuscript: thank you for going in detail through each line here written, even through the references and catalog numbers, that was a serious work), Samir (we made it for the amygdala!!! Clap clap), Sabine (thank you so much for your caring gestures and empathizing so deeply upon US craziness, also thank you for helping me understand electrophysiology! Wow, couldn't make it without you), Aline (thank you for teaming up for so long, your work constitutes a big technical component of this thesis – you made work the TOX2 IHC, you genotyped a big part of the animals protagonists of this story, you cut at least the 90% of the electroporated brains and your artistic side inspired me to pursue morphological reconstructions), Aurore (was an immense pleasure to work next to you and you've been my hands for so long too. Your contributions to this thesis were tremendously crucial: genotyping, IHC, cutting, but also you quantified TOX2, NPY and RXFP1 experiments and you were the one seeing for the first time the elusive 3rd type in cortex, thank you for pushing it and make it happen!), Eline (for these animal facility times together, shared struggles became buddy experiences together), Awais, Daniel, Clothilde, Laura, Ilaria, Pierre, Philipp, Giuseppe, Lea, Ricardo. All of you are part of this.

JabLab people have such a powerful energy, wow! They initiated the "Neurolounge" phenomenon: it emerged as a cohesive force in Covid times, that started by but extended beyond the JabLab and marked our generation. A memorable neurolounge night was, for example, Jimmy's farewell.

Thank you Jimmy, you are also a big part of this thesis and of the personal journey behind it. It is very unusual to connect with someone as much as we did. You are like family to me: we understood each other without the need to speak, we shared many weaknesses and strengths, you managed to convince me to stop working at lunch time, wow! (I didn't hold it after you left though, haha). Thank you also for the countless hours spent together at the animal facility and helping me setting and managing the head breaking triple transgenics. Thank you for starting exploring the ISreporter, at the end is part of this thesis. Hope to see you again soon and finally meet your beautiful family.

And you know, to make an interneuron, a combination of nature and nurture are necessary. You never met them but my parents are of course the producers of the atypical profile you trusted on and shaped.

Thank you mom for blessing me with your tireless strength for working, your perfectionism and attention to detail in everything you do. It is obvious to me that without those tools you gave me, this PhD would not be possible. Thank you dad for the legacy of your openness, communication skills and your tendency to get into more than what seems human to assume. The creativity behind this thesis emerged from those trait gifts as well as the thousand parallel things I accomplished during the PhD years. And of course, without your emotional and economic support I would never even made it to Switzerland. Thank you infinitely to understand it was time for me to leave the nest and fly, thank you for believing in me.

And just when the time seemed right, I finally found my life and love team mate: Luka. He is also part of the neurogliaform cell story because he is the one to remind me every day that frustration and guiltiness are not worthy of my time, that I deserve what I have achieved and that nothing I envision is impossible.

Thank you Luka, somehow you see my endless weak points as strengths and you know how to keep my emotions under control for producing at levels I never did before. You taught me how to flow managing the context shifts and setting boundaries, your love makes me feel capable of everything and through LuLuThons we grow together to be unstoppable. The strategy, logistics and timing for writing this thesis largely were enabled by you, and thank you for the post-writing adventures getting lost in the sea and breathing freedom aboard LeNiNo.

The defense will soon take place and the two people you chose to be jury members remain on board: Camila Bellone and Ludovic Telley. Denis Jabaudon will take on your role as you wished and Daphne Bavelier just came on board.

Thank you for accepting to be members of the thesis committee and assuming all the work and responsibility that come with the role. Looking very much forward to receiving your inputs to raise this work to a next level, your individual expertise will nourish the work and certainly strengthen it towards it upcoming publication.

I remember Camila and you used to share a lot of time together every day. Destiny gladly surprised me developing a bulletproof bond with Giulia, a PhD student from Camila.

Thank you Giulia, definitely you are my life counselor in the good and the bad. It feels you've been guiding me even before we met (life advisor since 1993). Your will and support strengthen me every day since I meet you and, because of it, of course you are part of this thesis too. For all the PhD struggles that were solved with you on balcony sessions and the personal growth path we travel together, Giulia you represent a legacy of the DayCam partnership. By the way, it seems a miracle you don't hate me after cutting apples at 6 a.m.

Finally, I' m very happy to announce you that the second chapter of the neurogliaform story will soon see the light thanks to Denis support. Hope this time no shade of doubt will remain for the academic minds: neurogliaform cells are POA derived. I ask the universe just one thing, for the world to associate your name with the discovery of neurogliaform cell birth and diversification paths.

Concluding, thank you Alex again for believing in me and for providing me the resources that will hopefully add a doctor next to my name. I would never be the neuroscientist I am if not thanks of you, and I would never have developed the passion for science that was so contagious from you. Thank you for opening me the doors of your lab, Switzerland, research, biology, compassion, care, altruism and a large etcetera.

Shine bright, see you there.

Lucia

Summary

GABAergic interneurons are key inhibitory regulators of cortical circuit function. Among the dozens of reported transcriptionally distinct types of cortical interneurons, neurogliaform cells (NGCs) are unique: they are the primary source of 'slow' cortical inhibition and are recruited by long-range excitatory inputs. Despite their functional importance, the developmental emergence and cellular diversity within this cell type remain unclear. Here, combining single-cell transcriptomics, genetic fate-mapping, electrophysiological characterization and morphological reconstruction, we show that discrete molecular subtypes of NGCs emerge from a common progenitor domain in the embryonic preoptic area (POA). Moreover, using *in-utero* electroporation, we show that the different NGC subtypes are generated in the POA at E14.5. By reconstructing NGC molecular architecture across development, we demonstrate that newborn NGCs and their postnatal progeny harbor shared molecular features and that the transcription factor *Tox2* constitutes an identity hallmark for the different members of the NGC family. Subsequently, using CRISPR-mediated genetic loss-of-function, we reveal that the transcription factor *Tox2* is critical for the development of these cells: POA-born cells lacking *Tox2* fail to differentiate into NGCs. Together, these results indicate that the different NGC subtypes are born from a spatially restricted pool of POA progenitors, after which subtype signatures are gradually acquired through development via diverging molecular programs and reach a stabilization plateau at early postnatal stages.

Resumé

Les interneurones GABAergiques sont des régulateurs d'inhibition clés dans la fonction des circuits corticaux. Parmi les multiples types d'interneurones corticaux moléculairement distincts, les cellules neurogliaformes (NGC) sont uniques : elles constituent la principale source d'inhibition corticale à cinétique "lente" et sont recrutées par des influx excitateurs distants. Malgré leur importance fonctionnelle, l'émergence développementale et la diversité cellulaire au sein des NGCs demeurent équivoques. Dans cette étude, en combinant quatre approaches à l'échelle de la cellule unique en transcriptomique, la cartographie du linage cellulaire, caractérisation électrophysiologique et reconstruction morphologique, nous montrons que des sous-types moléculaires discrets de NGCs émergent de progéniteurs communs conscrits dans un domaine topologique de la zone préoptique embryonnaire (POA). De plus, par électroporation *in-utero*, nous mettons en évidence que les différents sous-types de NGCs sont simultanément générés dans la POA au stade de gestation E14.5. En reconstruisant l'architecture moléculaire des NGCs, qui est conservée au cours du développement, nous démontrons que les NGCs nouvellement formées et leurs descendants postnataux présentent des caractéristiques moléculaires communes et que le facteur de transcription *Tox2* constitue une marque d'identité cellulaire commun à tous les différents sous-types de NGC. Enfin, en induisant une perte de fonction génétique médiée par CRISPR-Cas9, nous révélons que le facteur de transcription *Tox2* est critique au le développement de ces cellules: les cellules nées dans la POA dépourvues de *Tox2* ne parviennent pas à se différencier en NGCs. En conclusion, l'ensemble de nos résultats montrent que NGCs prennent leur source d'un groupe de progéniteurs POA spatialement restreint, puis que la diversité intraspécifique emerge progressivement au cours du développement par l'acquisition de programmes moléculaires divergents et arrivent à un plateau de stabilisation aux premiers stades postnatals.

Abbreviations

AAV	Adeno Associated Virus
ACSF	Artificial Cerebrospinal fluid
AHP	After Hyperpolarization potential
AP	Apical Progenitor
ATAC	Transposase-Accessible Chromatin
BC	Basquet Cell
BICCN	Brain Initiative Cell Census Network
BMPs	Bone Morphogenetic Proteins
BP	Basal Progenitor
BPC	Bipolar Cell
BRAIN	Brain Research Through Advancing Innovative Neurotechnologies
BTC	Bitufted Cell
CAM	Cell Adhesion Molecule
CCD	Charge-coupled Device
CCV	Canonical Correlation Vectors
CFSE	Carboxyfluorescein Succinimidyl Ester
CGE	Caudal Ganglionic Eminence
CRISPR	Clustered Regularly Interspaced Short Palindromic Repeats
DAPI	4',6-diamidino-2-phenylindole
DBC	Double-Bouquet Cell
DC	Deep-projecting Cell
DEG	Differentially Expressed Gene
DIC	Differential Interference Contrast
DL	Deep Layer
DMEM	Dulbecco's Modified Eagle Medium
DP	*Hmx3*-dtTOM+; *Htr3a*-GFP+ cell
EBSS	Earle's Balanced Salt Solution
EGTA	Ethylene Glycol Tetraacetic Acid
EN	Excitatory Neuron
FACS	Fluorescence-Activated Cell Sorting
FBS	Fetal Bovine Serum
FC	Fold Change

FFI	Feedforward Circuits
FGF	Fibroblast Growth Factor
FISH	Fluorescence in situ Hybridization
FT	Flash-Tag
GABA	Gamma-Aminobutyric Acid
GEM	Gel Beads in EMulsion
GO	Gene Ontology
GPCR	G-protein-coupled receptor
HBSS	Hank's balanced salt solution
HCA	Human Cell Atlas
HEPES	4-(2-hydroxyethyl)-1-piperazineethanesulfonic acid
HGNC	HUGO Gene Nomenclature Committee
HT	High Throughput
HuBMAP	Human BioMolecular Atlas Program
IFC	Integrated Fluidic Circuits
IHC	Immunohistochemistry
IN	Interneuron
IPSC	Inhibitory Postsynaptic Current
IS	Intersection-subtraction
IUE	*In-utero* Electroporation
IUPHAR	International Union of Basic and Clinical Pharmacology
KNN	K-nearest neighbors algorithmm
L	Layer
LGE	Lateral Ganglionic Eminence
LGIC	Ligand-gated ion channels
MC,	Martinotti Cell
MGE	Medial Ganglionic Eminence
MGI	Mouse Genomic Informatics
MT	Mitochondrial
NGC	Neurogliaform cell
NHS	Normal Horse Serum
P	Postnatal
PBS	Phosphate buffered saline
PC	Principal Component
PCA	Principal Component Analysis

PCR	Polymerase Chain Reaction
PFA	Paraformaldehide
POA	Preoptic Area
PSB	Pallial-Subpallial Boundary
QC	Quality Control
R	R programming language
R26	*Rosa26*
RA	Retinoic Acid
RMP	Resting Membrane Potential
ROI	Region Of Interest
RPM	Reads Per Million
RT	Room Temperature
S1	Primary Somatosensory Cortex
SBC	Single-Bouquet Cell
SC	Shrub cell
SDS	Sodium Dodecyl Sulfate
SHH	Sonic Hedgehog
STDB	Subthreshold depolarizing bump
STICR	scRNA-seq-compatible tracer for identifying clonal relationships
STRING	Database: Protein-Protein Interaction Networks Functional Enrichment Analysis
SVM	Support Vector Machines
SVZ	Subventricular Zone
TF	Transcription Factor
TGF	Transforming Growth Factor
tSNE	t-distributed stochastic neighbor embedding
UL	Upper Layers
UMAP	Uniform Manifold Approximation and Projection
UMI	Unique Molecule Identifier
V1	Primary Visual Cortex
VZ	Ventricular Zone
WM	White Matter
WNT	Wingless/Integrated
WT	Wild Type

Table of Contents

List of figures

List of tables

Introduction

"It was, above all, indispensable to explore the short axon corpuscles, insufficiently studied by the aforementioned scholars (...) my investigations demonstrated that the functional excellence of the human encephalon is intimately linked to the prodigious abundance and unusual luxury of forms of the so-called short axon neurons"

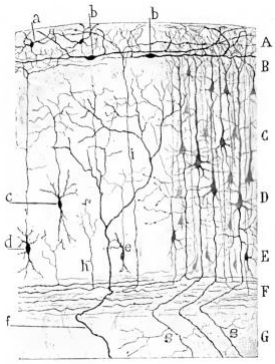

"Era, sobre todo, indispensable explorar los corpúsculos de axón corto, insuficientemente estudiados por los susodichos sabios (...) mis investigaciones demostraron que la excelencia funcional del encéfalo humano está íntimamente ligada a la prodigiosa abundancia e inusitado lujo de formas de las llamadas neuronas de axón corto"

Introduction figure 1. Cajal's neocortex drawing and quote on the importance of studying INs (Ramón y Cajal, 1923) pp. 252 & 350.

Architecture of the adult mouse neocortex

The thorough yet graceful neocortical design

The neocortex, the outermost anatomical structure of the mammalian brain in constant interaction with itself and other cerebral compartments, is in charge of enabling high-order functions such as perception, attention and memory as well as the generation of motor commands (Kirkcaldie, 2012) (Introduction figure 2). For instance, the ability to sense the outside world and react to it requires the neocortex to be connected to the thalamus (Shepherd & Yamawaki, 2021), while the complex regulation of memory, fundamental for everyday life functioning, is powered by the interplay between neocortex and hippocampus (Basu & Siegelbaum, 2015).

Although structural similarity exists along the neocortex, anatomical and functional specialization regions can be identified over two axes: dorso-ventrally through its organization into cortical columns and layers (Introduction figure 2) and rostro-caudally / medio-laterally through specialized functional areas (Introduction figure 2) (Capone et al., 2016; Douglas & Martin, 2004). Along the neocortex, distinctive intra-areal, inter-areal (associative or commissural) and long-range extracortical connectivity schemes can be found, which ultimately confer its characteristic functional heterogeneity and complexity (Kirkcaldie, 2012).

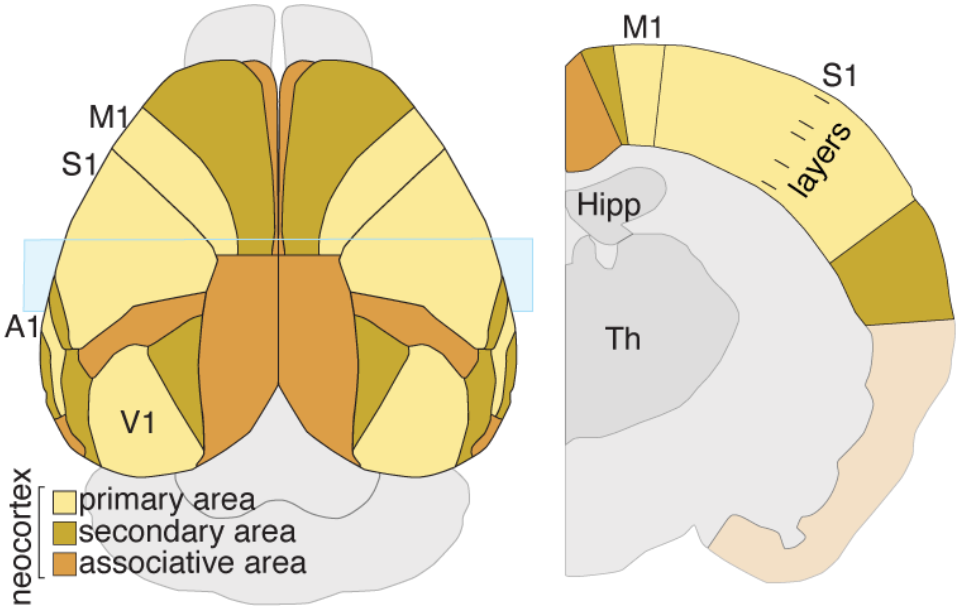

Introduction figure 2. Architecture of the mouse neocortex. Schematic illustration of the spatial distribution of the neocortical areas visible from a top view (left) and through a coronal plane placed at the level of the somatosensory barrel field (right). Primary areas are depicted in yellow, secondary in brown and associative in orange. Perpendicular lines to the cortical surface (pia) schematize cortical lamina.

Abbreviations: M1, primary motor cortex; S1, primary somatosensory cortex; A1, primary auditory cortex; V1, primary visual cortex; Hipp, hippocampus; Th, thalamus.

Despite of the variability driven by areal typology (primary, secondary or associative) (Introduction figure 2) (Kirkcaldie, 2012), primary sensory areas (visual, auditory or somatosensory) have been traditionally used to exemplify columnar intracortical architecture (Introduction figure 3) (da Costa, 2010; Douglas, 1989). As in other brain regions, the neocortex is built upon discrete cellular units among which neurons are the main functional actors and glial cells exert regulatory roles (Farhy-Tselnicker & Allen, 2018; Moore et al., 2020). Neuronal building blocks forming canonical cortical circuits come in two opposing flavors: excitatory (ENs) and inhibitory (INs). Balanced network activity is key to the fine regulation of cortical dynamic states resulting from the excitation/inhibition (E/I) interplay (D'amour & Froemke, 2015; Hennequin et al., 2017; Sukenik et al., 2021). In the neocortex, while ENs are the most abundant (~70-80%), INs, however, show a greater cell type diversity (Isaacson & Scanziani, 2011; Sultan & Shi, 2018; Tasic et al., 2018). Interestingly, cell type identity of ENs largely correlates with their connectivity patterns and thus varies across

neocortical areas while the vast array of IN genetic subtypes is shared across neocortical areas yet keeping presynaptic heterogeneity (Pouchelon et al., 2021; Tasic et al., 2018).

A close look at the neocortex reveals its hierarchical structure supported by the existence of functional boundaries between elementary computational units: the layers. Despite numerous exceptions, the neocortex is consensually seen as a laminar structure composed of six layers successively established during corticogenesis, which vertically communicate between each other in a columnar manner through excitatory connections (Larkum et al., 2018; Narayanan et al., 2017; Shepherd & Yamawaki, 2021).

Briefly, a primary sensory area such as the somatosensory cortex receives sensory input from the thalamus to layer (L) 4 neurons, which subsequently transfer the input to L2/3 neurons. In turn, L2/3 pyramidal ENs, after communicating with other neocortical regions and integrating information from many different structures of the brain, activate L5 neurons. Next, these cells communicate back to L2/3 neurons and ultimately generate appropriate output signals themselves and with L6 ENs. L6 ENs then initiate the L6-4 reciprocal loop (Introduction figure 3).

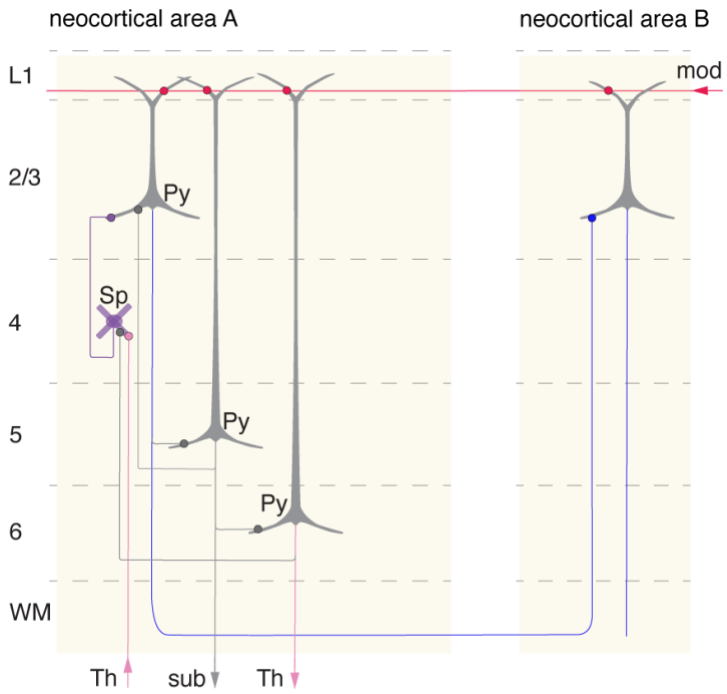

Introduction figure 3. Neocortical canonical excitatory connectivity map. Schema illustrating connection patterns between excitatory neurons in the neocortex and main extracortical inputs -

outputs (thalamic and subcortical). Excitatory neurons and their connections are depicted in grey (pyramidal) or purple (spiny stellate); Modulatory inputs to L1 and their contacts with EN dendrites are displayed in red. Thalamocortical and corticothalamic projections are indicated in pink. Intracortical connections are shown in blue. Subcortical efferent projections are shown in orange. Dashed lines represent cortical layers.

Abbreviations: L, layer; Th, thalamus; sub, subcortical; mod, modulatory; WM, white matter; Py, pyramidal; Sp, spiny stellate.

Behind the simplified canonical circuit schematic above lies a diverse cocktail of inhibitory and excitatory cell type combinations harmoniously distributed over different lamina (Tasic et al., 2018). INs are the connecting bridges of this tissular grid, ensuring fine-grained local connectivity (Tremblay et al., 2016).

Indeed, except for glial and excitatory Cajal-Retzius cells, only inhibitory INs reside in L1 (Introduction figure 4), surrounded by a mesh of axons from INs in and outside L1 (thalamic and neuromodulatory afferents from the midbrain and basal forebrain) (Ibrahim et al., 2020). Behaving as top-down hubs, L1 interneurons are crucial recipients of long-range inputs from many different brain areas and carry the critical mission of processing this information for regulating the activity of L2/3 and L5 excitatory neurons accordingly through inhibition (Hou & Capogna, 2018; Jiang et al., 2015).

"The short axon cells (...) side chains attached to the main pathways, to which they would provide stored nerve energy. They would come to be something like capacitors of potential destined to increase the tension of the nervous impulse in the main afferent and efferent vias."

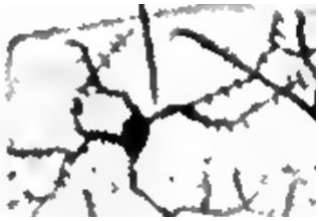

"Las células de axón corto (…) cadenas laterales anejas a las vías principales, a quienes proporcionarían energía nerviosa almacenada. Vendrían a ser algo así como condensadores de potencial destinado a aumentar la tensión del impulse nervioso en las vías principales aferentes y eferentes"

Introduction figure 4. Cajal's quote regarding IN connectivity (Ramón y Cajal, 1923) pp. 206, 405

Inhibitory interneurons in the neocortex are not restricted to L1. Also called GABAergic interneurons, they can be found across the entire cortical depth in various shapes (Introduction figure 5), displaying a complex array of connections with themselves and with precise sub-compartments of pyramidal ENs (Jiang et al., 2015; Kubota, 2014).

L1 hosts four types of INs: neurogliaform (NGC), canopy, α7-expressing single-bouquets, and VIP-positive (Schuman et al., 2019). The first two are very similar in morphology and are in continuous communication. However, the connection probability between L1 NGC and L2/3 ENs is much higher and, unlike NGCs, canopy cells are almost exclusively present in L1. α7 cells, also called single-bouquet (Jiang et al., 2013), have a characteristic vertically descending axon and connect with several types of L2/3 INs that, in turn, will contact L5 ENs, resulting in their disinhibition. Finally, L1 VIP-expressing INs, reside at the frontier of L1 and L2 and are morphologically identical to L2/3 bipolar VIP-expressing INs.

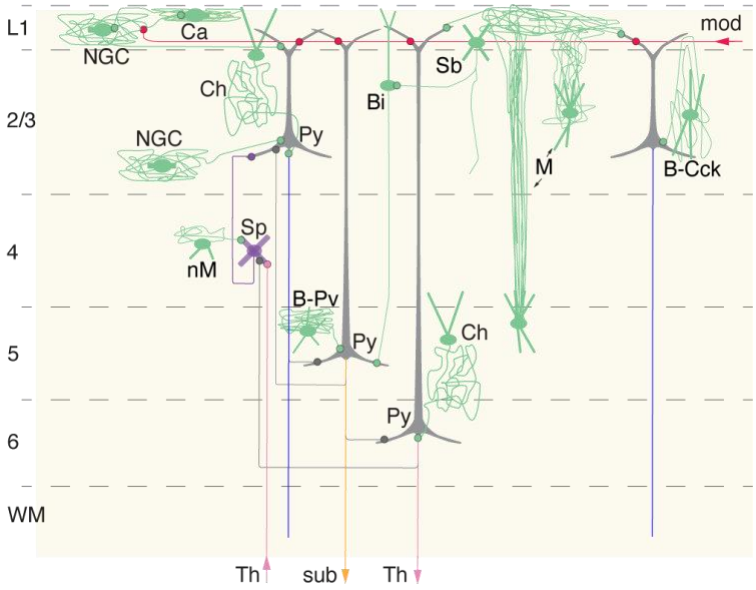

Introduction figure 5. IN morphological types and IN-EN connectivity in neocortical microcircuits. Schematic illustrating the variety of neocortical IN types according to their morphology and connectivity with ENs. INs and their connections to ENs are depicted in green. Excitatory neurons and their connections are shown in grey (pyramidal) or purple (spiny stellate). Modulatory inputs to L1 and their connections are displayed in red.

Abbreviations: L, layer; Th, thalamus; sub, subcortical; mod, modulatory; WM, white matter; Py, pyramidal; Sp, spiny stellate; NGC, neurogliaform; Ca, canopy; Ch, chandelier; Bi, bipolar; Sb, single-bouquet; M, Martinotti; nM, non-Martinotti; B-Pv, PV-expressing basket; B-Cck, CCK-expressing basket.

Cortical layers are not strictly segregated by anatomical boundaries. Unlike the discrete distribution of EN types along horizontal alignments in the cortex, IN types do not distribute in layers as markedly, although they do manifest laminar (Tasic et al., 2018). The spectrum of

IN diversity expands as we move down the cortical column (Jiang et al., 2015). NGCs and bipolar VIPs are also very abundant in L2/3. PV-expressing chandelier INs are sparsely found in the lower portion of L1 (Schuman et al., 2019). Connecting axo-axonally with nearby pyramidal ENs, chandeliers cells are slightly more abundantly in L2/3 and increase in number in deeper layers (Woodruff et al., 2009). Another type of PV-expressing interneurons found in L2/3 and L5, called basket cells, target ENs mainly within the same layer through their soma (Jiang et al., 2015). Dendrite-targeting SST-expressing basket cells and some-targeting CCK-expressing basket cells can be found in L2/3 and deep layers. SST- baskets, also called non-Martinotti cells, preferentially target L4 ENs (Scala et al., 2019). Finally, the abundant Martinotti cells, consisting of L2/3 and deep-layer SST-positive INs, send long axons to L1 and inhibit pyramidal cells by contacting their apical dendrites.

The connectivity specificity of IN types with precise compartments of ENs illustrates a carefully designed level of regulation. However, to understand the global complexity, it is necessary to consider that INs also connect, creating disinhibitory circuits (Pfeffer et al., 2013) (Introduction figure 6).

Disinhibition of ENs mediated by upstream IN-IN circuits is a powerful mechanism involved in pre-synaptic gain modulation, which is the amplification of neuronal firing that surpasses cell type-dependent target specificity (Letzkus et al., 2015; Salinas & Thier, 2000). Disinhibitory circuits in the neocortex are known to exist between different combinations of IN cell types and their functional implications are just starting to be deciphered (Letzkus et al., 2015). For instance, superficial VIP-expressing INs, and likely other L1 types mediating disinhibitory circuits have been suggested as candidates for relaying cholinergic neuromodulatory inputs to ENs, enabling processes such as memory expression, associative learning and activity-dependent plasticity (Letzkus et al., 2011; Pi et al., 2013).

However, schemes of IN-IN connectivity can be found across cortical layers and several rules can be drawn (Introduction figure 6): PV-expressing and NGC-canopy cells show a marked

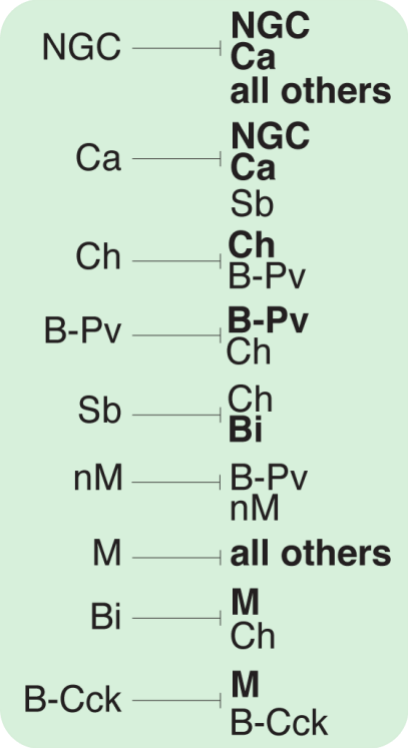

preference for contacting INs from the same type. In contrast, VIP- and SST-expressing cells tend to target other IN types. Specifically, VIP INs inhibit PV cells, although their principal targets are SST INs. The latter, are potent inhibitors of all IN types except themselves (Dávid et al., 2007; Jiang et al., 2015; Pfeffer et al., 2013; Salinas & Thier, 2000; Schuman et al., 2019; H. Xu et al., 2013).

Introduction figure 6. Disinhibition in the neocortex. Schematic illustrating cell type preferential disinhibition targets. Connectivity pairs with high probability are depicted in bold. Abbreviations: NGC, neurogliaform; Ca, canopy; Ch, chandelier; Bi, bipolar; Sb, single-bouquet; M, Martinotti; nM, non-Martinotti B-Pv, PV-expressing basket; B-Cck, CCK-expressing basket.

"Because the sovereign artifice of the gray matter is so intricate that it defies and will defy the stubborn curiosity of researchers for many centuries."	*"Porque el artificio soberano de la substancia gris es tan intrincado, que desafía y desafiará por muchos siglos la porfiada curiosidad de los investigadores".*

Introduction figure 7. Cajal's quote on cortical complexity. (Ramón y Cajal, 1923) pp. 203

The neocortical interneuron diversity dilemma in a breakthrough era

A challenge suited for the multi-dimensionality era

Constituting a clear numerical minority of neurons in the neocortex, GABAergic interneurons display an impressive level of heterogeneity. Thus, a long-standing effort to understand IN diversity began around 1980 (Introduction figures 8 & 9), which is still far from being completed (Huang & Paul, 2019).

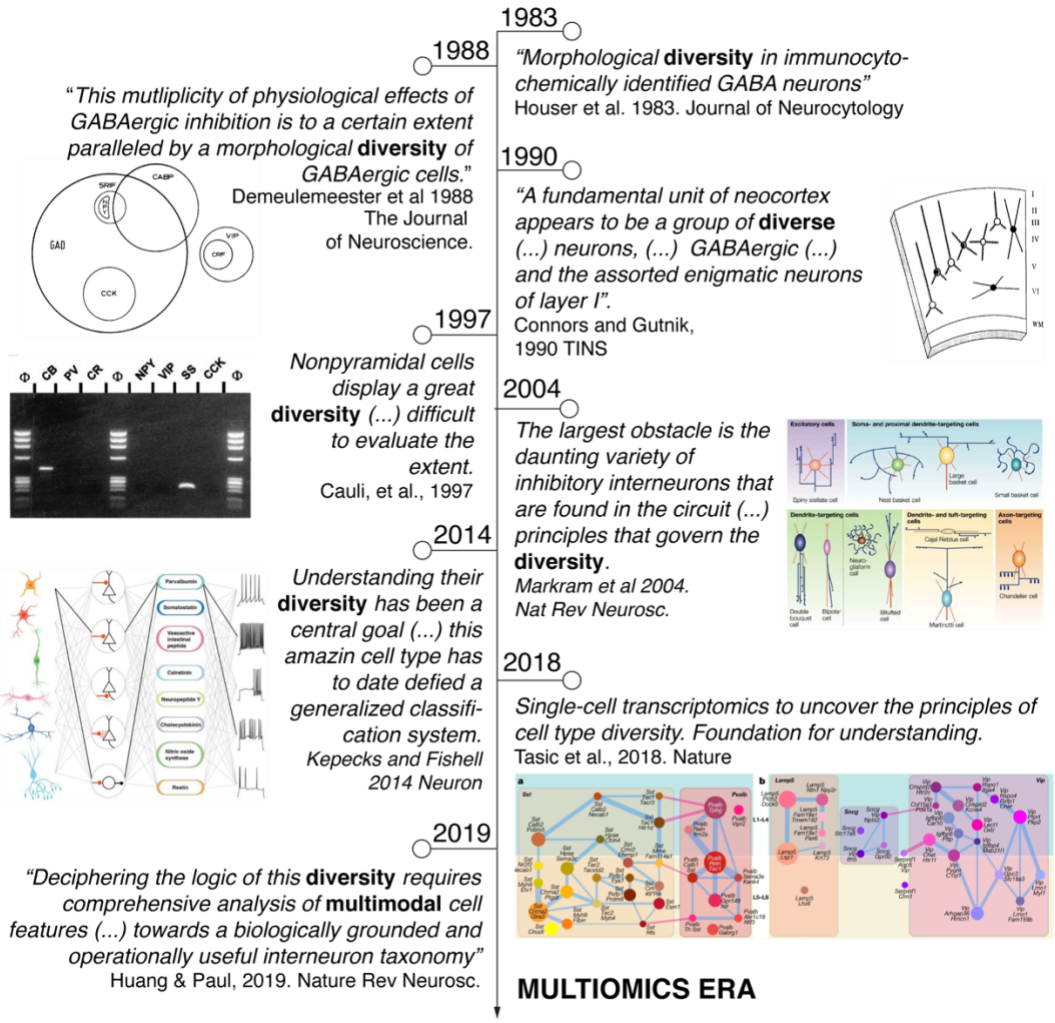

Introduction figure 8. **Timeline on IN diversity debate**. Examples of papers and passages discussing the reasons for which IN classification has been challenging at different moments in time. Illustrations within the timeline were obtained from source publications.

Data source: PubMed. Post-processing: R.

At the heart of the IN-classification debate lies a difficulty that pertains both to the observer and to the object: the multitude of angles from which the matter can be addressed (Introduction figure 9). Potentially, the methodological and technological revolution we are witnessing will be critical in linking the different interrogation viewpoints over the coming years (Introduction figure 9B). It is now technically possible to address far more questions than ever before and, more importantly, to integrate various data types for multidimensional analysis.

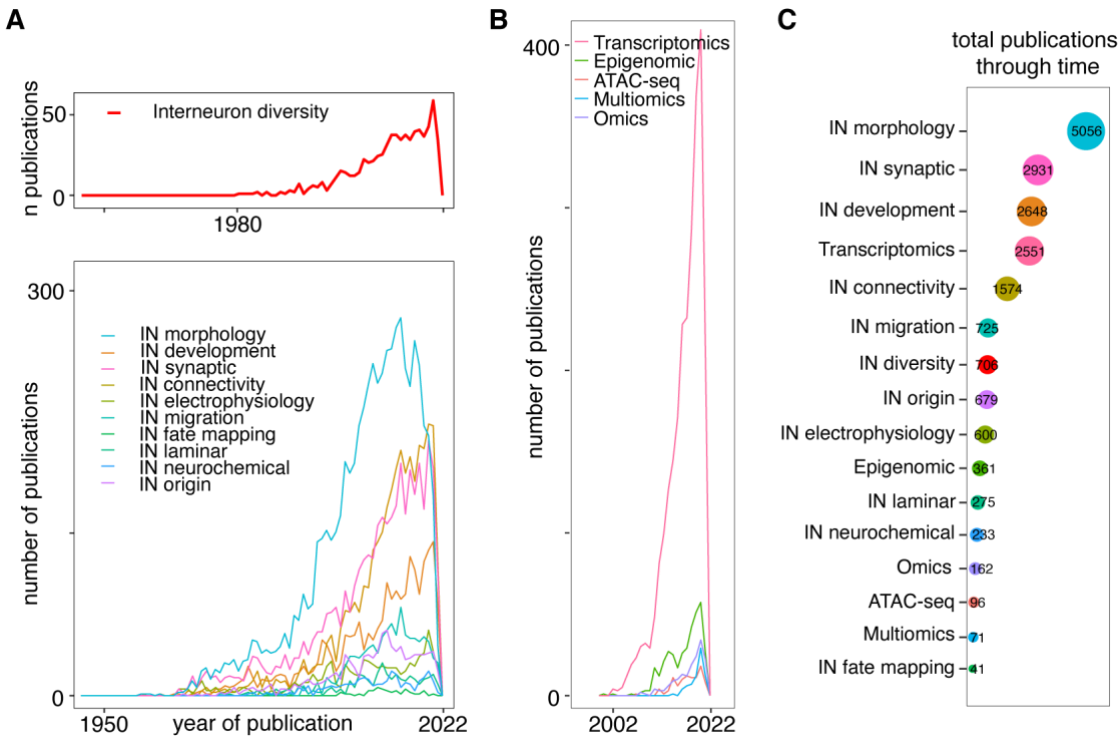

Introduction figure 9. Number of scientific publications on cortical research through time. (A-B) Line plots displaying number of publications per year color-coded by keyword or combination of them. **C.** Bubble plot depicting the total number of scientific publications through time color-coded by keyword or combination of them. Each color represents one or a combination of keywords.

Data source: PubMed. Post-processing: R. For queries on panel A, all keywords were additionally combined with "cortex" and "interneuron". For queries on panel B, all keywords were additionally combined with "cortex"

Taking a careful look at how the question of IN diversity has been addressed over time, the multidimensional nature of the subject is readily apparent (Figure I5 A). Approximately 100 years ago, the first dimension in which INs were described, their morphology, came with Cajal's discovery of neurons presented as the brain computational units and the use of the Golgi silver impregnation technique for morphological reconstruction (Introduction figure 10) (Ramón y Cajal, 1923).

"The protoplasm of the nerve cells, so rebellious to artificial colorations, possesses the precious attribute of attracting vividly the precipitate of silver chromate (...) the corpuscles of the gray substance show themselves to be tinged with chocolate black even in their finest ramuscules (...) dyed completely without the slightest tinctorial gap, my joy was immense".

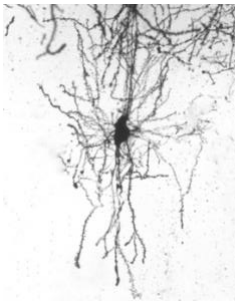

"El protoplasma de las células nerviosas, tan rebelde á las coloraciones artificiales, posee el precioso atributo de atraer vivamente el precipitado de cromato de plata (…) los corpúsculos de la substancia gris muéstranse teñidos de negro achocolatado hasta en sus más finos ramúsculos (…) teñidas por completo sin la menor laguna tintorial, mi alegría fué inmensa"

Introduction figure 10. Example of Golgi-stained IN and Cajal's quote about the method.
(Ramón y Cajal, 1923)

Morphology characterization is, by far, the dimension that led to the most extensive corpus of publications tackling IN diversity (Introduction figure 9). This way, Cajal's denomination of INs as "neurons with short axons" evolved through time into a complete catalog of highly detailed shapes (Mihaljević et al., 2018). Soon after, electrophysiological and connectivity characterizations appeared as two complementary sibling perspectives, which have been at the forefront of interneuron diversity description at high resolution. Many were the efforts that used one, the other, or a combination of both approaches until a

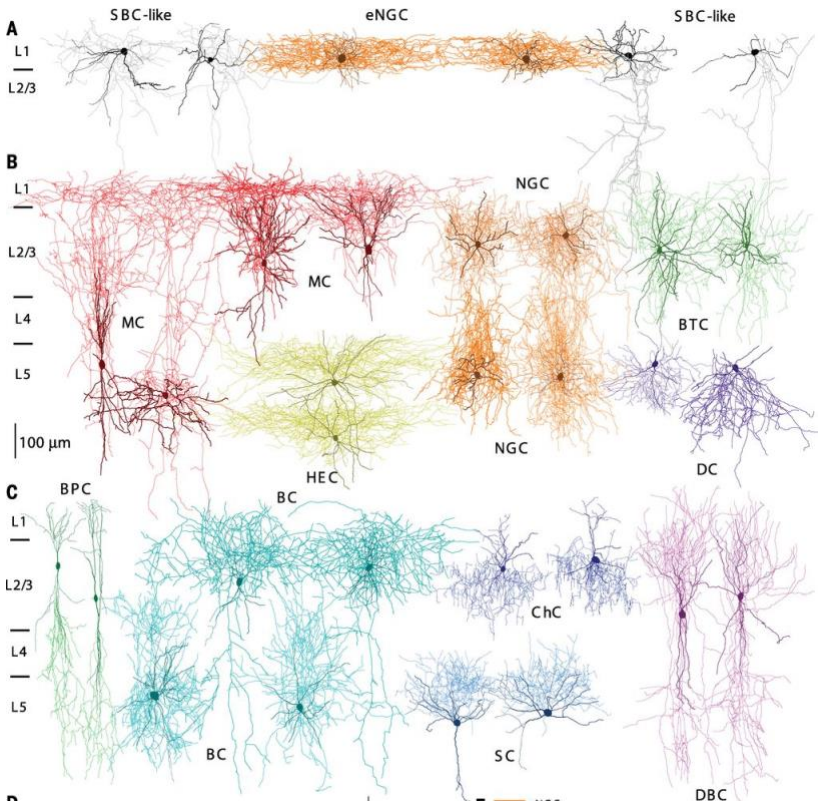

Introduction figure 11. Morphological IN types. (Jiang et al., 2015)

Abbreviations: SBC, single-bouquet cell; eNGC, elongated neurogliaform; MC, martinotti cell; NGC, neurogliaform; BTC, bitufted cell; DC, deep-projecting cell; BPC, bipolar cell; BC, basket cell; ChC, chandelier cell; SC, shrub cell; DBC, double-bouquet cell.

seminal turning point was reached in 2015 with the work of Jiang et al., who brought these two together with morphology (Jiang et al., 2015) (Introduction figure 11).

Although morphology, electrophysiology and connectivity were the canonical characterization methods historically, many other dimensions for IN classification were formulated based on molecular identity and neurochemical properties, laminar enrichment, synaptic partnership, migratory routes, birth-dating, genetic fate-mapping, embryonic origins, etc. Many publications addressing interneuron function used molecular identity or genetic fate-mapping. However, both approaches offer a low level of resolution because of summarizing the segmentation in two to four categories: the molecular groups PV, SST and 5-TH_{3A}R (VIP and REELIN), either by histological identification or fate-mapping via transgenic lines driven by genes such as *Nkx2.1*, *Lhx6*, *Htr3a*, *Vip*, *Pv* or *Sst*. In this regard, more refined fate-mapping strategies have been described and made available, combining CRE- and FLP-mediated recombination for lineage intersection and subtraction (He et al., 2016).

The power of using genetic fate-mapping strategies for IN population segmentation points toward the existence of an early embryonic determination of cell types or at least of large families. Being another of the most explored viewpoints (Introduction figure 9), it goes beyond being a dimension for describing IN diversity: the study of IN development aims at shedding light on how diversity is generated in the brain, which is crucial for understanding whether different function-anatomic IN units have specific underlying generative programs. Development diversification is potentially the most challenging dimension since it implies moving away from the already cumbersome end-point of cellular diversity in adulthood. Due to the subject's complexity and its strategical relevance in the context of this thesis, the following section will be explicitly dedicated to the developmental emergence of neocortical IN types.

In conjunction with the advancement of single-cell transcriptomics, one of the most influential technological breakthroughs in the field (Introduction figure 9), the matter of how many types of interneurons might exist in the adult neocortex recently reached an exhaustion point. In 2018, the Allen Institute for Brain Science reported the existence of 61 subtypes present across the different areas of the mouse adult cortex (Tasic et al., 2018) (Introduction figure 12).

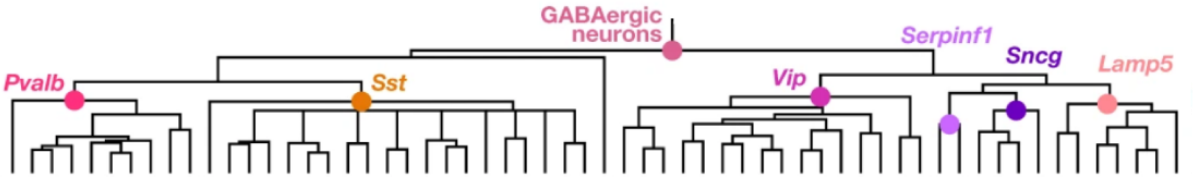

Introduction figure 12. Allen Brain taxonomy of adult transcriptomic IN subtypes. Hierarchical tree resulting from iterative clustering on single cell transcriptomes collected on two distant neocortical areas: Visual primary cortex and Lateral motor cortex (Tasic et al., 2018)

Tasic et al., 2018 cell type taxonomy set a turning point in the field for two main reasons: 1) the guarantee that the sampling and algorithm used give to account for all possible molecular subtypes and; 2) the gene expression similarity-based hierarchical understanding of interneuron diversity. Thereby, it was found that the vast range of interneuron subtypes can be grouped into five major subclasses (*Pv*, *Sst*, *Vip*, *Sncg* and *Lamp5*-expressing). The general IN class correspondence follows the traditional neurochemical classification (Introduction figure 12) (PV^+:*Pv*; SST^+-*Sst*; 5-$HT_{3A}R^+$:*Vip*, *Sncg*, *Lamp5*). However, refined subtype level precise correspondences to all classical classification schemes remains an active research effort.

The aforementioned taxonomy was the first high-throughput big-scale effort to catalog cell types in a high-throughput manner. From that moment on, international consortia got involved in the development of cell classification atlases (BICCN, HCA, HuBMAP, etc.), aiming to provide comprehensive reference systems. Such resources rapidly surpassed the transcriptomic revolution by aggregating other "-omics" to the equation: epigenomics, spatial-transcriptomics, chromatin profiling, proteomics, etc. (BRAIN Initiative Cell Census Network (BICCN) et al., 2021).

The literature of the past two years has been populated by a new term: "multi-omics" (Introduction figure 9). Multi-omics refers to the combination of several "-omics" methods for cellular profiling and will certainly become the methodological standard in the field as it enters yet a new era in brain science (Mimitou et al., 2021). With the release of new multi-omics dataset at a dizzying pace, countless bioinformatic tools are being developed and made openly available (Perkel, 2021).

"*Most if not all, important scientific advances are the result of technological progress*"
(Sotelo, 2020)

The multi-omics revolution could be the answer to concerns raised pointing out the artificiality of single-cell transcriptomic taxonomies if not in line with biological mechanisms and principles (Huang & Paul, 2019). Transcriptomic-morpho-electric atlases have been released in the last years, providing an unprecedented integrative level of description (Gouwens et al., 2020; Scala et al., 2021) (Introduction figure 13). One key message emerged from these comprehensive efforts and could constitute a paradigm shift: the idea of continuity (in identity) within cell types. Thus, categorization would be the first step for accessing subtle state-based variation. In this regard, a recent publication highlighted the possibility of accessing state-modulation profiles of cortical cell types using single-cell transcriptomics data (Bugeon et al., 2022).

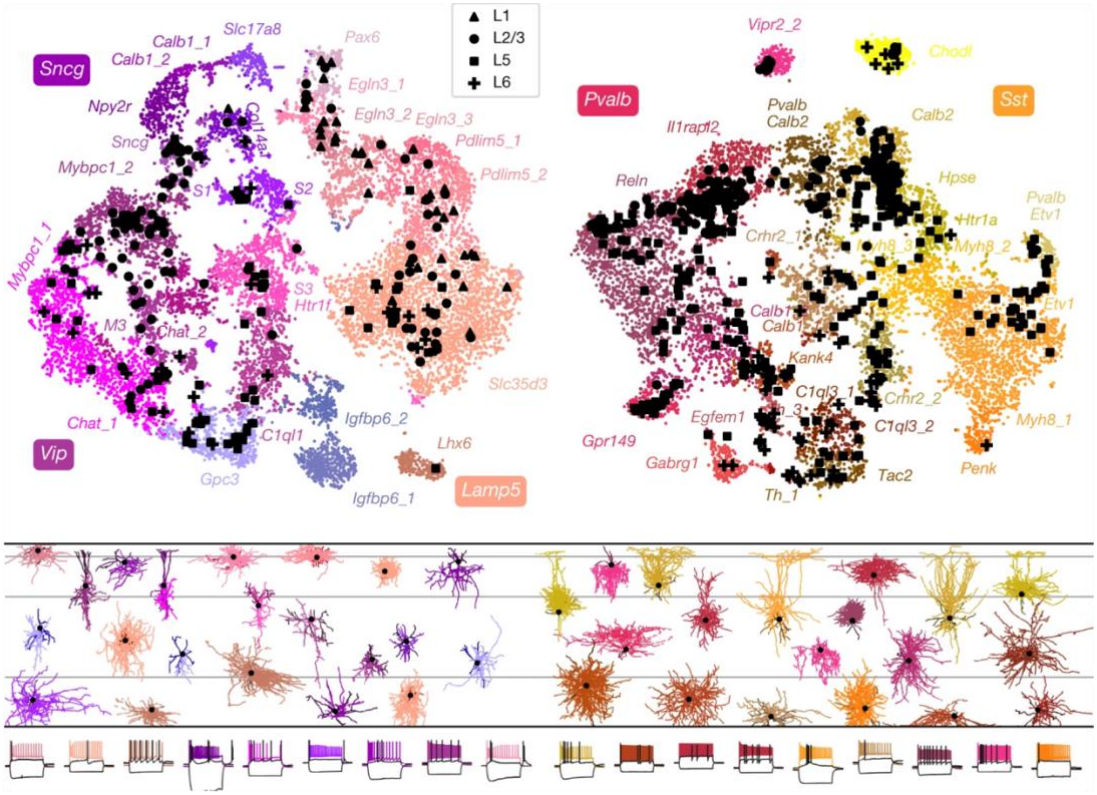

Introduction figure 13. Transcriptomic-Morpho-Electric IN subtypes. UMAP plots depicting IN single cell transcriptomic similarity and color-coded by cell type. Below, corresponding morphology and electrophysiological patterns for identified cell types. Y-position of morphology reconstructions is arranged respect to their radial position in the cortical column. (Scala et al., 2021)

While being very close to understanding the multidimensionality of cell types and their state transitions, one key question remains: how are these cell types generated in the first place?

With so much new knowledge in the playground, developmental trajectories for cell type differentiation at the type-subtype level are still largely unknown.

Developmental emergence of interneuron subtypes: a spatio-temporal interplay

"And if the encephalon and other organs (...) are too complex to allow us to discover their structural plan, why not systematically apply the method to lower animals or to the early stages of ontogenetic evolution, in which the nervous system must offer simple and, so to speak, schematic organization?"

"Y si el encéfalo y demás órganos (...) son demasiado complejos para permitir descubrir su plan estructural, ¿por qué no aplicar sistemáticamente el método á los animales inferiores ó a las fases tempranas de la evolución ontogénica, en las cuales el sistema nervioso debe ofrecer organización sencilla y, por decirlo así, esquemática?"

Introduction figure 14. Cajal's statement about development. Power of the developmental approach for accessing a simplified view of adult complexity. Cajal's drawing of neonatal mouse olfactive neurons (Ramón y Cajal, 1923) pp. 79 – 137.

Deciphering the mechanisms underlying the generation of cortical IN diversity is a still a puzzling task, despite an impressive number of publications over the last decades (Introduction figure 9). Cajal's reasoning for studying immature biological systems as a simplified proxy to understand their adult organization was paradoxical: we discovered the vast degree of complexity that is added when investigating a highly dynamic system in development. Hence, in times of exponential knowledge acquisition about the end result (mature neocortex), we still largely ignore how to get there.

Knowing how the neocortex is built is a highly relevant question for several reasons: a) answering fundamental questions: e.g., how diversity is generated (which in turn can shed light on tissue engineering for organoid development), how is the formation of different cell populations coordinated in space and time, how diverse cells can originate from a common progenitor pool, which mechanisms underlie cell-cycle exit and start of differentiation, how

and when cell fate is specified, how do cells find their path through migration, how cells are integrated into circuits, how synaptogenesis and pruning occur, how the different cell types interact with each other during development, etc.; b) Defining what is “normal” development and understanding how it occurs could be doors opening for disentangling what can go wrong and when, and thus contribute to the comprehension of how developmental disorders arise.

Research on interneuron development for more than 20 years (Introduction figure 9) has provided the first answers to the aforementioned questions. Specifically, many were the publications that linked environmental risk factors and defects in specific interneuron types to developmentally generated neuropsychiatric disorders (Paterno et al., 2020; Yang et al., 2022) and answers to fundamental questions uncovered, for example, the existence of common genetic early maturation programs for interneurons and the space and time windows for IN generation in the embryonic brain. However, a long way to go remains for a global understanding of the phenomenon since many fundamental questions have only partial answers and many processes seem to contribute to the generation of neuropsychiatric disorders, making it difficult to spot the full picture.

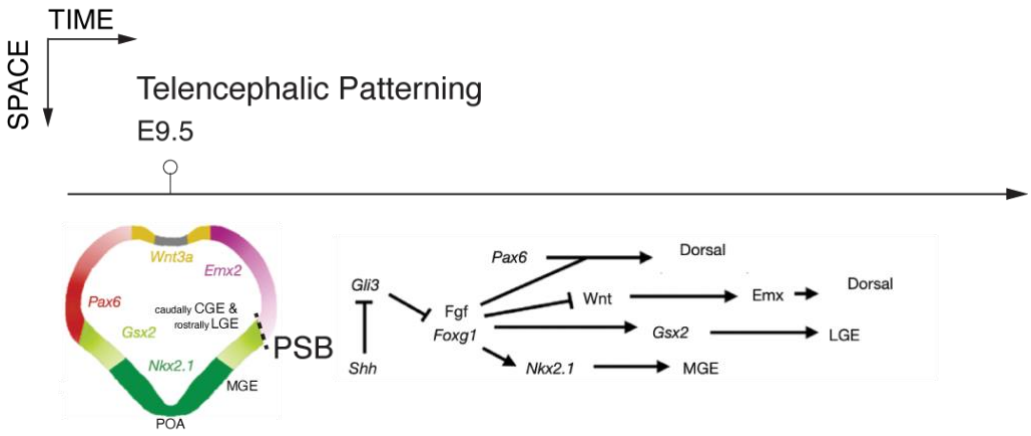

Introduction figure 15. Dorso-ventral telencephalic patterning through space and time.

Schematic illustrating the spatial expression of and the interaction between the factors implicated in D/V patterning (morphogens and transcription factors). Adapted from (Tole & Hébert, 2020).

Abbreviations: CGE, Caudal Ganglionic Eminence; LGE, Lateral Ganglionic Eminence; MGE, Medial Ganglionic Eminence; POA, Preoptic Area; PSB, pallial – subpallial boundary.

Mouse embryonic day (E) 9.5 marks the beginning of telencephalic patterning, a process through which the telencephalon will be shaped into its major territories according to two perpendicular axes: antero-posterior (A/P) and dorso-ventral (D/V). The competitive interplay

between the different cell-extrinsic signaling factors and cell-intrinsic transcription factors (TFs) is at the basis of these processes: BMPs, SHH, FGFs, WNTs, TGFs and RA families of morphogens and the TFs FOXG1, GLI3, PAX6, LHX2, GSX2, NKX2.1 and EMX2 are the main actors (morphogens modulating TF activity and TFs modulating morphogen secretion). Specifically, WNT - SHH and PAX6 - GSX2 counteract to delimitate a region called the pallial-subpallial boundary (PSB), a frontier between the dorsal cortical EN-producing and the ventral IN-producing telencephalic territories (Tole & Hébert, 2020). Ventral regions are further primarily shaped by FOXG1 to create spatial domains with specific TF-expression codes in which cells from the different IN families will be born. In particular, cortical INs will be generated in three regions at slightly shifted time windows: the Caudal Ganglionic Eminence (CGE), enriched in *Gsx2* expression from E10.5 on, starts neurogenesis after the Medial Ganglionic Eminence (MGE) and the Preoptic Area (POA), where *Nkx2.1* expression dominates from E9.5 on (Nasu et al., 2021; Nat et al., 2013).

Introduction figure 16. Neurogenesis in the ventral telencephalon through space and time. Schematic recapitulating time and space dynamics of interneuron generation in the different micro-domains of MGE, POA and CGE; combinatorial code of spatially enriched TFs; types of interneurons generated by microdomain.

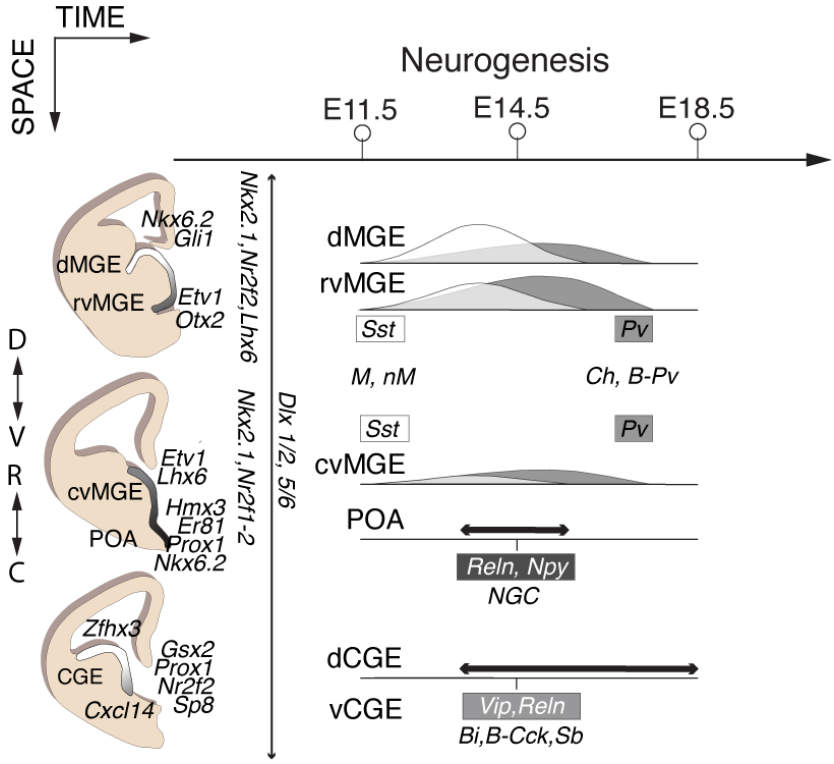

Abbreviations: dMGE, dorsal Medial Ganglionic Eminence; rvMGE, rostro-ventral Medial Ganglionic Eminence; cvMGE, caudo-ventral Medial Ganglionic Eminence; POA, Preoptic Area; dCGE, dorsal Caudal Ganglionic Eminence; vCGE, ventral Caudal Ganglionic Eminence; D, dorsal; V, ventral; R, rostral; C, caudal; M, Martinotti; nM, non-Martinotti; Ch, chandelier; B-Pv, PV-expressing basket; NGC, neurogliaform; Bi, bipolar; B-Cck, CCK-expressing basket; Sb, single-bouquet cell.

IN neurogenesis occurs approximately from E12.5 to E18.5 (Introduction figure 16), a process in which neuroblasts located adjacent to the ventricular wall of MGE, CGE and POA divide to give rise to cells that will ultimately become INs. Other ventral neurogenic niches exist, such as LGE and septum, but they are thought to not contribute to cortical IN generation (Kelly et al., 2018; Qin et al., 2017). While much is known about MGE neurogenesis, dynamics in CGE and POA remain largely unexplored (Gelman et al., 2009; Hu et al., 2017; Lee et al., 2022; Lim et al., 2018; Llorca & Deogracias, 2022; Niquille et al., 2018; Yang et al., 2022). Specifically, an explosion of scientific publications describing embryonic IN production in MGE started in the early 2000s', while the interest for other interneuron generative zones never achieved as much research attention (Introduction figure 17).

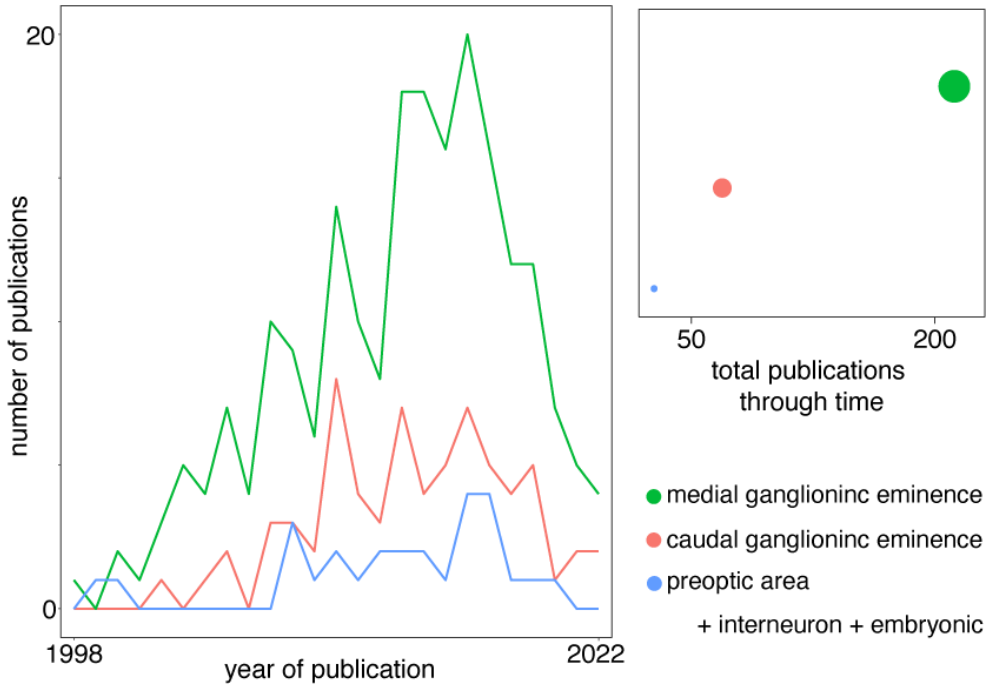

Introduction figure 17. **Number of scientific publications on MGE-, CGE- and POA-born IN development.** Line plot displays the number of publications per year color-coded by combination of keywords. Bubble plot depicts the total number of scientific publications through time color-coded combination of keywords.

Data source: PubMed. Post-processing: R. Queries: "medial ganglionic eminence" + "interneuron" + "embryonic" (green); "caudal ganglionic eminence" + "interneuron" + "embryonic" (orange); "preoptic area" + "interneuron" + "embryonic" (blue).

The spatial regulation for IN diversity generation, characterized by a very precise combinatorial code of TF-expression along the R/C and D/V axes, becomes even more apparent in the adjacent region of the proliferative ventricular zone (Introduction figure 16)

(Hu et al., 2017; Lee et al., 2022). The detailed granularity of TF-expression allows the description of subdomains within the MGE, CGE and POA. To mention some subdomain TF codes: dorsal MGE expresses *Nkx6.2* and Gli1 while ventral MGE is enriched in *Etv1* and *Otx2*; dorsal CGE displays *Zfhx3* specifically while the ventral CGE expresses *Nr2f2* strongly; POA spatial domains are drawn by *Hmx3* (rostro-dorsal and caudo-ventral) and *Nkx6.2* (ventral) (Gelman et al., 2009; Hu et al., 2017; Lee et al., 2022; Niquille et al., 2018) (Introduction figure 16). Time windows for IN neurogenesis vary depending on the ventricular niche: MGE starts producing them at E11.5 while CGE is thought to enter this process around E12.5. Little is known about the IN neurogenic time window in POA. Accordingly, the peak of IN neurogenesis is delayed in CGE (~16.5) compared to MGE (~E14.5) (Miyoshi et al., 2010). The different regions (space) generate very different interneuron cell types: MGE gives rise to SST and PV INs, CGE to VIP and REELN INs and POA to neurogliaform INs. The relative contributions of space and time dimensions become blurrier when studying the dynamics within each neurogenic region. For instance, spatiotemporal interplay in MGE for type generation draws a relatively flexible scenario in which both SST and PV types appear to be generated through space and time with different relative probabilities (Lim et al., 2018): SST types are preferentially generated earlier and in more dorsal regions than PV types, and PV-expressing chandelier cells are the last to be generated with a preference of birth in the ventral MGE (Inan et al., 2012). Spatiotemporal generative dynamics in CGE appear to be even fuzzier: up to date, no clear birthdate-dependent type enrichments or spatial subdomains were observed (Miyoshi et al., 2010).

Unraveling the precise elements that contribute to IN subtype diversification has proven to be a daunting challenge and remains to be resolved. The progenitor spatiotemporal heterogeneity contribution to interneuron diversity generation is unquestionable, but subtype production appears to be a relatively flexible process encoded by gradients of space and time.

Two non-mutually-exclusive alternate scenarios that have been theoretically formulated around the enigmatic question of neural commitment: progenitors could be either fate committed intrinsically (molecular Spatio-temporal encoding) or become progressively fate-determined progressively as they differentiate and interact with extrinsic cues (Telley & Jabaudon, 2018). Research evidence supports a mixed model between these two scenarios depending on the cell type (Bandler et al., 2022; Mayer et al., 2018; Nowakowski et al., 2017). Progenitor cells in different spaces and times largely share molecular programs and

simultaneously present subtle differences. As maturation progresses, molecular differences get sharper at the early post-mitotic stage, allowing for a rough fate alignment with mature types (Mayer et al., 2018). In the case of interneurons, lineage tracing experimental evidence suggests that progression in time of a given progenitor accounts for the production of cells aligning to different mature fates. Therefore, clonal divergence exists within a given pool of dividing cells (Bandler et al., 2022). In addition, early post-mitotic interneurons mapped to different adult identity fates can be molecularly distinguished, further indicating that subtype commitment starts upon cell-cycle exit (Bandler et al., 2022).

Introduction figure 18. Schema of lineage-divergence from a common progenitor pool (Bandler et al., 2022).

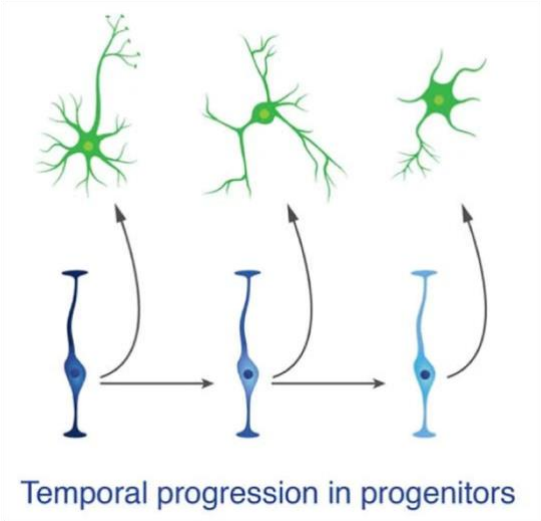

Congruently with the divergence scenario driven by the temporal progression of a shared progenitor pool, experimental evidence indicates that differential progenitor modes of division contribute to the production of different interneuron subtypes by the same progenitor clone (Bandler et al., 2017; Glickstein et al., 2007; Petros et al., 2015).

A given apical progenitor (AP), located at the ventricular zone (VZ) surface, can divide both symmetrically to amplify the AP pool or asymmetrically to produce both an AP and a basal progenitor (BP). On the other hand, BPs, located farther away from VZ in a zone called subventricular (SVZ), have neurogenic potential and also the capacity to keep expanding symmetrically (Adnani et al., 2018).

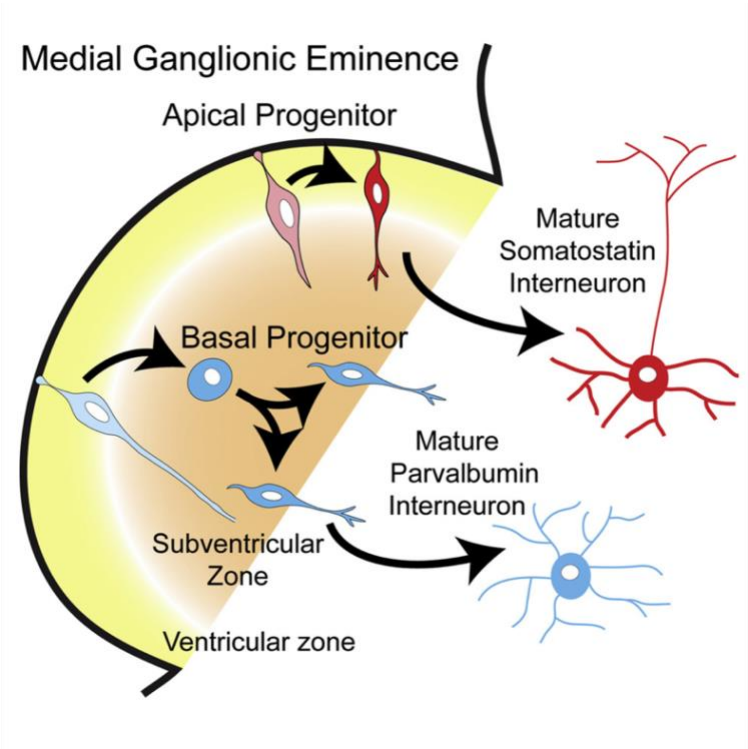

It was specifically demonstrated that PV-expressing interneuron progeny is reduced in BP marker *Ccnd2* null mice, while SST-expressing interneurons number remains unaltered (Glickstein et al., 2007). This finding, together with evidence from fate-mapping and progenitor division mode manipulations indicates that SST+ interneurons preferentially emerge from APs (Petros et al., 2015) that could later produce PV-generating BPs.

Introduction figure 19. Influence of progenitors' division mode on IN fate. (Petros et al., 2015)

Progenitor fate has also been associated with epigenetic regulation (Albert et al., 2017; Burney et al., 2013; Nord et al., 2015). Empirical evidence shows that the chromatin landscape of progenitors' promoters can be different when their gene expression profiles are still identical (Allaway et al., 2021). For instance, *Nkx2.1*, a gene expressed both in MGE and POA progenitors, can promote transcription repression in APs and activation in non-AP progenitors (Sandberg et al., 2016).

Once newborn INs have been generated in their respective birthplaces and times, they begin a long migratory journey towards their final destinations, where they will ultimately integrate into functional circuits and interact with other cell types (Lim et al., 2018).

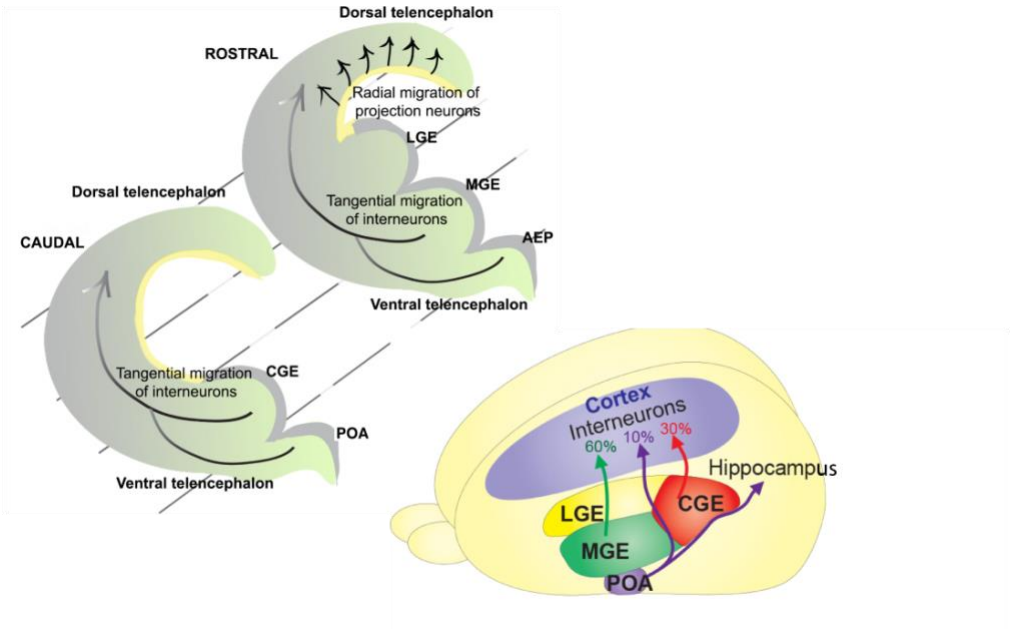

Introduction figure 20. IN migratory routes. 2D and 3D schemas of migratory routes from ventral neurogenic niches giving rise to neocortical interneurons (Adnani et al., 2018).

Abbreviations: LGE, lateral ganglionic eminence; MGE, medial ganglionic eminence; POA, preoptic area.

Interneurons born in the same spatiotemporal coordinates have the potential to populate regions all over the brain, including the neocortex. Indeed, no preferential destination places or circuit specificity relations existed on clonally related interneurons (Mayer et al., 2016; Turrero García et al., 2016).

Neurogliaform cells – a landmark subtype in neocortex

Numerously placed at the top of "the impenetrable jungle of the gray matter, a constellation of unknowns"

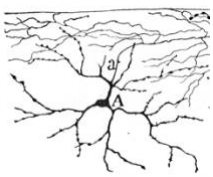

Numerously placed at the top of "*la selva impenetrable de la substancia gris, constelación de incónitas*"

Introduction figure 21. Cajal's illustration of a L1 neurogliaform cell and quote on the impenetrable jungle. (Ramón y Cajal, 1923) p 72.

Among the dozens of IN subtypes populating the postnatal neocortex, one of them stands out from the crowd: neurogliaform cells (NGCs), many of them located at the top of the cortical "impenetrable jungle" with dense intricated axons, are the only cortical INs able to communicate using a quadruple strategy: electrical coupling, GABA-A mediated synaptic release in two flavors (fast and slow) and GABA-B mediated volumetric transmission (Armstrong et al., 2012; Oláh et al., 2009; Overstreet-Wadiche & McBain, 2015).

Generally, INs are electrically coupled (sometimes forming gap junctions) preferentially with members of the same type, mechanism that allows them for a fast and tight regulation of firing synchronicity (Bennett & Zukin, 2004; Connors & Long, 2004). NGCs, however, are able to connect this way with a large range of IN types, including themselves as well as with excitatory neurons (Jiang et al., 2015; Simon, 2005), indicative of their role in network activity modulation (Overstreet-Wadiche & McBain, 2015). Electrical coupling between interneurons, in addition, orchestrates the formation of bidirectional NGC chemical synapses during early postnatal development (Yao et al., 2016). In these lines, NGCs do communicate bidirectionally through GABA release and, importantly, synchronous NGC firing is significantly impaired when GABA-A receptor mediated communication is blocked (Yao et al., 2016). It has been suggested that these two forms of reciprocal IN communication have complementary effects: while electrical coupling contributes to homogenize voltages between cells and reduce suppression, chemical inhibition enables fast synchronization (Kopell & Ermentrout, 2004). It is thought that, in this way, NGCs contribute to the maintenance of cortical oscillations, ultimately regulating the activity of excitatory cells in space and time (Roux & Buzsáki, 2015).

Importantly, NGCs can exert GABA-A communication in two flavors: fast and slow (Overstreet-Wadiche & McBain, 2015). Fast GABA-A mediated communication is the overarching inhibitory mechanism in the cortex and results in rapid IPSCs, while slow GABA-A transmission elicits slow rising and long-lasting ones (Capogna & Pearce, 2011). Importantly, it has been suggested that these two IPSC modalities are made possible by receptors with differential subunit compositions in target cells (Hentschke et al., 2009; Ramadan et al., 2003). An important factor for NGCs' ability for GABA-A slow communication is their particular axon morphology: they have a very thing and dense axonal plexus populated with numerous small boutons filled with synaptic vesicles (Armstrong et al., 2012; Capogna & Pearce, 2011; Karayannis et al., 2010). Such particular axonal shape, where postsynaptic target sites are subtle and distant, is known to elicit GABA spillover and is also

optimized for the fourth type of communication exerted uniquely by NGCs: GABA-B mediated tonic signaling resulting from volumetric GABA release (Armstrong et al., 2012; Capogna & Pearce, 2011; Price et al., 2008). This form of GABA transmission enables NGCs to massively inhibit all targets located in the extent of their intricated axons, affecting even extrasynaptic receptors. In addition, GABA-B mediated inhibition can occur unitarily in their targets upon one single NGC action potential (Oláh et al., 2009; Tremblay et al., 2016). The combination of GABA-A and GABA-B communication exerted by NGCs elicits biphasic responses in the target cells, with an early peak explained by the first and a late prolonged one enabled by GABA-B transfer.

Another unique characteristic of NGCs is that their axons can cross boundaries between brain regions (Jiang et al., 2015; Tremblay et al., 2016), thus contributing to inter-areal activity coordination and information sharing and integration (Armstrong et al., 2012). This process is thought to be mediated through GABA-B inhibition, forming the so-called feedforward circuits (FFI) (Price et al., 2008). FFIs are implicated in the regulation of neuronal excitation by the establishment of time-constrained intervals of inhibition, the improvement of sensory discrimination by favoring coincidence detection, the provision of gain modulation through input normalization and their contribution to associative functions (Cohen-Kashi Malina et al., 2021; Hou & Capogna, 2018; Price et al., 2008; Suzuki et al., 2022; Tremblay et al., 2016).

The positioning of NGCs within cortical circuits, mainly in superficial layers and very numerous in L1, appears to be strategical for bottom-up and top-down information integration through their implication in FFI and neuromodulation (Colonnese et al., 2021). In this lines, L4 NGCs play a role in somatosensory integration through their transient circuit modulation of thalamic-evoked FFI (Chittajallu et al., 2013). Also via their responsiveness to thalamocortical afferents, L1 NGCs are implicated in the induction of cortical DOWN states (low arousal) across cortical areas through GABA-B release, feature thought to contribute to memory consolidation (Cohen-Kashi Malina et al., 2021; Hay et al., 2021). In addition, L1 NGCs, have been proven to be rapidly recruited during learning, locomotion and attention given their expression of nicotine acetylcholine receptors and responsiveness to cholinergic long-range projections from the basal forebrain (Bloem et al., 2014; Poorthuis et al., 2018). NGC FFI functions mediated by cholinergic modulation can selectively control the effect of external inputs on current behaviors by tuning their salience (English et al., 2012). Long-range inputs to L1 NGCs such as the one previously described are numerous and include also those

from neocortical areas such anterior cingulate projections to visual cortex located NGCs (Colonnese et al., 2021). In this regard, L1 NGCs have are implicated in the integration of contextual and attentional signals (Speed & Haider, 2021), which in turn provide columnar bulk inhibition (Schuman et al., 2021). Some NGCs located in deep layers have been shown to coordinate memory consolidation processes during DOWN brain states (such as slow-wave sleep) (Hay et al., 2021; Valero et al., 2021). Those rare *Lhx6*-expressing NGCs, fired specifically when other INs are silent, are thought to prolongate cortical DOWN states across cortical areas and be crucial for memory consolidation. Finally, NGCs not only promoting inter-areal synchronization, also contribute to information transfer by coupling their activity and decoupling excitatory cell activity respect to gamma oscillations (Sakalar et al., 2022). This mechanism was described to gate the interaction of hippocampus and cortex for a tightly time controlled information transmission (Craig & Witton, 2022; Sakalar et al., 2022), crucial for memory acquisition and consolidation.

Thesis aims

Previous work from the laboratory has shown that NGCs derive from the POA, using an *Hmx3*-Cre::*Htr3a*-GFP;Rosa26-tdTOMfl/fl mouse model (Niquille et al., 2018). More specifically, these NGCs mature from a pool of E14.5 *Hmx3*;tdTOM+/*Htr3a*-GFP+ postmitotic cells that populate the entire brain, including the neocortex. These cortical NGCs were shown to be molecularly and functionally different from other L1 *Hmx3*;tdTOM-/*Htr3a*-GFP+ interneurons, thought to be derived from the CGE (Miyoshi et al., 2010). Electrophysiological characterization indicated a typical NGC functional profile of *Hmx3*;tdTOM+/*Htr3a*-GFP+ cells, which led to the observation of a scarce NGC population in L1 (so-called type 1B), for which AHP was shallower and spike latency shorter compared to the overarching NGC L1 (type 1A). Niquille et a., 2018 also reported the existence of non-L1 NGCs with activity patterns matching those of the 1A type profile.

The research project behind the present thesis aims at interrogating cortical NGC diversity from a developmental point of view. For this purpose, genetic fate-mapping using the *Hmx3*-Cre::*Htr3a*-GFP;Rosa26-tdTOMfl/fl mouse model enables us to study this restricted cell type, NGCs, through maturation and access to the highest possible resolution level for diversity interrogation. Furthermore, we sought to investigate cortical NGC molecular signatures using single-cell transcriptomics, combined electrophysiological characterization with whole-cell transcriptome (patch-sequencing), and morphological description. The objectives of this thesis can be summarized as follows:

- Describe NGCs (POA-derived) compared with their molecular neighbor INs (CGE-derived) throughout postnatal development combining genetic fate-mapping and scRNA-seq - how is the NGC identity card like? Are there molecular determinants of cell type identity traceable throughout development?

- Decipher whether molecular heterogeneity exists within the cortical population of POA-derived NGCs.

- Once postnatal NGC diversity was disentangled, we aimed to discover whether transcriptomic profiles corresponding to putative NGC subtypes were also functionally different. For this purpose, we combined the power of single cell transcriptomics with the electrophysiological characterization of single cortical NGCs.

- Trace NGCs back to their embryonic origins by reconstructing their maturation trajectory combining scRNA-seq and genetic fate-mapping to gain insights into the molecular profile of embryonic NGCs and the emergence of their diversity. We subsequently discovered that NGCs from diverse subtypes are simultaneously generated at E14.5, spanning different brain areas and cortical layers.

- With NGC developmental trajectories unraveled, we sought to challenge their maturation by genetically manipulating NGC progenitors. We disrupted by genetic loss-of-function what we identified as the most defining NGC molecular signature: the sustained expression of TOX2. Thus, we used *in-utero* electroporation using of a CRISPR-Cas9 construct targeting *Tox2* in POA progenitors at E14.5. We did not identify any cortical NGC following *Tox2* loss-of-function, indicative of disrupted maturation.

Materials and methods

Mouse strains

Animal experiments were performed according to international and Swiss guidelines and approved by the Geneva local animal care committee. Mice were housed in the conventional area of the animal facility of the University Medical Center, under controlled temperature (22±2°C) and dark/light cycles (12h each). Food and water were provided *ad libitum*. We crossed B6.Cg-*Gt(ROSA)26Sor*$^{tm14(CAG-tdTomato)Hze}$/J (Jax stock #007914) loxP flanked reporter mice with transgenic mice expressing the enhanced green fluorescent protein (eGFP) under the control of the *Htr3a* regulatory sequence (Tg(*Htr3a*-EGFP)DH30Gsat/Mmnc) (GENSAT Consortium) to obtain *Htr3a*-GFP;*Rosa26*-tdTOM$^{fl/fl}$ mice. To label NGCs, these mice were then crossed with Tg(*Hmx3*-icre)1Kess (also known as *Hmx3*-Cre) animals to obtain the *Hmx3*-Cre::*Htr3a*-GFP;*Rosa26*-tdTOM$^{fl/fl}$ mouse model reported in (Niquille et al., 2018). For elucidating whether NGC progenitors belong to an *Nkx2.1*+ lineage, *Hmx3*-cre animals were first bred to *Nkx2-1*$^{tm2.1(flpo)Zjh}$/J (JAX #028577, also known as *Nkx2.1*-ires-Flp) to generate *Hmx3*-Cre;*Nkx2.1*-ires-Flp mice that were finally crossed with B6;129S4-*Gt(ROSA)26Sor*$^{tm3(CAG-tdTomato,-EGFP*)Zjh}$/J (IS reporter, JAX #028582) (He et al., 2016). Timed-pregnant transgenic females were obtained by overnight mating. Mice were maintained on a C57BL/6 background and both female and male embryos and mice were analyzed in this study. WT mice were purchased from Charles River Laboratories and the embryonic day E0.5 (overnight-mated females) was established as the time of detection of the vaginal plug.

Surgical procedures

Pre- and post- operatory procedures

CD1 overnight-mated CD1 pregnant dams (age of embryos: E14.5) were used for in-utero experiments: FlashTag (FT) and electroporation. One hour before the surgery, pregnant females were treated subcutaneously with Temgesic (1.5ul of 0.5% Temgesic, Schering-Plough). Prior to the surgical intervention, mice were anesthetized by inhalation of 2.5% isoflurane (Baxter), placed on a sterilized surgery table (temperature controlled at 37°C), eyes protected with gel drops (Viscotears), abdomen was shaved, sterilized with Betadine

(MundiPharma) and covered with a sterile pad. For performing both types of in-utero surgeries, uterine horns were exposed by cesarean cut along the *linea alba*. Embryos were kept moisturized by continuous application of warm 0.9% NaCl. Once the surgical procedure on embryos was completed, another identical dose of subcutaneous Temgesic was applied and the abdominal wall was closed. Mice recovery on a warm pad was monitored for two hours post-surgery before placed in the animal house.

Flash Tag in-utero injection

For FT injections, half a microliter of 10 mM of a carboxyfluorescein succinimidyl ester (FlashTag, CellTrace™ CFSE, Life Technologies, #C34554) was injected into the lateral ventricle of the embryos' brain through a beveled glass pipette (Drummond Scientific) applied to a Picospritzer (Parker). They were let to develop for 2 hours prior collection aiming at stain the progenitors in the wall of the 3rd ventricle.

In-utero electroporation

For in-utero electroporations, 10ul of 2ug/ul (1% Fast Green, Sigma) plasmid was delivered into embryo's lateral ventricle of the embryos' brain through a beveled glass pipette (Drummond Scientific) applied to a Picospritzer (Parker). Tweezers-type electrodes (CUY611P3-1, NepaGene) were placed on the embryo's brain at an appropriate angle to target electrically the region of interest (for POA see Results figure 11A; for dorsal pallium see Results figure 11B), with the positive pole of the electrode directed towards the desired area. Five square pulses of 45V (50ms on/950ms off) for E14.5 electroporation and five square pulses of 35V (50ms on/950ms off) were applied with a square wave electroporator (ECM830, Harvard Apparatus). Embryos were let to develop until the age of interest (E16.5 or P10).

Two different plasmids were used for *in-utero* electroporation, either independently delivered or in combination. Final concentration was always kept at 2ug/ul (1% Fast Green). Used DNA constructs were: pcag-IRES-tdTOM (purchased from addgene) and Ef1a-sg*Tox2*Cas9-2A-GFP (purchased from abm, 473231140591, subcloned, transformed and amplified following manufacturer's protocol; Results figure 12A).

Histology

Tissue preparation

For postnatal ages, mice were anesthetized with intraperitoneal injection of pentobarbital (50 mb/kg) and transcardially perfused with 0.9% saline solution with Liquemine (2ml/L) followed by ice-cold paraformaldehyde dissolved in PBS 1X at 4%. Brains were dissected and post-fixed overnight at 4°C in 4% PFA under agitation in the dark.
For embryonic ages, pregnant females were euthanized with intraperitoneal injection of pentobarbital and embryos exposed by cesarian cut. Brains were dissected on ice-cold PBS 1X and post-fixed overnight at 4°C in 4% PFA under agitation in the dark.

Both for postnatal and embryonic brains, if used for smFISH, after overnight fixation, brains were prepared for fresh freezing by consecutive embedding in increasing percentages of sucrose solution (first day sucrose 15% and second day sucrose 30%; diluted in PBS1x, Sigma). Each brain was placed into a plastic cube filled with O.C.T Compound (Tissue-Tek, 4583) and freezed on isopentan (2-Metylbutan, ReagentPlus, >=99%; Sigma) placed on dry ice. Brain cubes were stored at -20°C until cutting.

Single-molecule Fluorescent In-Situ-Hybridization

Twelve µm-thick coronal sections were prepared from fresh frozen embryonic (E14.5) and adult brains (P56) from *Hmx3*-Cre::*Htr3a*-GFP; *Rosa26*-tdTOM$^{fl/fl}$ or WT (CD1) animals. A Cryostat was used for slicing (-19°C to -21°C; Leica CM3050) and brain slices were immediately placed on microscope slides (Superfrost Plus 25 x 75 x 1.0 mm; Thermo scientific). Sliced were stored at -20°C after drying.
Sections were then incubated at room temperature for 1 hour and then fixed with 4% PFA for 15 min and processed for the staining according to the manufacturer's instructions, using the RNAscope Multiplex Fluorescent kit (Advanced Cell Diagnostics, 323110) for fresh frozen tissue. Briefly, sections were dehydrated using 50%, 70% and 100% successive baths. A 10 min treatment in SDS (4% in 200 mM sodium borate) was added to the protocol after the Protease IV incubation as proposed in Zeisel et al., 2018. *Gfp*, *Nkx2.1* (Channel 1), *Tomato*, *Hmx3* (Channel 2), *Tox2*, *Rxfp1* (Channel 3) probes were then incubated on sections for 2 hours at 40°C and processed for amplification steps. Finally, sections were counterstained with DAPI and mounted with Mowiol medium (Merck, 9002-89-5).

Probe	Channel	Reference
Mm-*Hmx3*	C2	518641
tdTomato	C2	317041
eGfp	C1	409971
Mm-*Dock5*	C3	872971
Mm-*Lsp1*	C3	511811
Mm-*Tox2*	C3	552611
Mm-*Rxfp1*	C3	458001
Mm-*Nkx2.1*	C3	434721

Table 1. RNA-Scope probes.

Immunohistochemistry

Brains were sliced coronally at 70um using a vibratome (VT100S, Leica). Slices were stored at -20°C in an ethylene-glycol-based cryoprotective solution.

Brain slices were permeabilized in PBS/0.3% Txt-100/Na-Azide and blocked in 2% normal horse serum (NHS) for 2h on a rotating shaker at room temperature (RT) in the dark. Primary antibodies were applied at the appropriate dilution (see Table 1) in permeabilization solution and left at 4°C on a rotating shaker in the dark overnight. Secondary donkey antibodies Alexa 488, 567 and 647 (Abcam, Invitrogen) raised agains the appropriated species were diluted at 1:500 in permeabilization solution and incubated for 2h on a rotating shaker at RT in the dark. After three washes in PBS1X, sections were counterstained with Hoechst 33342 for 15 minutes (1:10000, Sigma), washed again and mounted using Mowiol mounting media.

Target Protein	Species	Dilution	Company	Reference
GFP	Chicken	1:2000	Abcam	ab13970
TOMATO	Goat	1:500	Sicgen	ab8181-200
CASPASE3	Rabbit	1:200	Cell Signaling	9661
NKX2.1	Rabbit	1:500	Santa Cruz	sc-13040
TOX2	Rabbit	1:100	Abcam	ab220985
nNOS	Goat	1:500	Abcam	ab1376

Table 2. Primary antibodies.

Histological analysis

Imaging

Fluorescent images were acquired using:

- Nikon A1 inverted confocal microscope, equipped either with a 20x (0.45 CFI Plan Fluor) or an oil-immersion 40X (0.6 CFI Plan Fluor 40x) objective (Nikon). This equipment was used for histological preparations for colocalization assessment and Z-stack acquisitions for morphology reconstruction.
- Widefield scanner Zeiss Axioscan Z1 with a 20x (0.8 Plan Apochromat) objective (Zeiss). This equipment was used when no colocalization assessment was required.

Image preprocessing

Custom Matlab scripts for preprocessing smFISH images were prepared and executed by the members of the UNIGE Bioimaging Platform. This preprocessing aimed at sharpening smFISH signal for single molecule quantitative quantifications.

Quantification and analysis

For cell quantifications, Fiji software (Image J) and custom R scripts were used. Images were rotated using Fiji for homogeneity across acquisitions: specifically, for cortical images, rotation aimed at pial surface to be the upper-horizontal limits; for POA or hypothalamic slices, the wall of the 3rd ventricle was aimed at the right-vertical limit. Using Fiji ROI manager plugin, an oval region of interest was drawn and saved for each single cell of interest. ROI manager coordinates for each cell as well as for the pial or ventricular limits were stored in a zipped file per image. For each ROI, the cell status for each staining was dummy-encoded in an excel file (cells were named with an unique identifier both in ROI and excel files, containing information about the brain, slice, side and cell number) Using R, for each experiment, ROI manager objects and excel files were matched by cell unique identifiers and assembled into a dataframe used for calculating population percentages and density estimates on their radial position respect to the pial surface or the 3rd ventricle (for cortical pictures, y-position was normalized respect to pial surface; for POA or hypothalamic pictures, x-position was normalized respect to ventricular wall. The coordinate axis not subjected to normalization was jittered according to an scaled interval within the region limits). For smFISH quantitative analysis, R software

was used to count and illustrate the number of molecules per region of interest as well as their normalized position similarly as was done for dummy-encoded IHC.

Paired Kolmogorov-Smirnov test was used to assess whether cell type distribution along the cortical depth is statistically different depending on different tissue stainings (non-parametric test evaluating the equality of one-dimensional distributions).

Morphological reconstruction and feature extraction

3D 40x confocal stacks of *in-utero* electroporated neurons were processed for high-resolution semi-automated tracing using Neutube 1.0z software (Feng et al., 2015), followed by manual correction and set of cell body as root. Reconstructions were scaled and exported in SWC format.

Feature extraction was performed on SWC scaled reconstructions using stats function from the NeuroM python software, developed by the Blue Brain project, with default settings (Palacios et al., 2022).

For plotting SWC reconstructed neurons as well as those obtained from the open dataset provided by (Scala et al., 2021), nat R package was used.

scRNA-seq dataset collection

Microfluidic based scRNA-seq

For postnatal tissue dissociation, P15 and P30 *Hmx3*-Cre::*Htr3a*-GFP; *R26R*-tdTOM$^{fl/fl}$ brains were extracted in ice cold Hanks' balanced Salt Solution (HBSS, Sigma) and coronal slices (600 µm) were cut using a Mcllwain tissue chopper. Upper layers of somatosensory cortex were microdissected under a stereomicroscope and further split into ~6mm fragments. Each time point consisted of pooled brains (n=5, at P15 and n=6 at P30). For tissue digestion, a modified protocol for the Worthington Papain Dissociation kit (Worthington Biochemical Corporation #LK003150) was used. Tissue was placed in EBSS#1 solution composed of EBSS provided in the kit, AP5 (0.05 mM, Tocris #0106), Kynurenic acid (0.8 mM, Sigma #K3375) and Trehalose (0.135 M, Sigma #T9531) and then transferred to a papain bath during 15 or 30 minutes at 37°C under gentle agitation for P15 and P30 respectively. Trituration with 1 ml pipette was performed and the obtained cloudy cell suspension was centrifuged at 300g during 5 minutes. The pellet was resuspended with 3 ml of EBSS#2 composed of EBSS, AP5 (0.05 mM), Kynurenic acid (0.8 mM), 350 µl of ovomucoid and 250 µl of DNAse provided in the kit and Trehalose (0.135 M). After adding the suspension in 5 ml of ovomucoid solution, the

mixture was centrifugated at 70g during 6 minutes. The final pellet was resuspended in 1 ml of DMEM/F12 complemented with 10% FBS, 10% Horse serum, AP5 (0.025 mM), Kynurenic acid (0.4 mM) and Trehalose (0.135 M). Finally, cells were incubated with Hoechst 33342 (1 µg/ml, Sigma #H1399) during 15 minutes at 37°C and FAC-sorted using a Beckman Coulter MoFlo Astrios set for selecting GFP^+ cells on one side and $GFP^+/Tomato^+$ cells on the other side. A mix of 1 µl of Cell Suspension Reagent (Fluidigm) and 9 µl of each of the two FAC-sorted cell suspensions (500 cells/µl) was loaded on a C1 Single-Cell AutoPrep intregated fluidic circuit (IFC) designed for 10-17 µm cells (HT-800, Fluidigm #100-57-80). Immediately after the single-cell capture, the IFC plate was imaged in two different filters (GFP 3035B and Cy3 4040B) in addition to the brightfield using the ImageXpress Micro Widefield High Content Screening System (Molecular Devices).

For embryonic tissue dissociation, either FT E14.5 + 2h injected brains either E14.5 brains from *Hmx3*-Cre::*Htr3a*-GFP; *R26R*-$tdTOM^{fl/fl}$ mice were used. Embryonic brains were extracted in ice-cold HBSS and sectioned using a Mcllwain tissue chopper. The embryonic tissue from regions of interest was micro-dissected under a stereomicroscope and incubated in 0.05% trypsin at 37°C for 5 minutes. Following tissue digestion, fetal bovine serum was added to the mix and cells were manually dissociated via up-and-down pipetting. Cells were centrifuged 5 min at 300 G and the pellet was suspended in 1 ml of HBSS then passed on a 70 µm cell strainer. FT+ cells were FAC-sorted on a MoFloAstrios device (Beckman) gated to include only the top 5% brightest cells. *Hmx3*-Cre; tdTOM+; *Htr3a*-GFP+ POA cells were FAC-sorted on a MoFloAstrios device for selecting $GFP^+/Tomato^+$ cells. Each previously described FAC-sorted embryonic single cell populations was captured using integrated fluidic circuits, imaged and sequenced as previously described for postnatal datasets

Droplet-based scRNA-seq

E14.5 C57BL/6 WT embryos were used for droplet based RNA-seq. Tissue dissociation was performed as previously described for microfluidic embryonic preparation. Cell suspension was loaded into a 10x Chromium Controller (10x Genomkics, Plesanton, CA, USA).

Single-cell cDNA library preparation and RNA-sequencing, mapping, counting

All single cell RNA capture, library preparation and sequencing procedures were performed within the Genomics Core Facility of the University of Geneva. For microfluidic-based scRNA-seq, lysis, cDNA synthesis and preamplification steps were performed into the C1

instrument according to the manufacturer's protocol using the SMARTer Ultra Low RNA kit (Takara, #635026). For each IFC, 20 libraries were prepared using Nextera XT DNA Library Preparation Kit (Illumina, #FC-131-1096), multiplexed and sequenced in paired-end mode consisting of a 5bp Unique Molecular Identifier (UMI) on read 1 and 90bp on read 2 using an HiSeq2500 instrument (Illumina) to an expected depth of 1M reads per cell. Sequenced reads were aligned to the mouse genome (GRCm38) using the read-mapping algorithm STAR (Dobin et al. 2013). Unique Molecular Identifiers (UMI) were used to correct for cDNA PCR amplification biases. Duplicated reads were identified and corrected using the deduplication step from the UMI-tools software (Smith et al. 2017). Non-ambiguously mapped exonic reads (STAR mapping quality ≥ 255) were quantified using summarizeOverlaps() function from the GenomicAlignments R-Package (mode IntersectionStrict) considering their mapping strand. Unmapped reads were further aligned onto eGFP and Wpre-TdTomato sequences to identify *Htr3a*-GFP and *Hmx3*-Cre;tdTOM positive cells respectively. This transcriptomic information was cross-compared with fluorescent levels observed after IFC plate picture annotation. All the analyses were computed on the Vital-It cluster administered by the Swiss Institute of Bioinformatics. For droplet-based scRNA-seq, single-cell suspensions were loaded and processed into a 10X Chromium Controller (10X Genomics, Plesanton, CA, USA) with the Single Cell 3' v2 reagent kit (10X genomics) according to the manufacturer's protocol. Briefly, single cells were partitioned into Gel beads in EMulsion (GEMs) in the GemCode instrument followed by cell lysis and barcoded reverse transcription of RNA, amplification, shearing and 5' adaptor and sample index attachment. On average, 10.000 single cells were loaded on each channel with 4978 cells recovered for the CGE and 2736 cells recovered for the POA library after sequencing on a HiSeq 4000 instrument (Illumina) at an expected depth of 70k reads per single cell. "Cell Ranger" software (10X Genomics, version 3.0.2) was used for mapping reads to the mouse genome provided by the instrument manufacturer (10X Genomics, mm10 refdata v3.0.0) and for generating feature-barcode matrices.

scRNA-seq analysis

Quality Control on microfluidic-based datasets

Doublet cells or empty wells identified on the Fluidigm C1 plate imaging were excluded. At P15 and P30 time-points, cells expressing < 1000 genes or <100.000 UMIs or <50.000 mapped reads or > 20% of reads from mitochondrial genome were excluded from the analysis (Methods figure 1). At E14.5 time-point, C1 cells expressing < 1000 genes or <100.000 UMIs or <50.000

mapped reads or > 15% reads from mitochondrial genome were excluded from the analysis. Non-GABAergic populations were filtered by clustering on 2000 most variable genes (9.7% among E14.5 *Hmx3*-dtTOM+; *Htr3a*-GFP+ cells and 15.7% among FT+ cells) (Methods figure 2). A total of 897 *Hmx3*-dtTOM+; *Htr3a*-GFP+ single cells (E14.5: 418, P15: 200 cells, P30: 313 cells), 431 *Hmx3*-dtTOM-; *Htr3a*-GFP+ (P15: 197 cells, P30: 234 cells) and 352 E14.5 FT+ cells were kept for further analysis.

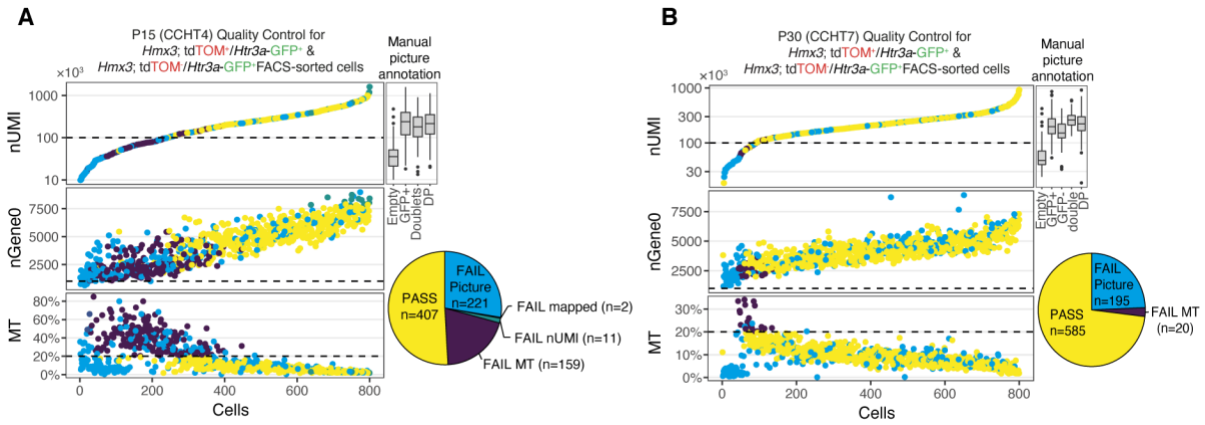

Methods figure 1. Quality Control procedure applied on postnatal scRNA-seq datasets.

A-B. Scatter plots illustrating QC procedures for P15 and P30 microfluidic-based datasets containing both *Hmx3*-dtTOM+; *Htr3a*-GFP+ and *Hmx3*-dtTOM-; *Htr3a*-GFP+ FACSorted cells. Number of UMIs detected (nUMI), number of genes detected (nGene0) and percentage of mitochondrial reads (MT) are detailed in respective y-axes. X-axes represents cell index. Barplots illustrate the nUMIs per fluorescent condition of the single cells as they were manually annotated following microscopy acquisition on microfluidic plates. Pie charts illustrate the proportions as well as number of cells by QC status (yellow: QC successfully passed; blue: QC failed because of bad quality picture or empty plate chamber; purple: QC failed because too high % MT; dark green: QC failed because of too low nUMI count; light green: QC failed because of too low mapped reads).

Abbreviations: nUMI, number of Unique Molecule Identifiers; nGene0, number of detected genes; MT, mitochondrial reads; DP, *Hmx3*-dtTOM+; *Htr3a*-GFP+ cell.

Quality Control on Droplet-based datasets

We considered filtered cells from the "Cell Ranger" output, and additionally discarded cells expressing <1000 genes or >15% reads from mitochondrial genome. We additionally identified by clustering on 2000 variable genes and filtered cells expressing known markers of vascular or endothelial (0.62%), red-blood (2.96%), cajal-retzius (3.40%), immune (0.93%) and

glutamatergic (11.10%) cell types in order to remove non-GABAergic cell populations. Remaining 6221 GABAergic were used for further analysis (Methods figure 2).

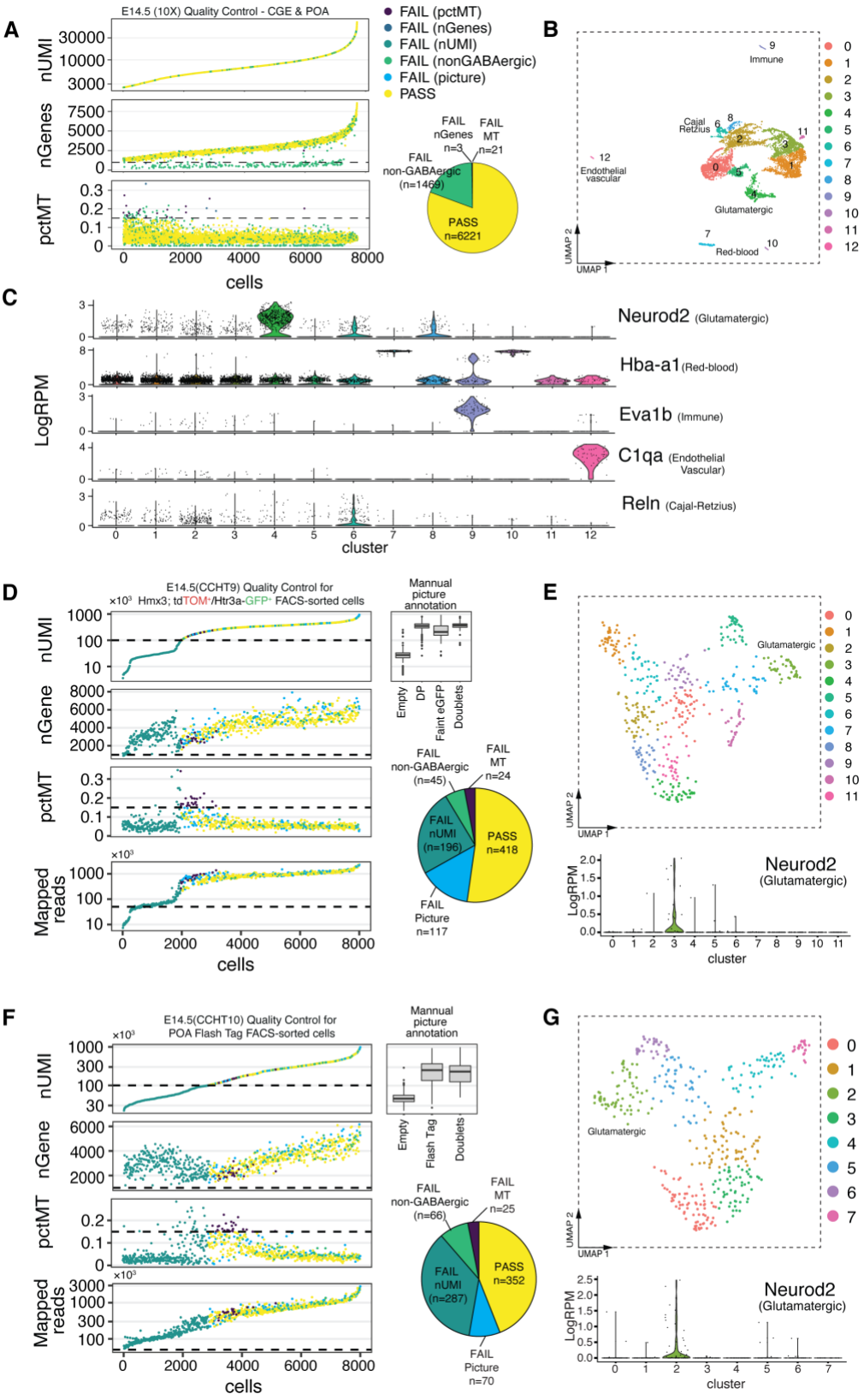

Methods figure 2. Quality Control procedure applied on E14.5 scRNA-seq datasets.

A,D,F. Scatter plots illustrating QC procedures for E14.5 datasets containing: A, dropled-based sequenced WT cells; D, microfluidic-based *Hmx3*-dtTOM+; *Htr3a*-GFP+ FACSorted cells or F, microfluidic-based FT+2h FACSorted cells. Number of UMIs detected (nUMI), number of genes detected (nGene0), percentage of mitochondrial reads (MT) and mapped reads are detailed in respective y-axes. X-axes represents cell index. Barplots illustrate the nUMIs per fluorescent condition of the single cells as they were manually annotated following microscopy acquisition on microfluidic plates. Pie charts illustrate the proportions as well as number of cells by QC status (yellow: QC successfully passed; blue: QC failed because of bad quality picture or empty plate chamber; purple: QC failed because too high % MT; dark green: QC failed because of too low nUMI count; light green: QC failed non-GABAergic cell).
C,B,E,G. UMAP and Violin plots illustrating cell populations in E14.5 datasets highlighting non-GABAergic cell populations that were excluding during QC and representative markers signaling their cell identity.

Abbreviations: nUMI, number of Unique Molecule Identifiers; nGene0, number of detected genes; MT, mitochondrial reads; DP, *Hmx3*-dtTOM+; *Htr3a*-GFP+ cell.

Cell type assignment on postnatal datasets

In order to assign a cell type identity to each single cell in postnatal datasets (P15 n=397 and P30 n=547), we used as reference the mouse transcriptomic cell types database from Allen Brain Map (Tasic et al 2018.). Only core cells from adult cortical interneurons belonging to Htr3a-expressing cardinal classes (Lamp5, Vip, Sncg and Serpinf1, n=4751), both from visual and anterior motor cortex (Allen Cell Types Database) where considered. We performed pairwise integrations (P15 to reference and P30 to reference) using two independent methods in parallel with the aim of assigning core identities to single cells with a consensus type assignment. One method was Seurat R package v2 dataset integration pipeline. Briefly, for each integration, we normalized, scaled and calculated 2000 top variable genes on each dataset independently (variable genes in the two datasets were combined using Seurat union function). 20 canonical correlation vectors (CCV) were calculated and aligned between query and reference data and only those with a biweight midcorrelation >0.15 with at least 30 genes of the normalized and scaled expression matrix (bicor function from WGCNA R package) were used. This CCVs were then used as input for a 2D t-SNE non-linear transformation, followed by a k-nearest neighbors (KNN) classifier to assign the identities to P15 and P30 cells. As second method we used Multiclass Bagging Support Vector Machines Classification from the

bmrm R package. Briefly, we trained 25 classifiers on random subsets of single cells and genes using the reference dataset that were used to predict cell identity independently on P15 and P30 datasets. Majority vote prediction on the 25 classification models for each single cell was aggregated. Finally, in order to obtain a consensus identity prediction between Seurat-KNN and SVM approaches, identity predictions obtained with each method were cross-compared. P15 and P30 single cells whose predictions agreed and had a consistent fluorescence profile were considered core cells (n=158 at P15 and n=207 at P30) while cells whose prediction differ between the two methods or had an inconsistent fluorescence profile were considered as intermediate cells (n=239 at P15 and n=340 at P30). For P15 and P30 datasets, only core cells where considered for further analysis and an equivalent number of cells were selected per identity class in reference dataset.

Cell assignment enrichment

For understanding the extent of Dock5 / Lsp1 subtype enrichment among *Hmx3*;tdTOM+/*Htr3a*-GFP+ cells, we contrasted the proportion of these NGC fate-mapped cells assigned to each subtype respect to the cell type distributions when no genetic fate-mapping is used, as in Tasic et al., 2018, and when *Hmx3*;tdTOM-/*Htr3a*-GFP+ cells are considered (non-NGC fate-mapping).

Postnatal maturation reconstruction

P15 and P30 core cells as well as an equivalent number of P56 reference cells were used to train a regularized ordinal regression model to order them on a quantitative maturation score. Inspired by the approach used in Telley et al., 2019, a 10-fold cross-validated linear model was trained using a small set of variable genes for each timepoint. Prediction weights allowed to order single cells as a continuum in accordance with their developmental maturation stage.

Postnatally conserved differential expression

In order to characterize NGC-enriched gene expression both at the type and the subtype level, we performed differential gene expression analysis followed by functional characterization. To do so, we built two cross-validated SVM classifiers, one to classify NGC vs other *Htr3a*-expressing interneurons and another to differentiate NGC enriched subtypes (Lamp5 Plch2

Dock5 and Lamp5 Lsp1) versus other *Htr3a*-expressing interneurons. Selected NGC cells contained 69 P15 (36 Dock5 and 33 Lsp1), 111 P30 (76 Dock5 and 35 Lsp1) and 90 P56 (56 Dock5 and 34 Lsp1). Selected non-NGC cells contained 89 P15, 96 P30 and 96 P56 non-NGC cells. Both models were trained using genes expressed across development and maturation variation was regressed in order to discover genes with stable patterns of expression through postnatal development. Top 150 genes across 10 cross validations were selected for each model/cell type (NGC, non-NGC, Dock5, Lsp1) according to model weights.

Postnatal gene enrichment analysis

To explore the functional relevance of differentially expressed genes on postnatal contrasts (NGC vs nonNGC and Dock5 vs Lsp1), we performed GO-term and HGNC gene family enrichment analysis. Mouse Genomic Informatics (MGI) database (http://www.informatics.jax.org/downloads/reports/gene_association.mgi.gz) was used for GO-term analysis with its corresponding gene-ontology (release 2018-12-28, http://purl.obolibrary.org/obo/go/go-basic.obo) to retrieve enriched GO term ancestors. Similarly, HGNC enriched gene families were identified using the MGI mouse homologs for the Human Gene Nomenclature Committee (HGNC) database (ftp://ftp.ebi.ac.uk/pub/databases/genenames/). A hypergeometric test was conducted for enrichment analysis in populations of interest as compared to the universe of expressed genes across all *Htr3a*-expressing interneuron subtypes. Significant HGNC associations were manually grouped into the so-called “gene superfamilies” for simplicity of representation.

Embryonic maturation reconstruction

Embryonic maturation trajectory for E14.5 single cell datasets was calculated following methods previously described in Telley et al., 2016. Briefly, all E14.5 single cell datasets were normalized and scaled regressing for number of genes expressed in order to remove sequencing depth biases. Variable genes common to the different datasets (n=675) were identified using FindVariableGenes function from Seurat R package with default parameters. Data dimensionality was reduced using Principal Component Analysis and only the principal components explaining at least 3% of the data variance were kept. A principal curve was fitted on significant PC components and its orientation determined by the expression of *Nes* and *Dcx*. A maturation score value was attributed to each single cell according to their position when

projected along the principal curve and scaled between 0 and 1. Mitotic to posmitotic transition was determined by fitting a smooth curve (loess, span=0.25, degree=1) along the coordinates of S-G2/M to maturation score and setting a threshold at the point where the curve falls below the S-G2/M half average.

Integration and characterization of POA embryonic datasets

POA-derived E14.5 single cells collected using droplet-based 10X technology (n=2106) were used as reference for the integration of the two population-restricted datasets using microfluidic-based C1 technology: 1) E14.5 fate-mapped *Hmx3*-tdTOM+/ *Htr3a*-GFP+ cells (n=418) and 2) E14.5 FT+ POA-derived progenitors (n=352). For the simultaneous integration of three datasets we used the Seurat v3 R pipeline. Briefly, each dataset was log-normalized and integration anchors were calculated with default parameters using the union of the 2000 most variable genes for each dataset. Datasets were integrated using 20 principal components and 20 neighbors, scaled and a 2D UMAP was used for representation and clustering using Seurat standard pipeline.

Markers for each cluster were identified using FindAllMarkers Seurat function and most differentially expressed transcription factors per cluster were illustrated.

For calculating cluster enrichment of *Hmx3*-tdTOM+/ *Htr3a*-GFP+ cells accounting for biases on cluster size, we calculated a seeded random sample of 95 cells per cluster (sample size determined according to the smallest cluster) for assessing the percentage of *Hmx3*-tdTOM+/ *Htr3a*-GFP+ integrated cells by POA population.

Identification of NGC conserved markers and embryonic pseudogene scoring, thresholding

For identifying the genes that characterize NGC cells across development (from progenitors to adulthood), we intersected postnatally-conserved NGC vs non-NGC SVM identified genes respect to the universe of genes expressed in the embryonic POA (>0.05 logRPM). NGC pseudogene was calculated by mean gene expression of NGC conserved markers normalized by the number of genes expressed on each embryonic cell. The threshold for assignment embryonic POA cells to the NGC-lineage was stablished at the 80th percentile on NGC pseudogene across POA embryonic cells. For assessing the likelihood of each gene in the NGC pseudogene to be developmentally conserved, we calculated its Z-Score both embryonically and postnatally respect to non-NGC cells (*Htr3a*-expressing INs postnatally and POA cells with an NGC pseudogene score below the previously described 80th percentile cutoff).

Integration of NGC datasets with STICR-lineage data and subtype embryonic prediction

Openly available STICR-lineage data from (Bandler et al., 2022) annotated as belonging to the NGC lineage was further annotated by subtype identity using (Tasic et al., 2018) data for Dock5/Lsp1/Lhx6 prediction using Seurat v3 standard pipeline for integration and label-transfer. Tasic et al., 2018, E14.5, P15 and P30 NGC were integrated into the transcriptomic space of Bandler et al., 2022 NGCs (reference) for obtaining a cross-dataset NGC subtype landscape and predicting E14.5 NGC subtype identity using Seurat v3 integration pipeline and label-transfer. Percentage of Bandler et al., 2022 cells according to their birthdate annotation was calculated per NGC subtype to assess NGC subtype neurogenesis rates.

Embryonic NGC subtypes gene enrichment

Seurat function FindMarkers was used to calculate differentially expressed genes between Dock5 and Lsp1 E14.5 NGCs. Pseudotime axis was regressed for discovering embryonic NGC markers not dependent on maturation.

IUE Morphology UMAP and cell type identity prediction

Feature extraction datasets (NeuroM) from: a) Scala et al., 2022 NGCs and b) morphologically reconstructed NGCs obtained from control POA E14.5 in-utero electroporation experiments (pcag-tdTOM) were integrated Seurat v3. This morphological integration space was used for predicting subtype identity of IUE reconstructed cells by label-transfer.

Single-cell patch-seq

Hmx3-Cre::*Htr3a*-GFP; *R26R*-tdTOM$^{fl/fl}$ mice between 14 and 25 postnatal days were used for electrophysiological recordings followed by patch-seq.

Whole-cell recording and RNA extraction

Dissected brains were immediately transferred into ice-cold sucrose cutting solution equilibrated with 95% O_2 and 5% CO_2 containing (in mM) Sucrose (75), NaCl (85), $CaCl_2$ (0.5), $MgCl_2$ (4), $NaHCO_3$ (24), KCl (2.5), NaH_2PO_4 (1.25) and glucose (25). 300-µm thick coronal slices were obtained using a vibratome (Leica VT 1200S). Slices were transferred and incubated at 35 °C for 20 min in a slice recovery chamber filled with artificial cerebrospinal fluid (ACSF) containing (in mM) NaCl (125), $CaCl_2$ (2.5), $MgCl_2$ (1), $NaHCO_3$ (26), KCl (2.5), NaH_2PO_4 (1.25) and glucose (25). Slices were kept in the recovery chamber at room

temperature until recording. For recording, slices were transferred to a continuously superfused with oxygenated ACSF maintained at 30±0.3°C using an in-line heating system (TC-01, Multichannel systems). *Hmx3*; tdTOM+ / *Htr3a*-GFP+ neurons in cortical layers 1-6 were visualized by using an upright microscope (BX51WIF, Olympus), equipped with a 40x water-immersion objective, infrared/differential interference contrast (DIC) optics and epifluorescence (GFP and mCherry filter set and two single fixed wavelengths. LED sources: 470 nm and 565 nm, COO-LED2LLG-470-565, CoolLED). Neurons were digitally visualized using a CCD camera system attached to BX51WIF (SciCam Pro CCD camera, Scientifica). Autoclaved borosilicate glass capillaries (1.5 mm OD, GC150TF-7.5, Harvard Instruments) were used to pull recording pipettes with resistance between 2-4 MΩ using Zeitz DMZ puller (Zeitz instrument). Pipettes were filled (up to 1µL) with RNase-free internal solution containing (in mM): potassium gluconate (123), KCl (12), HEPES (10), EGTA (0.2), MgATP (4), NaGTP (0.3), sodium phosphocreatine (10), glycogen 20 µg/ml, and 0.4 U/µl recombinant RNase inhibitor (Takara, 2313A), pH~7.3.

Once a gigaohm seal was established, neuronal membrane was ruptured with mild negative pressure to enter in the whole-cell configuration. Whole-cell recordings were acquired using a Multiclamp 700B amplifier (Molecular Devices) and digitized at 10 kHz (National Instruments) using a custom-written script in Igor pro (Wave Metrics). After break-in, the capacitive transients were compensated and capacitance values were recorded from the Multiclamp 700B commander. Cells were held at -70 mV in voltage-clamp mode and a repetitive pulse of -4 mV was given 0.1 Hz to monitor series resistance (R_s). Neurons with a stable R_s and a stable resting membrane potential (RMP) below -60 mV were subjected to a battery of current injection protocol to study electrophysiological properties, namely input resistance (R_{input}), action potential (AP) properties, and sag ratio. For computing R_{input}, -40 pA pulse for 120 ms was given and R_{input} values were calculated using Ohm's law. AP properties were studied by delivering consecutive current pulses, 500 ms duration each, from +5 to +300 pA with a 5 pA increment. For sag calculation, a hyperpolarizing current injection step of -200 pA for 500 ms was delivered. This current injection protocol (sweep) was repeated up to 10 times and averaged traces were used for data analysis. All the acquisitions were digitally stored for further offline analyses.

Single-cell RNA material was collected at the end of the recording (4-6 min from break-in to extraction) by applying light suction until most of the cytoplasm and nucleus had entered in the recording pipette. Contents of the pipette were transferred quickly to RNAse-free PCR tubes each containing 8.5 µl of nuclease-free water and 1 µl of a mix composed of 19 µl of

10X lysis buffer from the SMART-Seq v4 3' DE kit (Takara) and 1 µl of 40U/µl of RNase inhibitor. Samples were flash-frozen in dry ice and stored at -80°C until further processing.

Electrophysiological analysis

Neurons with > 25 MΩ initial R_s or fluctuation of > 20% during recording were excluded from the analysis. Offline analysis of electrophysiological data was carried out using Igor pro (Wave metric), several electrophysiological parameters were manually computed. The subthreshold depolarizing bump (STDB) was measured as a small depolarization exhibited at sub-threshold current injection. The first AP elicited in response to threshold depolarizing current injection was used to calculate the single AP parameters**.** AP train elicited in response to the current injection of +300 pA for 1000 ms was used for calculation of spike frequency and other AP train parameters. The membrane time constant (tau) was computed by monoexponential fit to the first 100 ms after current injection of -40 pA. The sag ratio was calculated using this equation: $(V_{min} - V_{end})/V_{min}$; V_{min} is the minimum voltage reached during the hyperpolarizing pulse of -200 pA, and V_{end} is the final voltage reached at end of current injection.

Bioinformatic analysis

Sequencing and Quality Control

Procedure applied to patch-seq dataset sequencing was identical respect to those applied for postnatal datasets (see previous section).

QC determined cells as valid if meeting the following criteria: imaging confirming the cell to be *Hmx3*; tdTOM+ / *Htr3a*-GFP+, containing at least 10000 sequenced reads, out of those 25% exonically mapped and with less than a 15% of microchondrial reads.

Cell type assignment

SVM model trained for Dock5/Lsp1 categorization was used for predicting cell type identity of patch-seq cells. For this purpose, among the 300 genes differentiation Dock5/Lsp1, only those that were expressed at least 10% patched cells (n=237) were kept. Because of dropout events, patched cells that were expressing less than 20% of the 237 selected genes were discarded. Cell type assignment was annotated for cells which SVM prediction weight (decision value) was superior to 0.2. (94%, n=47).

Feature extraction and first spike isolation

AllenSDK anaconda environment with python version 3.7 was used for R reticulate calling of the "allensdk.ephys.epys_extractor" function

Electrophysiological PCA and biplot

Electrophysiological feature extraction dataframe and manually annotated features were scaled and used as input for PCA using the "prcomp" R function. R function "ggbiplot" from the R package with identical name was used to draw a biplot indicating the PCA eigenvectors associated with electrophysiological features.

Gene-electrophysiological correlates

SVM Dock5/Lsp1 genes contained in the IUPHAR database (Harding et al., 2022) were used for calculating correlations (pearson, R) between gene expression and electrophysiological measurements for each patch-seq cell. Significantly correlated genes for each NGC subtype were separately imputed to string-db.org multi protein network inference software using whole mus musculus genome as reference for significance assessment.

Correlations between the different electrophysiological measurements were also calculated for each NGC predicted subtype.

Layer-electrophysiological correlates

Overall correlation for each electrophysiological parameter on each NGC subtype was correlated (pearson, R) respect to the quantitative annotation of patch-seq cell radial position. To assess the relation between each electrophysiological feature and each cortical layer (or sublayer) independently, chi square pearson residuals were calculated using "chisq.test" R function.

Results

Cortical-UL NGCs consist of two transcriptionally defined subtypes

Cortical NGCs are labelled explicitly in *Hmx3*-Cre::*Htr3a*-GFP;*Rosa26*-tdTOM$^{fl/fl}$ mice (Niquille et al., 2018). To determine whether molecular diversity exists within cortical NGCs, we collected *Hmx3*;tdTOM+/*Htr3a*-GFP+ (POA-derived) and *Hmx3*;tdTOM-/*Htr3a*-GFP+ (CGE-derived) cortical upper-layers (UL) cells for scRNA-seq. These two cell populations were isolated by fluorescence-activated cell sorting (FACS) at postnatal (P) days 15 and 30, corresponding to the beginning and end of synaptogenesis in interneurons (INs) (Llorca & Deogracias, 2022).

To assess whether UL POA-born fate-mapped NGCs are a molecularly homogeneous cell population or comprise several subtypes, we aligned their gene expression profiles (at P15 and P30 separately) to a transcriptomic atlas of *Htr3a*-expressing P56 interneurons (Tasic et al., 2018) (Results figure 1A, 2A). Cell type was predicted by combining two independent label-transfer algorithms (Results figure 2B, 3A-B). On one side, we first trained a cross-validated K-Nearest Neighbors (KNN) classifier on the tSNE embeddings of P56 reference cells to confidently predict their subtype, which was then used to assess the identity of FACSorted integrated cells. On the other side, we trained a cross-validated Support Vector Machines (SVM) binary classifier on P56 gene expression matrix which was then used to label-transferring P56 identity on FACSorted cells. To offset methodological constraints, we combined the KNN-based approach with the coordinate-free prediction SVM approach. Cells whose identity prediction coincided at the subtype level by both classifiers were considered core cells and used for further analysis.

Label transfer on transcriptomic alignment resulted in a very robust assignment of fate-mapped NGCs to the *Lamp5*-expressing family of cortical interneurons (Tasic et al., 2018) (88.4% and 76.6% of NGCs mapped on Lamp5 at P30 and P30 respectively) (Results figure 1A, 2A). Specifically, two transcriptomic subtypes were extensively mapped by FACSorted NGCs:

Lamp5 Plch2 Dock5 (hereafter called Dock5) (46.5% of all cells at P30 and 34.8% at P15) and *Lamp5 Lsp1* (hereafter called Lsp1) (29% of all cells at P30 and 29.4% at P15). Globally, Dock5 and Lsp1 subtypes accounted for 75.5% and 64.2% of sequenced NGCs at P30 and P15, respectively. We observed a bigger proportion of core assigned NGCs at P30 than P15, indicative of a sharper on subtype-specific gene expression correlating with IN maturity. In addition, cell type assignment results indicated that while both subtypes are equally represented among P15 NGCs, more cells got assigned to the Dock5 subtype among P30 NGCs..

NGC Dock5 and Lsp1 mapping enrichment robustness was addressed by comparing it with *Htr3a*-expressing IN subtype enrichments described in Tasic et al. 2018 (Results figure 1A). When no *Hmx3*-lineage cell enrichment occurs (Tasic et al., 2018), more non-*Lamp5*-expressing cells are sampled, suggesting that Dock5 and Lsp1 enriched subtype assignment in *Hmx3*;tdTOM+/*Htr3a*-GFP+ cells reflects a high probability of NGCs to carry one of these two genetic signatures (60.2% of non-Lamp5 in Tasic et al., 2018 versus 11.5% of non-Lamp5 among P30 *Hmx3*;tdTOM+/*Htr3a*-GFP+ cells; 23.4% at P15). Consistent with this view, non-Lamp5 mapping enrichment on *Hmx3*;tdTOM-/*Htr3a*-GFP+ cells draws similar proportions as in a pan-IN context (60.4% and 66.4% non-Lamp5 cells among P30 and P15 *Hmx3*;tdTOM-/*Htr3a*-GFP+ cells respectively).

In light of NGC preferential assignment to the Dock5 and Lsp1 adult cortical IN subtypes, we validated the expression of *Dock5* and *Lsp1*, subtype-name genes assigned in Tasic et al., 2018, by Fluorescence *in situ* hybridization (FISH) on coronal section of adult *Hmx3*-Cre::*Htr3a*-GFP;R26-tdTOMfl/fl mice (P56) (Results figure 1B). We assessed the colocalization and cortical positioning of genetically fate-mapped NGCs labeled by *Dock5* or *Lsp1* FISH independently and unlabeled NGCs (pink, purple and yellow color-coding, respectively). We confirmed that cortical adult NGCs do express the genes associated with subtype names from Tasic et al., 2018. For consistency with transcriptomic data, we quantified the number of NGCs populating upper cortical layers and found a bigger abundance of *Dock5* cells respect to *Lsp1*-expressing NGCs: 77.4% and 31.75%, respectively. Importantly, we found that the relative presence of these two subtypes is strongly correlated with cortical depth (p=0.001). Specifically, Dock5 subtype was found mainly in NGCs populating L1, while Lsp1 subtype NGCs are primarily positioned in layers 2/3. Both subtypes can be found across ULs, but *Lsp1*-expressing cells show a spreader radial position distribution and can occasionally populate deep cortical layers (DLs) (not accounted for displayed quantification). The distribution of unlabeled

UL NGCs matches the combined individual distributions of *Dock5*- and *Lsp1*-expressing cell types. *Dock5* and *Lsp1* FISH experiments were also quantified across the entire cortical depth to test whether *Dock5* subtype is population majority when considering all cortical NGCs together. Importantly, we found that subtype abundance gets balanced when all cortical lamina are considered. This finding shows that Lsp1-NGCs are enriched in deep layers of the cortex compared with Dock5-NGCs (data not shown). A recent study by (Valero et al., 2021) suggested the existence of an *Nkx2-1*/*Nos1*-expressing NGC subtype restricted to deep cortical layers. To test this hypothesis, we performed genetic fate-mapping using the *Hmx3*-Cre::*Nkx2.1*-Flp;ISreporter mouse line, and confirmed that this subtype belongs to the *Hmx3*-NGC lineage (Results figure 8), is localized in deep cortical layers, and is immunoreactive for nNOS. The Lamp5 Lhx6 described in Tasic et al., 2018, placed next to the Dock5 and Lsp1 subtypes according to their transcriptomic hierarchy, expresses the markers of the *Nkx2.1*/*Nos1*-expressing NGC subtype (Results figure 8). Finally, this NGC subtype represents a very minor cell population in the cortex but can be found in bigger proportions in the hippocampus (data not shown) (Scala et al., 2021; Tasic et al., 2018; Valero et al., 2021).

Cell type assignment was also performed and analyzed from FACSorted *Hmx3*;tdTOM-/*Htr3a*-GFP+ cells (CGE-derived) (Results figure 3A, 3B), resulting in a weak mapping onto the NGC-enriched Dock5 and Lsp1 subtypes. Instead, CGE-derived INs mapped preferentially to *Vip*-expressing IN subtypes (78.8% at P15 and 77.4% at P30), as described for the subtype distribution on pan-IN collection performed by Tasic et al. 2018.

Altogether, cell type assignment on cortical CGE-derived and POA-derived INs confirms the findings described by previous work in the laboratory (Niquille et al., 2018). The *Hmx3*-Cre::*Htr3a*-GFP;Rosa26-tdTOM$^{fl/fl}$ mouse line targets two complementary cell populations: NGCs by *Hmx3*;tdTOM+/*Htr3a*-GFP+ cells and mainly *Vip*-expressing non-NGCs by *Hmx3*;tdTOM-/*Htr3a*-GFP+ cells. In addition, we demonstrate that NGCs located in upper cortical layers consist of two transcriptionally-defined subtypes, Dock5 and Lsp1, displaying markedly different laminar distributions: Dock5 subtype populates UL preferentially. In contrast, Lsp1 subtype can be found across cortical layers and is likely more abundant in DL. In addition, we provide proof of the existence of a third NGC subtype populating deep cortical layers. This evidence suggests that diversity exists within NGCs derived from the same genetic lineage (*Htr3a*+*Hmx3*+), a heterogeneity that likely reflects functionally different entities with specific roles in cortical microcircuit regulation.

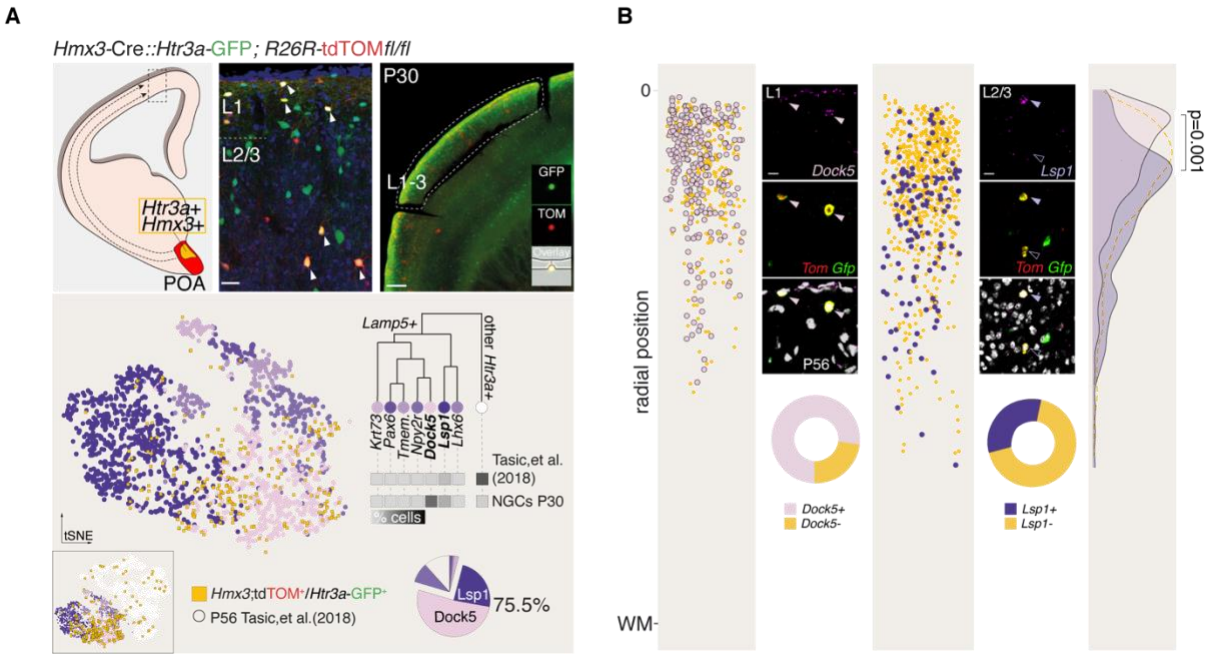

Results figure 1. UL NGCs consist of two transcriptionally-defined subtypes.

A. Schematic describing the procedure for microdissection and FACSorting UL cortical INs from *Hmx3*-Cre::*Htr3a*-GFP;*Rosa26*-tdTOM$^{fl/fl}$ postnatal mice and capturing them for single-cell RNA-seq. tSNE plot illustrating the integration of sequenced NGCs (*Hmx3*;tdTOM+/*Htr3a*-GFP+) onto a transcriptomic atlas of P56 cortical *Htr3a*-expressing interneurons (Tasic et al., 2018) (low-magnification tSNE inset depicts all *Htr3a*-expressing IN subtypes while high-magnification tSNE displays only *Lamp5*-expressing INs). Hierarchical tree (Tasic et al., 2018) illustrates the transcriptomic proximity between *Lamp5*-expressing subtypes and the splitting point among their parent node of *Htr3a*-expressing INs (*Lamp5*-expressing subtypes: Krt73, Pax6, Tmem., Npy2r, Dock5, Lsp1 and Lhx6). Heatmap illustrates subtype enrichment using the percentage of cells among NGC sequenced or pan-driver INs from (Tasic et al., 2018). Pie chart displays the percentage of P30 NGCs mapping to the different *Htr3a*-expressing IN subtypes (highlighted NGCs mapping to Dock5 and Lsp1 subtypes, 75.5% at P30). **B.** FISH gene expression validation for the markers *Dock5* and *Lsp1* in P56 *Hmx3*;tdTOM+/*Htr3a*-GFP+ cells (NGCs). High-magnification pictures detail mRNA localization of these markers in fate-mapped NGCs. Pie charts represent the percentage of NGCs expressing either *Dock5* or *Lsp1* mRNAs (77.4 and 31.75% respectively). Scatter plots detail the position of quantified NGCs on the y-axis compared to their radial position (distance from pia surface) color-coded by either absence of marker expression (yellow), expression of *Dock5* (pink) or expression of *Lsp1* (purple). Density plot displays the distribution of quantified NGCs according to their gene expression profile (dashed yellow line represents Dock5 or *Lsp1* negative NGCs) (pvalue=0.001 according to Kolmogorov-Smirnov statistical test).

Scale bars: A, 500um; B, 10um.

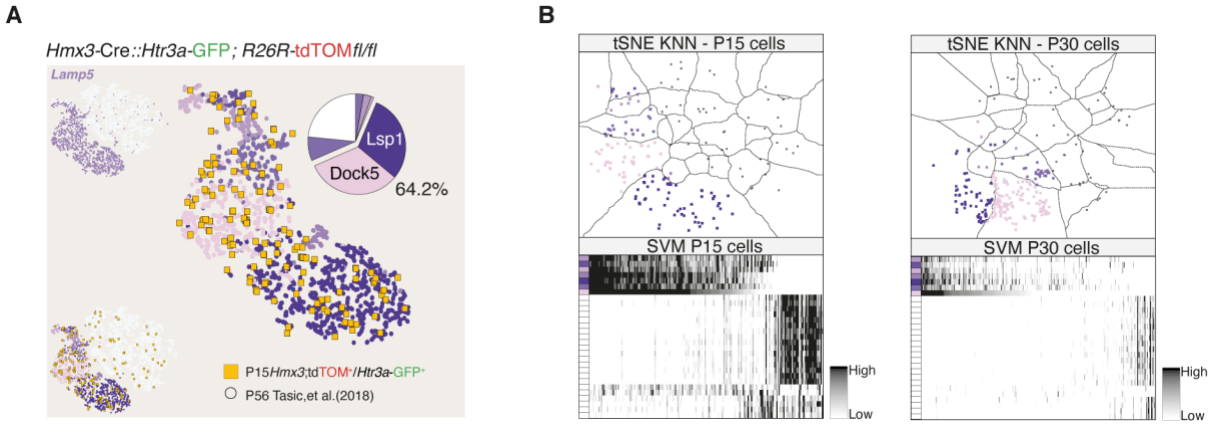

Results figure 2. Cell type assignment of early postnatal UL NGCs and classifier prediction confidence.

A. tSNE plots illustrating the integration of sequenced P15 NGCs (*Hmx3*;tdTOM+/*Htr3a*-GFP+) onto a transcriptomic atlas of P56 cortical *Htr3a*-expressing interneurons (Tasic et al., 2018) (lower-left inset), main tSNE displays only cells belonging to *Lamp5*-expressing clusters. Upper-left inset tSNE displays *Lamp5* logRPM RNA expression among *Htr3a*-expressing interneurons. Pie chart shows the percentage of P15 NGCs mapping to the different *Htr3a*-expressing IN subtypes (highlighted NGCs mapping to Dock5 and Lsp1 subtypes, 64.2% at P15). **B.** Scatter plots and heatmaps depicting cell type prediction results for P15 and P30 *Hmx3*;tdTOM+/*Htr3a*-GFP+ cells. Scatter plots represent the tSNE coordinates resulting from dataset integration and schematic decision frontiers learned by the KNN classifier trained on (Tasic et al., 2018) subtypes. Heatmaps show the decision confidence of the SVM classifier for each cell (columns) compared to each subtype (rows).

Abbreviations: KNN, K-nearest neighbors; SVM, Support Vector Machines; tSNE, t-distributed stochastic neighbor embedding.

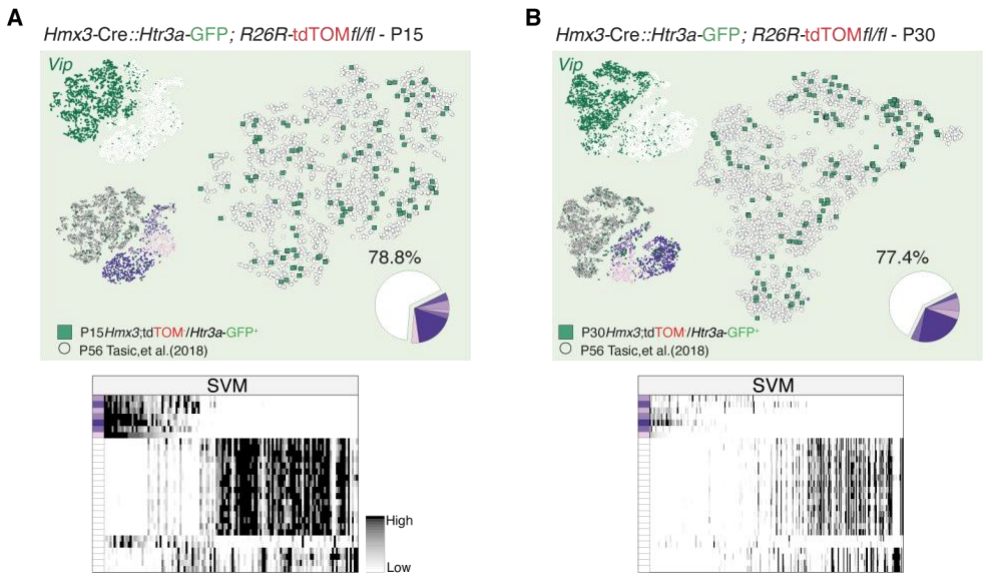

Results figure 3. Cell type assignment on P15 and P30 non-NGC *Htr3a*-expressing INs.

A. tSNE plots illustrating the integration of sequenced P15 non-NGCs (*Hmx3*;tdTOM-/*Htr3a*-GFP+) onto a transcriptomic atlas of P56 cortical *Htr3a*-expressing interneurons (Tasic et al., 2018) (low-left inset), main tSNE displays only cells belonging to *Vip*-expressing clusters. Upper-left inset tSNE displays *Vip* logRPM RNA expression among *Htr3a*-expressing interneurons. Pie chart shows the percentage of P15 non-NGCs mapping to the different *Htr3a*-expressing IN subtypes (highlighted NGCs mapping to Vip-expressing subtypes, 78.8% at P15). Heatmap depicting cell type prediction results for P15 *Hmx3*;tdTOM-/*Htr3a*-GFP+ cells: decision confidence of the SVM classifier for each cell (columns) for each subtype (rows). **B.** Same as A, for non-NGC P30 cells. P30 nonNGCs map preferentially to *Vip*-expressing subtypes (77.4%).

Abbreviations: SVM, Support Vector Machines; tSNE, t-distributed stochastic neighbor embedding.

Molecular architecture of NGC type and subtypes

Cortical canonical NGC-type is a heterogeneous cell population comprised of two main subtypes transcriptionally different from other *Htr3a*-expressing INs and mainly populating ULs. They can be further segregated into subtypes according to their laminar positioning and molecular profiles. Therefore, we aimed to understand the molecular fingerprints of NGC cells as an unique entity compared to the different subtypes of NGCs and non-NGCs (Results figure 4A, 4B, 8A). We used cross-validated SVM modeling for ordinal regression and binary classification on single-cell transcriptomic data. An ordinal SVM model allowed to reconstruct a continuous postnatal pseudotime axis in which a subtype-balanced subset of adult cells from Tasic et al., 2018 was included, and binary SVM classifiers were used for discovering the time-conserved molecular architectures of CGE-derived non-NGCs, POA-derived NGCs, Dock5 and Lsp1 NGC subtypes. Both type and subtype classifiers were robustly discriminative, and the 300 top SVM genes were further analyzed for disentangling enriched biological pathways and gene families. Fold change range of values revealed a sharper gene signature for type compared to subtype contrasts (Results figure 4A, 4B). This finding is in line with a hierarchical consideration of IN diversity: IN subtype molecular signatures constitute a fine-grained granularity level where gradients of gene expression draw subtle but robust transcriptomic frontiers. Molecular architectures of IN types are, by far, more discriminative in terms of gene expression fold changes.

NGC canonical type contrast with other *Htr3a*-expressing cortical interneurons revealed the existence of a robust and time-conserved orthogonal combinatorial code of TF expression. While NGC molecular fingerprint is characterized by the expression of two members of the TOX TF family (*Tox2* and *Tox3*), non-NGC cells have an NPAS TF genetic code (*Npas2*, *Npas3*) (Results figure 4A). *Tox2* enrichment in NGCs was confirmed in P56 *Hmx3*-Cre::*Htr3a*-GFP;*Rosa26*-tdTOM$^{fl/fl}$ mice at the mRNA level using smFISH (Results figure 4A) as well as at the protein level (data not shown). *Tox2* differential expression proved robust, with an associated p-value below 0.0001. Aiming to clarify what characterizes the NGC type compared to other *Htr3a*-expressing INs, we performed gene ontology analysis for biological processes and gene family enrichment interrogation using the HGNC database (Results figure 5). Results indicate that NGCs, in contrast to other *Htr3a*-expressing INs, have an enriched expression of genes regulating synaptic release via vesicle exocytosis (HGNC superfamily), specifically synaptotagmins (*Syt1* and *Syt7*) and exocytosis regulating genes such as *Rims1* (Results figure 5A). This finding, together with their relative lower proportion of CAMs compared to non-NGCs, aligns with the description of NGCs as volumetric GABA releasers (Overstreet-Wadiche & McBain, 2015). Indeed, NGC-enriched synaptotagmins have been described as essential elements for fast and slow vesicle exocytosis (Bacaj et al., 2015).

NGC-subtype comparison highlighted a robust time-conserved graded gene expression complementarity. Notably, the top 2 SVM ranked genes were *Npy* and *Ndnf*, canonical markers for identifying cortical NGCs. A high SVM weight combined with a high fold change between NGC subtypes indicates that some level of expression of these two genes is present in both subtypes but they vary strongly in Dock5 and Lsp1 subtype cells. *Npy* is enriched in Lsp1 NGCs while *Ndnf* is enriched in Dock5 NGCs, which might explain the distinction within L1 INs between NGC and Canopy cell types made recently by (Schuman et al., 2019). Moreover, we discovered an enriched expression of *Rxfp1* within the Dock5 NGC population. Rxfp1 expression distributions was assessed *in situ* via smFISH in P56 *Hmx3*-Cre::*Htr3a*-GFP;*Rosa26*-tdTOM$^{fl/fl}$ cortices and matched the distribution of *Dock5*-expressing NGCs. This result validated *Rxfp1* as a suitable marker for Dock5 NGCs throughout postnatal development, hence allowing the identification of this subtype before *Dock5* expression itself at later postnatal stages (data not shown). *Rxfp1*, a gene encoding the Relaxin Family Receptor 1, is scarcely expressed in the neocortex and has recently been found to be expressed by some deep layer ENs as well (Gundlach et al., 2009). It is a peculiar receptor due to its unusual responsivity to the H1 relaxin peptide, recently described as involved in neocortical pain

processing (Abboud et al., 2021) . Gene-ontology analysis and HGNC enrichment showed that all HGNC super-families are represented in both NGC-subtypes, with a more considerable proportion of CAMs in Dock5 NGCs. Interestingly, we observed a differential enrichment on glutamate versus GABA receptor expression in NGC-subtypes: while Dock5 NGCs have an enriched expression of four glutamate ionotropic receptor subunits (*Grik1*, *Grik2*, *Grin3a* and *Grid1*), Lsp1 NGCs show a more robust expression of GABA type-A receptors (*Gabrd*, *Gabra5*), indicating their potential differential synaptic partners and roles in cortical microcircuits.

Altogether, these results demonstrate time-conserved robust molecular architectures of the NGC type and its subtypes, respectively characterized by sharper and more subtle gradients of gene expression. Unlike *Dock5* and *Lsp1* genes, which define NGC subtypes only from adulthood (data not shown), we provide here core constitutively expressed gene sets defining NGC type and subtypes across development, thus indicators of cell type identity definition and maintenance. Similarly, we found complementary orthogonal TF families discriminating INs at the type level. Indeed, NGC INs maintain through postnatal development the expression of two members of the TOX TFs family, which roles have been described in neural stem and progenitor cells during corticogenesis (Artegiani et al., 2015) but remain unexplored in INs. *Tox2* and *Tox3* emerge as potential IN type identity regulators or fate-specification factors since they are constitutively expressed by all NGC subtypes (Results figure 4A, 8) while largely absent in other *Htr3a*-expressing INs. Postnatally-conserved NGC-subtype gene expression signatures were also found and were gradual with few exceptions such as the Dock5 NGC-specific expression of the *Rxfp1* gene, indicating potential functional specificities of NGC subtypes.

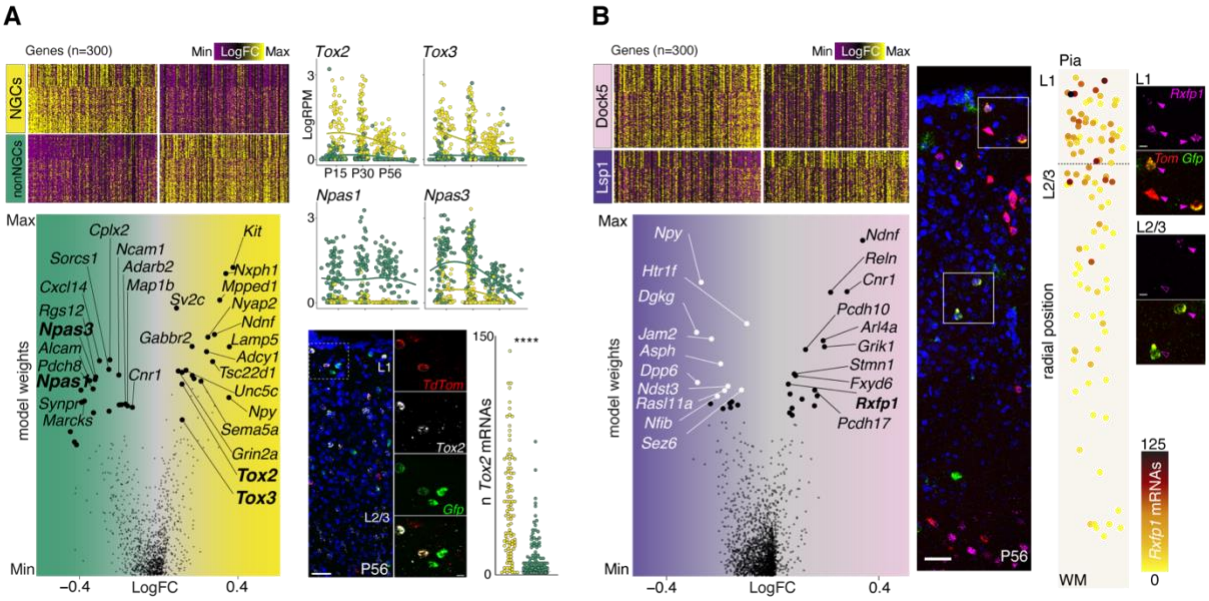

Results figure 4. Time-conserved molecular architecture of NGC type and subtypes.

A. Heatmap representing logRPM fold change (FC) in expression of the SVM-identified NGC vs non-NGC core set of time-conserved genes (columns) (magenta-black-yellow color gradient where yellow indicates high foldchange). Heatmap rows represent single cells ordered by SVM ordinal decision value (from P15 to P56). Scatter plot represents the ranking of genes by FC and SVM decision value. The names of 15 out of the most relevant genes for each type are detailed (green shading represents non-NGC genes while yellow shading represents NGC genes). Members of the two complementary TF families distinguishing NGCs vs non-NGCs are highlighted in bold text. Scatter plots illustrating gene expression through postnatal timepoint (SVM ordinal score) for the members of the complementary families of TFs distinguishing NGCs and non-NGCs. Loess function was fitted for representing time series expression and the levels of the gene expressed by each single cell (color-coding represents cell type: NGCs in yellow and non-NGCs in green). Low-magnification and high-magnification pictures representing smFISH experiment against *Tox2, Gfp and Tom* at P56 in *Hmx3*-Cre::*Htr3a*-GFP;Rosa26-tdTOM$^{fl/fl}$ mice cortices. Scatter plot represents the quantitative assessment of *Tox2* expression *in situ* for NGCs (yellow) and non-NGCs (green). Y-axis represents the number of mRNA molecules detected on single cell. A p-value of <0.0001 was obtained by comparing *Tox2* expression between the two populations. **B.** Heatmap representing logRPM FC in expression of the SVM-identified Lsp1- vs Dock5- subtype core set of time-conserved genes (columns) (magenta-black-yellow color gradient where yellow indicates high FC). Heatmap rows represent single cells as ordered by SVM ordinal decision value (from P15 to P56) and grouped by subtype (purple Lsp1-subtype and pink Dock5-subtype). Scatter plot represents the ranking of genes by FC and SVM decision value. The names of 15 out of the most relevant genes for each subtype are detailed (purple shading represents Lsp1-subtype genes while pink shading represents Dock5-subtype genes). *Rxfp1* gene is highlighted in bold text as it

was validated *in situ*. Low- and high magnification pictures representing smFISH experiment against *Rxfp1*, *Gfp* and *Tom* at P56 using *Hmx3*-Cre::*Htr3a*-GFP;*Rosa26*-tdTOM$^{fl/fl}$ mice cortices. Scatter plot illustrates in y-axis the radial position of the quantified cells and color-coding indicates the number of *Rxfp1* mRNA molecules detected on each single cell (yellow-brown-black color gradient where black indicates highest amount of mRNAs).

Scale bars: A, low-mag 50um; A, high-mag 10um; B, low-mag 25um; B, high-mag 10 um.

Abbreviations: FC, fold change; Min, minimum; Max, maximum.

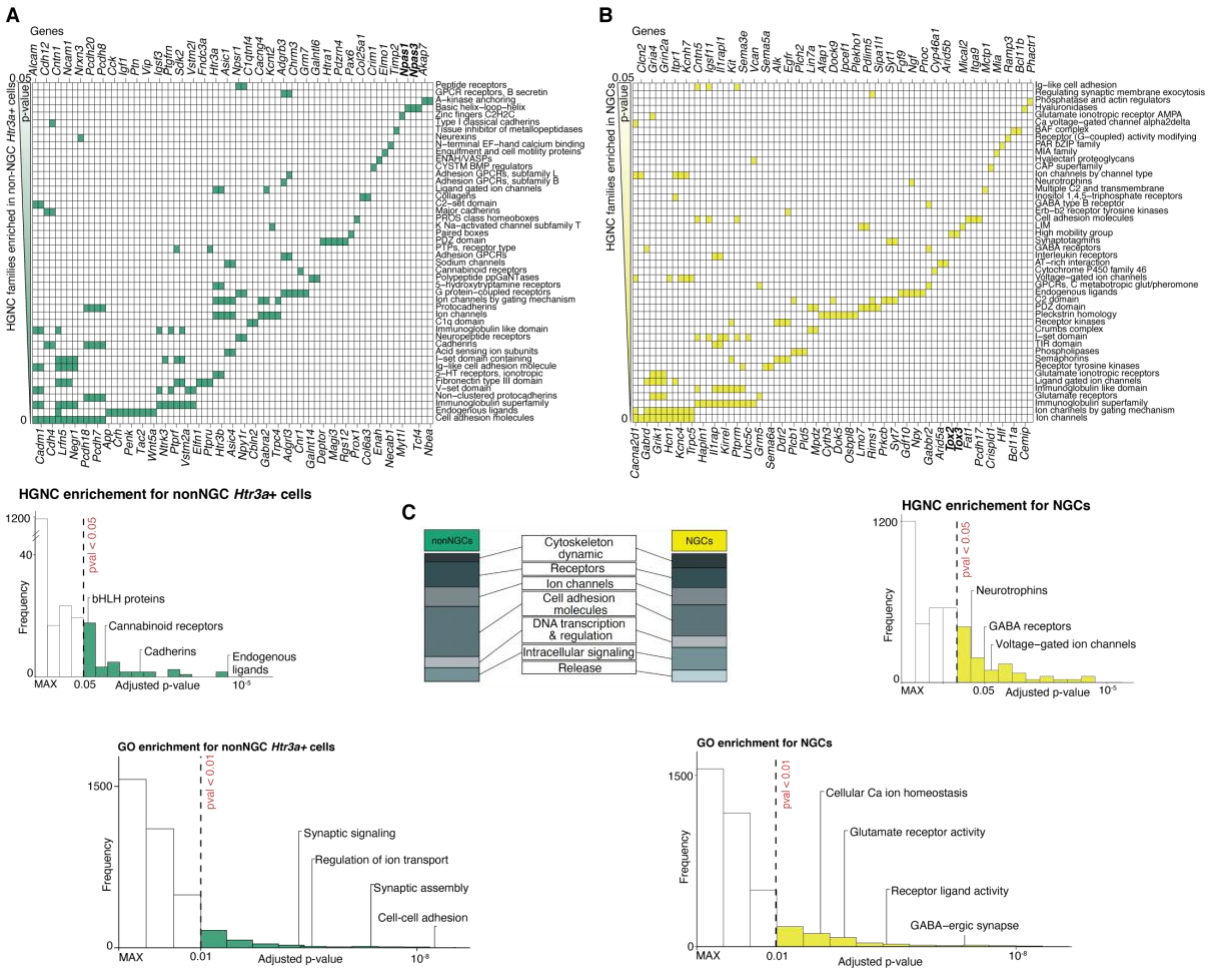

Results figure 5. Gene Enrichment Analysis on NGC vs non-NGC time-conserved molecular signatures.

A. Heatmap detailing results from HGNC enrichment on non-NGC SVM identified core genes (columns). Significantly enriched HGNC families are annotated in rows and heatmap filling shows HGNC term-to-gene association color-coded in shades of green representing p-value score (white-green gradient with low p-values on white side). Histograms displaying the frequency in which different HGNC or GO terms were defined across non-NGC SVM geneset according to their p-value. Significant

HGNC or GO term groups (histogram bins) are colored according to type color-coding (green). Dashed line indicates the p-value threshold of significance considered 0.05 for HGNC families and 0.01 for GO terms. **B.** Heatmap detailing results from HGNC enrichment on NGC SVM identified core genes (columns). Significantly enriched HGNC families are annotated in rows and heatmap filling shows HGNC term-to-gene association color-coded in shades of yellow representing p-value score (white-yellow gradient with low p-values in white side). Histograms displaying the frequency in which different HGNC or GO terms were represented across NGC SVM geneset according to their p-value. Significant HGNC or GO term groups (histogram bins) are colored according to type color-coding (yellow). Dashed line indicates the p-value threshold of significance considered 0.05 for HGNC families and 0.01 for GO terms. **C.** Barplot comparing relative proportions on major groups of HGNC gene families between NGC and non-NGC gene sets.

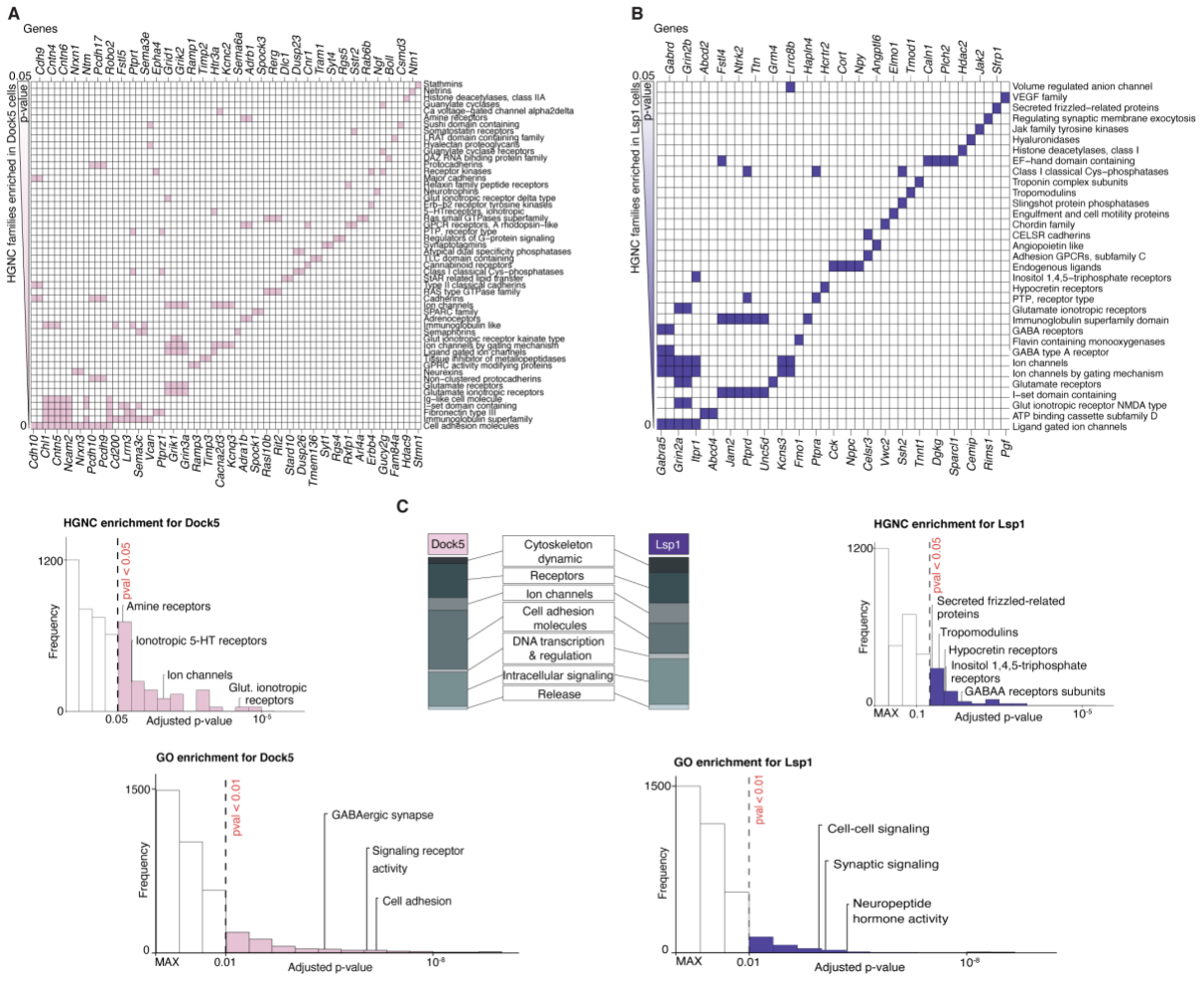

Results figure 6. Gene Enrichment Analysis on Dock5-subtype vs Lsp1-subtype time-conserved molecular signatures.

A. Heatmap detailing results from HGNC enrichment on Dock5-subtype SVM identified core genes (columns). Significantly enriched HGNC families are annotated in rows and heatmap filling shows

HGNC term-to-gene association color-coded in shades of pink representing p-value score (white-pink gradient with low p-values in white side). Histograms displaying the frequency in which different HGNC or GO terms were represented across Dock5-subtype SVM geneset according to their p-value. Significant HGNC or GO term groups (histogram bins) are colored according to type color-coding (pink). Dashed line indicates the p-value threshold of significance considered 0.05 for HGNC families and 0.01 for GO terms. **B.** Heatmap detailing results from HGNC enrichment on Lisp1-subtype SVM identified core genes (columns). Significantly enriched HGNC families are annotated in rows and heatmap filling shows HGNC term-to-gene association color-coded in shades of purple representing p-value score (white-purple gradient with low p-values in white side). Histograms displaying the frequency in which different HGNC or GO terms were represented across Lsp1-subtype SVM geneset according to their p-value. Significant HGNC or GO term groups (histogram bins) are colored according to type color-coding (purple). Dashed line indicates the p-value threshold of significance considered 0.05 for HGNC families and 0.01 for GO terms). **C.** Barplot comparing relative proportions on mayor groups of HGNC gene families between Dock5-subtype and Lsp1-subtype gene sets.

Functional and anatomical correlates of NGC-subtypes

NGC Dock5 and Lsp1 subtypes are characterized by differential laminar distributions and distinctive molecular architectures that get sustained through postnatal development. These findings indicate that NGC subtypes might be discrete functional types, not merely NGC state variations or transcriptomic granularity artifacts.

To test whether NGC subtypes are functionally different, we patched and RNA-sequenced (patch-seq) *Hmx3*;tdTOM+/*Htr3a*-GFP+ cells to investigate the electrophysiological properties of Dock5 and Lsp1 subtypes subtypes in ~P20 *Hmx3*-Cre::*Htr3a*-GFP;*Rosa26*-tdTOM$^{fl/fl}$ mice (Results figure 7, 8). The previously developed SVM binary model (Results figure 4) was applied to cells collected through patch-seq to predict their subtype identity. 47 out of 50 collected cells were confidently predicted to be either of the two subtypes and used for further analysis (Results figure 7A, 8A). Among 12 electrophysiological parameters assessed for each single cell (Results figure 8B), 8 were sufficient for segregating NGC subtypes in a PCA space: (Results figure 7B) after hyperpolarization potential (AHP) ($p<0.0001$), spike latency ($p<0.0001$), subthreshold depolarizing bump (STDB) ($p<0.001$), capacitance ($p<0.001$), spike frequency ($p<0.01$), R-input ($p<0.01$), membrane-Tau ($p<0.01$) and threshold potential ($p<0.01$) (Results figure 8C). This result, therefore, indicates the

existence of a functional specialization underlying NGC subtypes. PCA dimension 1 recapitulated the NGC-subtype segregating power of these parameters while PCA-2 represented the correlation of the different parameters between them irrespectively of cell type segregation (Results figure 7B, 8D). For instance, spike frequency and latency are positively correlated and are thus located in the top-left PCA space, while spike frequency and threshold are anti-correlated, explaining the opposite polarity of their PCA eigenvectors (Results figure 7A, 8D). These results confirm and extend the observations made by (Niquille et al., 2018) describing heterogeneity in NGCs regarding their AHP width and spike latency: Lsp1 NGCs had a significantly wider AHP that resulted highly correlated with spike latency. Dock5 NGCs, on the contrary, displayed a shallower AHP and showed a non-late-spiking behavior, typical of the recently called Canopy cells (Schuman et al., 2019) (Results figure 7A, 8C). In addition, they showed a characteristic STDB at sub-threshold current injection, absent in most Lsp1 NGCs. Dock5 NGCs display thus unique membrane potential oscillations that could underlie a role for UL NGCs in regulating cortical rhythmicity. Indeed, the presence of STDB was anti-correlated with cortical depth both in Dock5 and few Lsp1 cells (Results figure 7A, 8B), indicating that it is a characteristic of superficially located NGCs. Lsp1-specific features also varied linearly with cortical depth: deeper located Lsp1 NGCs showed even wider AHPs and spiked with higher latency (Results figure 7A, 8B). These results suggest that Dock5 and Lsp1 NGC subtypes might have distinct functional roles within cortical circuits.

We next aimed to discover whether specific molecular signatures underlie NGC differential functional profiles. First, we calculated correlation coefficients between SVM-identified NGC subtype molecular architectures and measured electrophysiological (e) parameters from patch-seq data (Results figure 7B). We observed that gene to e-parameter clusters exist (view heatmap): groups of genes behave as ensembles for explaining groups of e-parameters. For instance, 8 genes enriched in Dock5 NGCs were positively correlated with the 4 more distinctive electrophysiological parameters of this subtype while 10 Lsp1-subtype enriched genes were found to be correlated with the 3 best Lsp1 NGCs defining e-parameters. The existence of gene to e-parameter clusters suggests that these gene groups are together implicated in the observed NGC-subtypes functional specialization. Particularly, opposing families of presynaptic ligand-gated ion channels (LGICs), underlie the differential functional profiles of NGC subtypes: while *Grin3a* and *Grik1* gene expression correlated with Dock5 NGC e-features, *Gabra5* and *Gabrd* correlated with Lsp1 NGC physiology (Results figure 7B). These findings suggest that NGC subtypes could have differential synaptic-tunings and

microcircuit roles. Interestingly, GPCRs were only explanatory of Dock5 NGCs e-features. For instance, *Cnr1* protein product, which is specifically expressed in axon terminals, modulates GABA release (Freund et al., 2003). Another finding of particular interest was the link between *Ptprd* expression and Lsp1 physiology: notably, this receptor-like tyrosine phosphatase was pointed to as a synaptic specifier protein associated with an abundant presence of vesicular GABA transporter (*Slc32a1*) in cells expressing *Slitrk2* and *-3*, as it is the case in Lsp1 cells (data not shown) (Uhl & Martinez, 2019).

Altogether, these results strongly suggest that NGC subtypes are functionally and anatomically different. Indeed, their electrophysiological properties are sufficient for segregating Dock5- and Lsp1- subtypes, and subtle intrinsic physiology gradients are drawn within NGCs of the same subtype across cortical layers. In addition, marked molecular signatures underlie NGC subtype physiology by expressing a distinct set of synaptic receptors, suggesting that NGC subtypes might contact different synaptic partners and play different roles in cortical microcircuits. Moreover, we illustrated the gradients on electrophysiological properties distinguishing subtypes through laminar positioning, suggesting that NGC subtypes could be part of a specialization continuum. In line with this hypothesis, morphological reconstructions of the different NGC types across cortical layers (Results figure 8F) (Scala et al., 2021) confirmed anatomical subtype laminar differences.

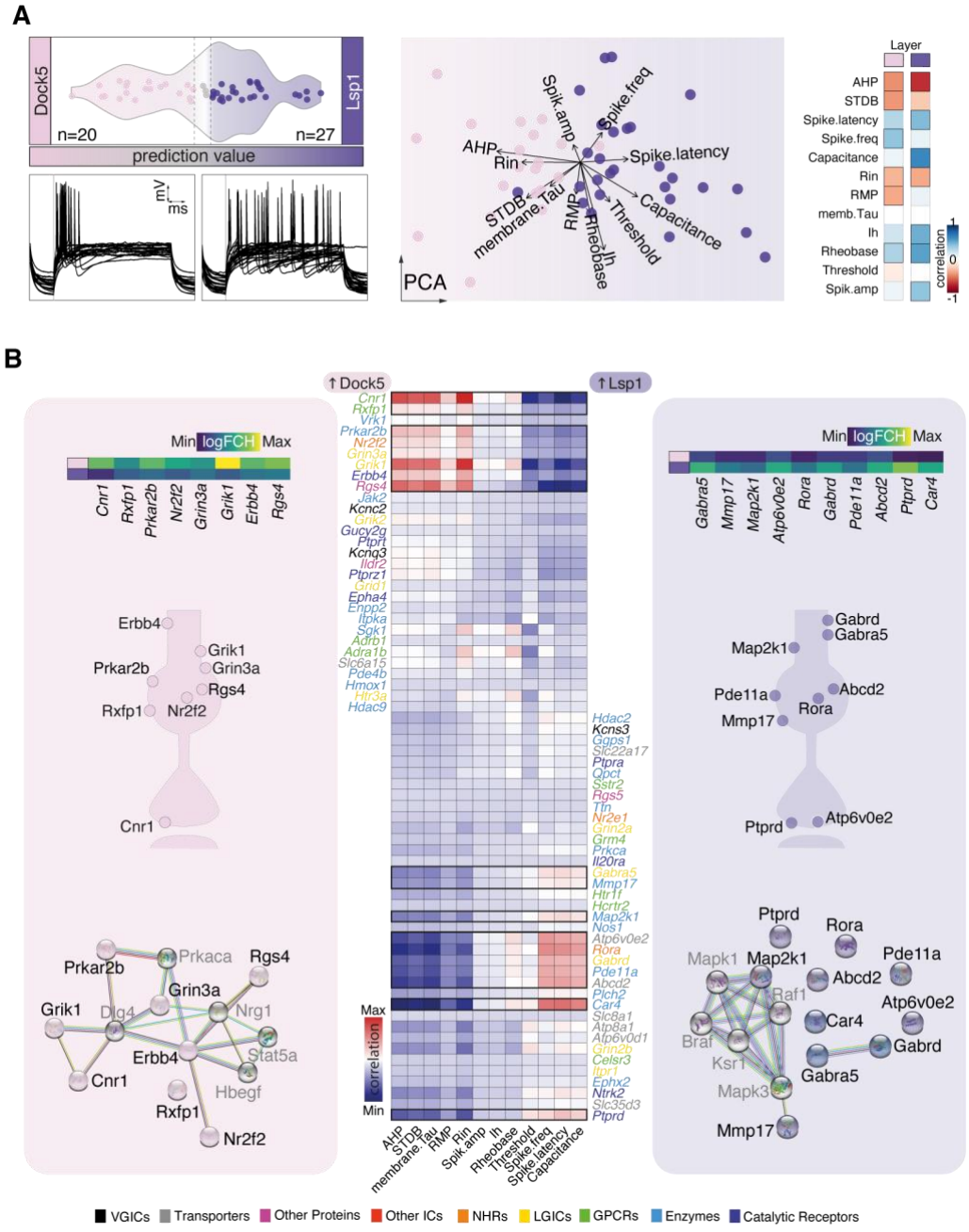

Results figure 7. Functional correlates of NGC-subtypes.

A. Violin plot representing SVM decision values for each NGC collected using patch-seq (*Hmx3*;tdTOM+/*Htr3a*-GFP+) color-coded by SVM NGC-subtype assignment (Dock5 NGC, pink (n=20); Lsp1 NGC, purple (n=27), non-assigned, grey (n=3). First-spike electrophysiological traces for each cell are represented and grouped by NGC-subtype. PCA plot calculated on measured electrophysiological features for each single cell and color-coded by NGC-subtype assigned to each cell and the gradient of Dock5-like features to Lsp1-like features that correlates with PC1 dimension. Heatmap of Pearson correlation coefficients depicting the overall relation between electrophysiological parameter values and cortical radial position of NGCs. **B.** Heatmap representing the correlation between

electrophysiological feature scores and gene expression patterns (SVM genes contained in IUPHAR database) on patch-sequenced single cells (correlation color-coding in gradient red-white-blue were red represents positive correlations and blue anticorrelations). Gene names depicted in y-axis-left were classified as Dock5-NGC-like and those in y-axis-left as Lsp1-NGC-like by SVM modeling. Gene-name color-coding represents gene categories as annotated in IUPHAR database. Highlighted rows on heatmap signal clusters of genes and e-features for each NGC-subtype. Pink and purple squared side panels contain a heatmap representing logFC values for electro-molecular cluster genes grouped by NGC-subtype, a schematic of a neuron synapse in which predicted gene localization is spotted and a STRING database protein network inference for electro-molecular gene clusters per NGC-subtype (pink side – Dock5 NGC associated; purple side – Lsp1 NGC associated).

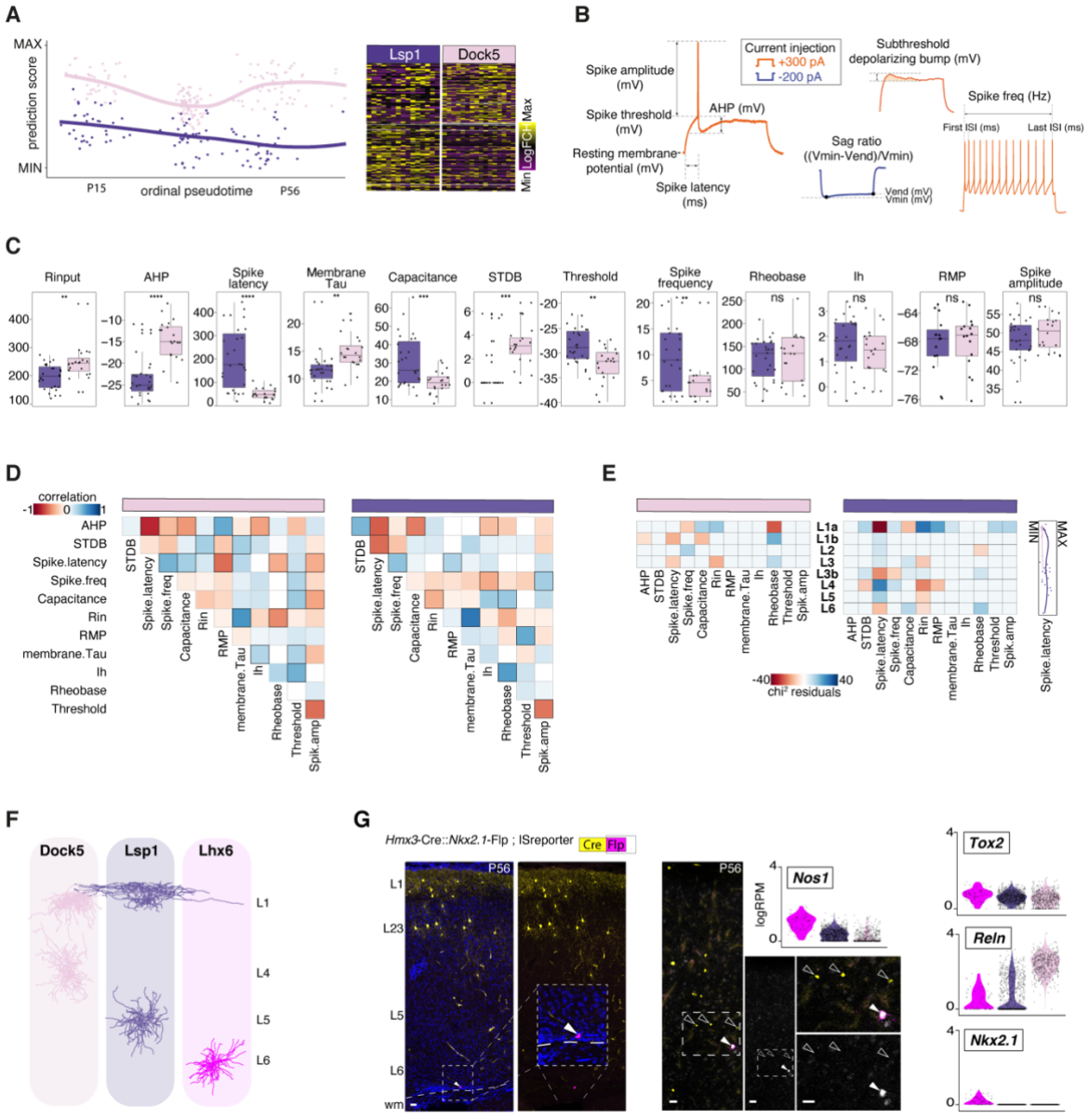

Results figure 8. Functional and anatomical correlates of NGC subtypes.

A. Scatter plot representing ordinal and sigmoid SVM scores for each NGC cell: x-axis represents ordinal pseudotime (left-most P15 and right-most P56) and x-axis sigmoid decision value. A loess fitted curve is represented for each NGC subtype across pseudotime. Color-coding represent NGC subtypes (Dock5, pink; Lsp1, purple). Heatmap illustrates the log FC value for each cell and SVM gene on patch-seq cells. **B.** Schematic representation of measured electrophysiological parameters in patch-seq protocol. **C.** Boxplots illustrating the scores for each electrophysiological parameter on each single cell split and color-coded by NGC subtype. Stars represent the p-values obtained when comparing NGC subtypes on each measured parameter. **D.** Pearson correlation heatmap between the different electrophysiological features within each NGC subtype (correlation color-coding gradient: brown-white-blue, brown anticorrelated; blue correlated). **E.** Chi-square residuals heatmap illustrating the relation between the cortical layer of the patched NGC compared to electrophysiological parameters (residuals color-coding gradient: brown-white-blue, brown anti-related; blue related). Scatter plot with NGC-subtype color-coding representing the radial position in the cortex of patched cells (y-axis) with respect to their spike latency values (x-axis) and loess fitted curves illustrate the variation of latency compared to cortical depth. **F.** Examples of morphological reconstructions for each NGC subtype across cortical layers (Scala et al., 2021). **G.** Pictures depicting examples of Lhx6 NGC subtype cells genetically fate-mapped using *Hmx3*-Cre::*Nkx2.1*-Flp;ISreporter mice and their nNOS protein expression. Violin plots representing log FC values for upregulated and downregulated genes in Lhx6 NGC subtype compared to other NGCs (color-coding represents NGC subtypes: Lhx6, dark pink; Lsp1, purple; Dock5, light pink (Tasic et al., 2018).

Scale bars: E, low and high-magnification 25 um.

NGC embryonic emergence and diversification

NGCs, a specialized and distinctive cell type in the neocortex with a common embryonic origin, are more heterogeneous than previously thought according to the four subtype determinants explored above: molecular, functional, synaptic and anatomic. Thus, NGCs can be considered a family of cell types. However, while many recent publications affirm that NGCs derive from the CGE (references), results obtained using genetic fate-mapping indicate that NGCs originate from the embryonic POA. Thus, we aimed to examine how NGC molecular identity and diversity emerge during embryonic development using single-cell transcriptomics in *Hmx3*-Cre::*Htr3a*-GFP;*Rosa26*-tdTOM$^{fl/fl}$ mice.

Embryonic post-mitotic NGCs can be found at E14.5 in the POA organized as a cluster of cells that defines a spatial microdomain for NGC generation (Results figure 10 F-H). Since the identification of NGCs relies on the combined expression of *Hmx3* and *Htr3a* postmitotically (Results figure 10C), identification of NGC progenitors for studying earlier NGC genesis is challenging. To overcome this limitation, we aimed to capture the entire NGC POA embryonic lineage using single-cell transcriptomics (Results figure 9A). Hence, we performed scRNA-seq covering different cellular population subsets at E14.5: 1) POA progenitors that underwent one cell cycle after Flash-Tag injection, 2) *Hmx3*;tdTOM+/*Htr3a*-GFP+ cells from *Hmx3*-Cre::*Htr3a*-GFP;*Rosa26*-tdTOM$^{fl/fl}$ mice and, 3) the entire cell populations from the POA and CGE germinal (Results figure 9A).

We first aimed at reconstructing an embryonic maturation axis from the three combined scRNA-seq datasets. To do so, we scored single cells according to their positions in a PCA-fitted principal curve built using variable genes common to POA and CGE datasets and which root was set based on *Nes* expression (Results figure 10A). This allowed us to identify a set of ~300 genes whose expression pattern explains early maturation across CGE and POA (Results figure 10A-D). Single-cell cell-cycle scoring and the pseudotime position of cells collected via Flash-Tag confirmed the biological correctness of this maturation score. Notably, the set of maturation genes identified overlaps with the ones described previously for MGE, CGE and LGE (Mayer et al., 2018), further revealing the existence of a pan-IN early maturation genetic program. Specifically, IN apical progenitors (APs) express genes such as *Nes* or *Hes5*, and intermediate progenitors switch on the expression of *Ccnd2* and *Top2a* among others. At the same time, cell-cycle exit and begimming of IN differentiation are characterized by the expression onset of genes of the *Dlx* family (Results figure 10D). This finding indicates the existence of common molecular programs for regulating IN-precursor development across all subpallial IN-generative regions.

We next aimed to investigate IN diversity in the embryonic POA and identify NGCs. Therefore, we integrated the three E14.5 POA transcriptomic datasets, resulting in an UMAP projection that greatly recapitulated the previously mentioned maturation score (Results figure 9A). We next applied clustering for partitioning the POA UMAP landscape into different cell populations. As expected by the UMAP representation of maturation, left-most clusters contain POA progenitors (light-grey, grey, light-blue and orange) while right-most clusters were formed by postmitotic cells (dark-red, dark-blue, green and magenta). Importantly, clustering

results revealed distinct TF codes expressed by each of these eight clusters (Results figure 9B), among which *Hmx3* was enriched in the blue postmitotic cluster (Results figure 10E) and which gene expression pattern indicates it is expressed transiently in early postmitotic cells. To identify NGCs among POA clusters, we assessed cluster enrichment of fate-mapped NGCs and found that the *Hmx3*-expressing cluster also shows the greatest proportion of NGCs (23%). We next established a gene set intersecting POA-expressed genes with postnatally-conserved NGC type SVM-genes to identify discrete single cells whose transcriptome resembles the most to postnatal NGCs (Results figure 4, 9C). The resulting NGC pseudogene (NGC geneset, n=88, Results figure 9C) was used for scoring embryonic POA cells at the 80th percentile and thus identifying the cells most likely belonging to the POA NGC lineage and spanning the entire E14.5 maturation axis (Results figure 9C) (n=376; 117 progenitors and 259 postmitotic cells).

NGC developmentally conserved gene set contained *Tox2,* which occupied a central position in the embryonic-to-postnatal Z-score landscape (Results figure 9C). Its sustained strong expression along NGC lifespan and its presence in all NGC subtypes suggest that *Tox2* might play a role in NGC cell fate specification. Moreover, *Tox2* IHC and FISH in embryonic POA at E14.5 revealed its colocalization with fate-mapped NGCs (~80%) and its overarching presence among POA progenitors, suggesting it could be a pan-POA marker. *Tox2* expression was completely absent in the embryonic CGE, further rejecting the hypothesis of NGCs to be CGE-born (Results figure 10G). Importantly, we identified a set of 88 NGC core genes, constitutively expressed in NGCs although at variable levels. Enrichment analysis on this gene set (https://version-11-5.string-db.org/cgi/network?networkId=bH5G8ut1eM6o) highlighted cellular processes such as neurogenesis, differentiation, migration, and axonogenesis, indicating that genes there contained might underlie a wide range of NGC biological processes at different developmental stages. For instance, one of these genes is *Reln*, encoding for REELIN, a critical secreted molecule involved in most of the highlighted processes. This finding opens the door for gene-functional interrogations accounting for their dynamism through development within a restricted cell type.

Having elucidated putative NGC lineage cells at E14.5 in the embryonic POA, we next ought to investigate whether NGC subtype heterogeneity can be identified embryonically and to validate the inferred lineage. To do so, we used the previously characterized postnatal NGC datasets together with the subset of adult Tasic et al., 2018 NGCs, embryonic predicted NGCs and another third-party set of data: the STICR (scRNA-seq-compatible tracer for identifying clonal relationships) postnatal lineage tracing dataset from Bandler et a., 2021. The SVM NGC-

subtypes geneset was used to integrate these datasets and label-transfer NGC-subtype categories (Results figure 9D) both to Bandler STICR single cells and embryonic NGC lineage POA cells. When visualized in the integration UMAP, driven by cell identity because of using postnatal NGCs as reference, NGC subtypes resulted clearly segregated along the UMAP2 dimension. However, POA embryonic integration UMAP space, driven by cell maturation, displayed NGCs dispersed all along the UMAP1 and 2 dimensions. In order to disentangle the molecular determinants of NGC subtypes embryonically, we regressed out maturation and cell cycle to calculate differentially expressed genes between Dock5-NGC and Lsp1-NGC embryonically predicted cells (Results figure 9E). The resulting DEG list showed enriched nuclear or cytoskeletal predicted localizations (https://version-11-5.string-db.org/cgi/network?networkId=bovKPVZF0I50). Of particular interest was to discover an NGC subtype complementary gene expression enrichment of the Eph receptors *Epha4* (Dock5-NGCs) and *Epha3* (Lsp1-NGCs), which are implicated in the selection of alternative migratory routes by developing INs (Rudolph et al., 2010; Steinecke et al., 2014; Zimmer et al., 2011). In support of this hypothesis, we found migrating NGCs taking a path through both the dorsal and the superficial migratory streams (Results figure 10F).

Here exposed transcriptomic interrogation of embryonic NGC type and subtype emergence pointed to the generation of both NGC subtypes simultaneously in space and time. Given the well know space-time interplay occurring in neurogenesis, we next interrogated whether time dynamics may exist in NGC subtype generation. To do so, we explored the lineage reconstructions traced by Bandler et al., 2021, with a view on NGC subtype birth-dating (Results figure 9D). Results indicated that NGC subtypes are not homogeneously generated throughout embryonic development: we observed the existence of a time gradient for subtype generation similar to the one reported for MGE SST and PV cell type genesis (Lim et al., 2018). Specifically, Lsp1-NGC neurogenesis starts first (already at E10) and only at later time points, from E13, both NGC subtypes (Dock5 and Lsp1) are generated simultaneously (Results figure 9D). This finding aligns with the outside-in hypothesis of neurogenesis: cell types populating deep layers are earlier born as compared to those populating upper cortical layers. The very scarce cortical Lhx6 NGC subtype was also hard to track using STICR: such a low number of cells do not allow to conclude their preferential birthdate. Thus, we aimed at investigating whether we can find Lhx6 NGC precursors in the embryonic POA and if a restricted spatial subdomain exists for them (Results figure 10H). Results indicate that, indeed, NGC Lhx6 type precursors can be found in the embryonic POA and that their spatial distribution follows a

microdomain logic (not randomly located across the POA) that apparently partially overlaps with the broader NGC microdomain comprising all subtypes.

Taken together, the findings exposed here indicate that embryonic NGCs harbor molecular elements in common with postnatal NGCs, enabling us to distinguish them both at the type and subtype level. Interrogating NGC diversity using STICR lineage-tracing (prediction) indicates that both NGC subtypes are generated at a single Spatio-temporal point: E14.5 POA simultaneously produces Dock5 and Lsp1 NGCs. The NGC family, sharing a common origin and genetic background, can be defined using a unique set of 88 genes whose expression is conserved through development (although implicated in different biological processes at different points of maturation). Remarkably, *Tox2* TF stands out as a member of the NGC gene set, given its potential role in regulating NGC fate acquisition and maintenance.

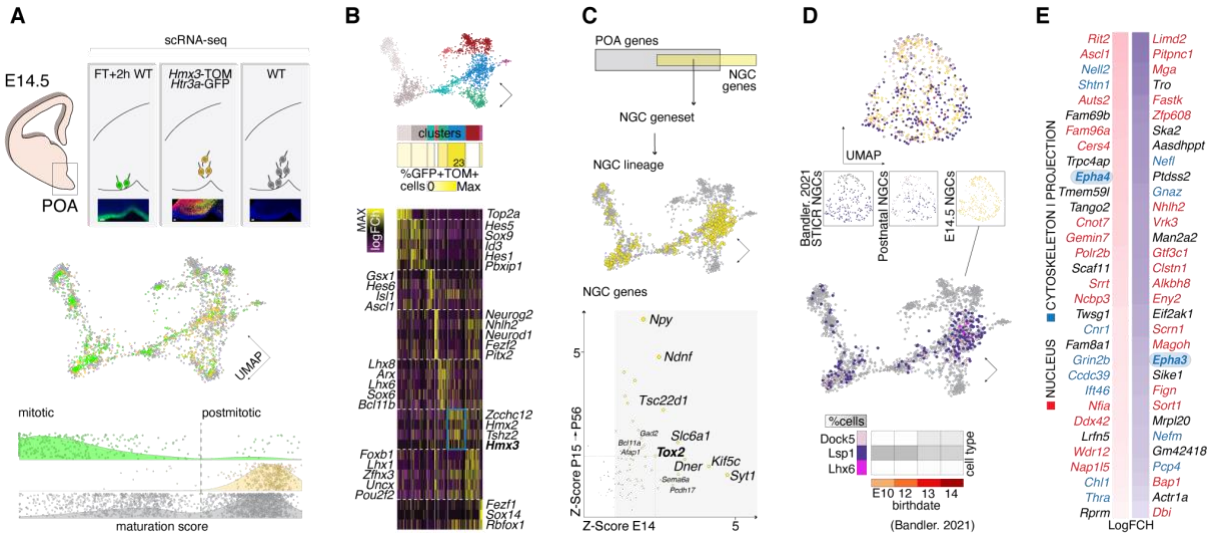

Results figure 9. Embryonic characterization of the NGC type and subtypes.

A. Schematic illustrating RNA-seq captures performed at E14.5 in POA and microscopy images of dissected regions for each protocol. Three independent datasets were generated: FlashTag + 2h (green), NGC fate-mapping (yellow) and WT (grey). UMAP projection of POA E14.5 dataset integration color-coded by capture type. Density plots depicting cell distribution along their maturation trajectory (PCA-pseudotime), color-coded and split by dataset. **B.** UMAP plot color-coded by cluster. Heatmap in shades of yellow indicates the percentage of fate-mapped NGCs populating each cluster (cell number differences were balanced). Heatmap depicting the gene expression log fold change for the main TFs enriched on each cluster (yellow indicates high fold-change). **C.** Schematic illustrating the feature selection strategy for defining the NGC geneset and lineage (intersection between POA variable genes,

grey; and NGC genes identified postnatally, yellow). UMAP plot highlighting in yellow the cells that were labeled as belonging to the NGC lineage. Scatter plot illustrating genes belonging to the NGC geneset, size and color intensity (grey-yellow scale) indicate the strength of the gene-expression log fold change value. X and y axis denote log fold change value; embryonic and postnatal respectively. **D.** UMAP plot illustrating integration results for three datasets: bandler, 2021 STICR, postnatal NGCs and embryonic NGCs. Shape/color-coding: pink circles, bandler Dock5; purple circles, bandler Lsp1; dark pink circles, bandler Lhx6; pink squares, postnatal Dock5 NGCs; purple squares, postnatal Lsp1 NGCs; yellow circles, embryonic NGCs. POA UMAP highlighting E14 cells belonging to the NGC lineage color-coded by label-transfer on bandler, 2021 NGC subtypes (pink-Dock5, purple-Lsp1;dark pink-Lhx6). Heatmap illustrating the percentage of Bandler, 2021 cells by NGC subtype and birthdate (color-filling white-grey gradient). **E.** Heatmap depicting gene-expression fold change for the most differentially expressed genes between NGC subtypes at E14.5 (color-filling gradient of pink for Dock5 cells and gradient of purple for Lsp1 cells). Gene names are color-coded by their predicted localization at the nucleus (red) or process / growth cone (blue).

Scale bars: A, 25um.

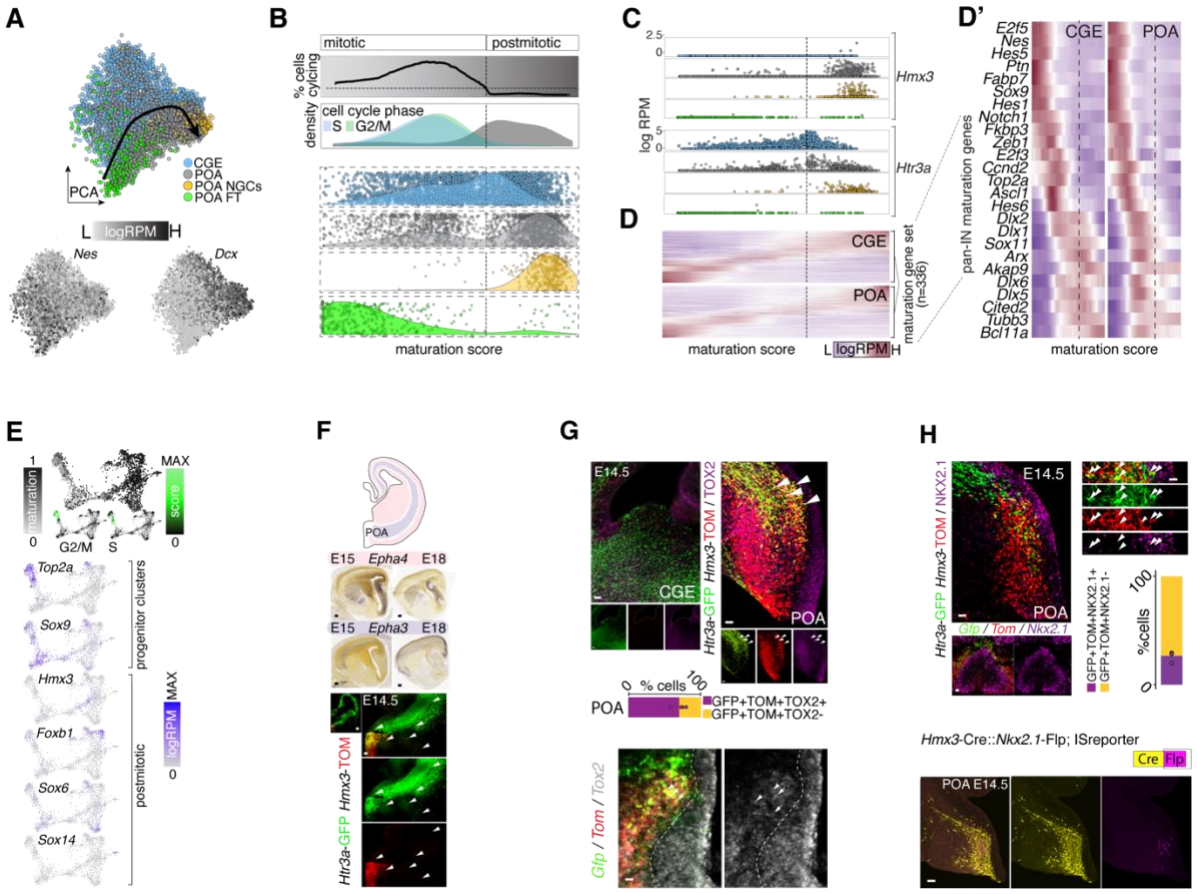

Results figure 10. Embryonic NGC maturation and characterization.

A. PCA plots displaying cells from all collected E14.5 scRNA-seq datasets (CGE, blue; POA WT, grey; POA FT, green; POA NGCs, yellow), the pseudotime curve and the expression of two time-genes: *Nes* and *Dcx* (logRPM white-grey gradient). **B.** Scatter and density plots illustrating the reconstructed E14.5 maturation score according to the percentage of cycling cells and their cycle phase at each moment in development (S phase, blue; G2/M phases green). Jittered density plots showing the position in maturation of each cell color-coded and slit by dataset (CGE, blue; POA WT, grey; POA FT, green; POA NGCs, yellow). **C.** Scatter plots showing the expression of the genes used to fate-map NGCs across maturation score and dataset. **D.** Heatmap illustrating the set of genes used for reconstructing the POA-CGE maturation trajectory (n=336) ordered by their peak expression in pseudotime and color-coded by their logRPM value (violet-white-brown gradient). **D'** Highmag of heatmap depicted in **D** - the subset of genes highlighted by Mayer et al., 2018 as maturation genes in MGE and LGE (pan-interneuron maturation genes). **E.** POA-dataset integration UMAP color-coded by: maturation score (white-black gradient), cell cycle score (black-green gradient), logRPM expression of cluster markers (grey-blue gradient). Marker-belonging to progenitor or postmitotic clusters is detailed. **F.** Schematic of putative migratory routes used by cells expressing Eph receptors A4 and A3. Allen Brain Atlas ISH pictures of sagittal E15 and E18 brain sections stained against Epha4 and Epha4 mRNAs. High magnification and low magnification pictures of one E14.5 coronal brain section from the *Htr3a*-GFP; *Hmx3*-tdTOM mouse line. White arrowheads signal migrating NGC spreading across migratory streams. **G.** *Htr3a*-GFP; *Hmx3*-tdTOM E14.5 coronal sections at the level of CGE and POA immunostained against TOX2 (magenta). Barplot depicts in magenta the percentage of POA NGCs (GFP+TOM+) expressing TOX2 (~80%) (TOX2- NGC fraction shown in yellow). FISH E14.5 coronal section illustrating the *Tox2* mRNA expression (grey) among postmitotic NGCs in POA. **H.** *Htr3a*-GFP; *Hmx3*-tdTOM E14.5 coronal section illustrating POA NGCs and NKX2.1 expression (magenta). Barplot depicts in magenta the percentage of NKX2.1+GFP+TOM+ cells found at E14.5 in POA (~20%) while NKX2.1- NGCs fraction is displayed in yellow. FISH E14.5 coronal at the level of POA displaying the complementary expression of *Nkx2.1* mRNA (magenta) in the space microdomain where NGC postmitotic cells are located. POA 14.5 coronal section from the *Hmx3*-Cre;*Nkx2.1*-Flp;ISreporter mouse line indicating the microdomain of *Hmx3* & *Nkx2.1* mixed lineage (Lamp5 Lhx6 NGCs) (*Nkx2.1*-Flp, magenta; *Hmx3*-Cre, yellow).

Scale bars: F, Low mag: 100um, High mag: 25um; G, 25um, 10um FISH; H, 25um, low mag 15um.

Tox2 plays a critical role in NGC development

Investigating NGCs through development led to the discovery of their time-conserved expression of *Tox2* and *Tox3*, both NGC type-specific and members of TOX family of TFs. Absent at the embryonic CGE and in postnatal cortical non-NGC *Htr3a*+ interneurons, *Tox2* expression (stronger embryonically in comparison with *Tox3*) spans the entire POA VZ surface at E14.5, is also observable in early postmitotic NGCs (both at mRNA and protein levels) (Results figure 10G) and sustains its expression until adulthood (Results figure 4A). Although *Tox2* role in brain development is undescribed, abundant evidence exists in other biological systems pointing to its crucial role for cellular development, regulation of chromatin accessibility and transcription (Aliahmad et al., 2011; Minton, 2020; W. Xu et al., 2019).

To better understand the role that *Tox2* plays in NGC development and whether it could be implicated in their fate acquisition or maintenance, we used *in-utero* electroporation for down-regulating it in POA E14.5 progenitors (Results figure 11B). For this purpose, we delivered a CRISPR-Cas9-GFP (sg*Tox2*GFP) plasmid containing three single guidance sequences against *Tox2* (Results figure 12A), co-electroporated with a brighter tdTOM-encoding plasmid. This last, when delivered alone, was used as control.

We first assessed the efficacy of the sg*Tox2*GFP plasmid on a sub-population of lower-layer cortical neurons endogenously expressing *Tox2* (Results figure 11A) with respect to control tdTOM cells. To do so, we electroporated the dorsal pallium of E12.5 CD1 embryos and analyzed the results at P10. We observed a 65% decrease in TOX2 protein presence among lower layers sg*Tox2*GFP+ electroporated excitatory cells at P10 compared to their control counterparts (tdTOM+sg*Tox2*GFP-), confirming the efficacy of the loss-of-function approach (Results figure 11A).

We then electroporated the sg*Tox2*GFP construct in the POA at E14.5 and, at P10, we observed a complete depletion of NGCs in the neocortex (Results figure 11B). In addition, alterations in cell distribution in the hypothalamus were noticeable by their aberrant periventricular accumulation (Result figure 11C). These results indicate that *Tox2* embryonic down-regulation

results in differential levels of phenotypic alteration depending on the targeted cell type: NGC proper development gets completely compromised while hypothalamic POA-born cell populations display alterations in their positioning.

To understand whether cell death could contribute to the observed phenotype, we examined sg*Tox*GFP electroporated brains at E16.5, finding a proportion of POA-derived cells expressing CASP3. To rule out if the CRISPR manipulation could mediate these apoptotic events, we examined hippocampal off-targeted precursors (endogenously lacking *Tox2* expression): no CASP3+ cells were observed, indicating that caspase3 activation is not merely due to CRISPR-induced apoptosis (Results figure 12C). The presence of CASP3+ cells exclusively in POA suggests that *Tox2*-expression is required for the survival of embryonic POA-derived cell populations.

On the other hand, when only the tdTOM plasmid (control) was electroporated in the POA at E14.5, NGCs maturated appropriately and settled in the neocortex expressing TOX2+ (Results figure 11B, 12B). Interestingly, tdTOM+ electroporated cortical NGCs were found in diverse cortical areas and across layers (Results figure 12B), demonstrating that E14.5 POA-born NGCs migrate dispersing across functional neocortical borders. Moreover, cortical tdTOM NGCs morphological reconstruction and cell type prediction (by morphology feature representation using as reference Scala et al., 2021 reconstructions) confirmed their NGC identity and indicated their heterogeneity (Results figure 12B). Thus, POA generates at E14.5 the three subtypes of NGCs simultaneously as predicted using STICR Bandler, 2021 dataset (Results figure 9D). NGC subtype diversity can be generated simultaneously in space and time, emerging from a shared pool of progenitors.

Altogether, this piece of data provides further evidence about the POA origin of cortical NGCs, since targeting POA progenitors at E14.5 via *in-utero* electroporation resulted in the labeling of cortical NGCs. Moreover, these results prove that the POA, at E14.5, can simultaneously generate several subtypes of NGCs, as evidenced by their different morphologies and laminar distributions. Finally, CRISPR-mediated down-regulation of *Tox2* in NGC progenitors resulted

in a severe disturbance of their maturation/specification, since no electroporated NGC was ever observed in the cortex.

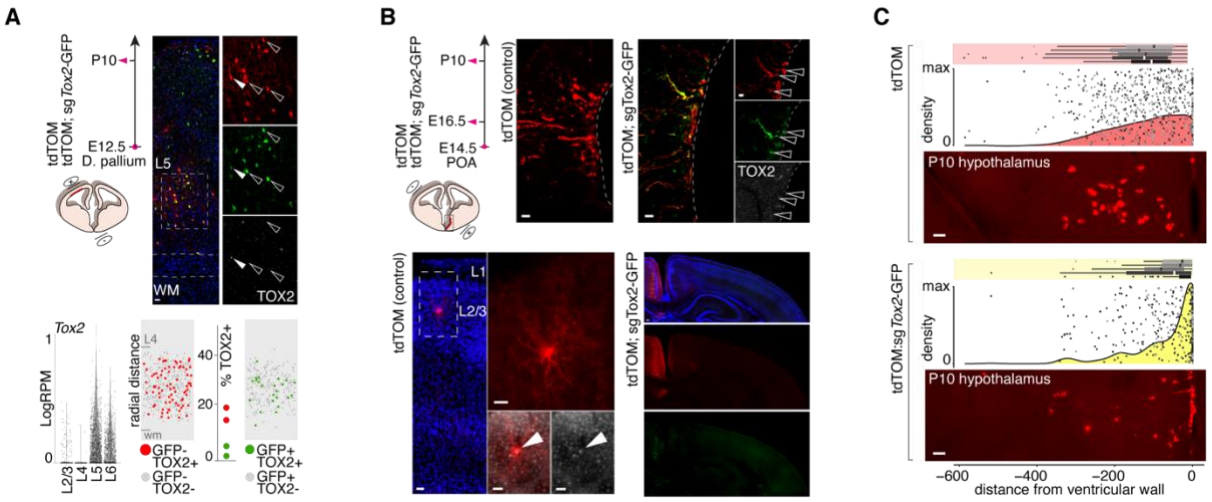

Results figure 11. *Tox2* plays a critical role in NGC development. A. Schema illustrating *in utero electroporation* experimental strategy and analysis pipeline for downregulating *Tox2* in dorsal pallium at E12.5 (phenotype analyzed at P10). Violin plot depicting *Tox2* LogRPM RNA-expression on adult excitatory neurons by cortical layer. High- and Low-magnification pictures of electroporation results at P10: excitatory neurons in L5 and TOX2 protein expression (arrowheads:GFP+TOM+TOX2, empty arrowheads:GFP+TOM+TOX2-). Quantification results of sg*Tox2*GFP electroporation in dorsal pallium: scatter plot depicting the radial cortical position of analyzed cells colored by their expression of TOX2 (grey, absence of TOX2 in either experimental condition; red, TOX2+ in tdTOM+; green, TOX2+ in tdTOM+;sg*Tox2*GFP+ cells). Dot plot displays the % of electroporated cells expressing TOX2 depending on the experimental condition: tdTOM (control) or tdTOM;sg*Tox2*GFP (split by biological replicates). **B.** Schema illustrating illustrating *in utero electroporation* experimental strategy and analysis pipeline for down-regulating *Tox2* in POA cells at E14.5 (phenotype analyzed at E16.5 and P10). Low and high mag illustrations of electroporation results at E16.5 and P10 (left: tdTOM; right: tdTOM;sg*Tox2*GFP). **C.** Box plots, density plots and pictures of the P10 hypothalamus following *in-utero* electroporation (top: tdTOM; bottom: tdTOM;sg*Tox2*GFP) illustrating the altered cell distribution patterns observed following *Tox2* downregulation.

Scale bars: A 25um, B-E16.5 low mag 10um, B-E16.5 hig hmag 10um, B-P10 low mag 50um, B-P10 high mag 1-2 20um, B-P10 hemisphere 50um, C 25um.

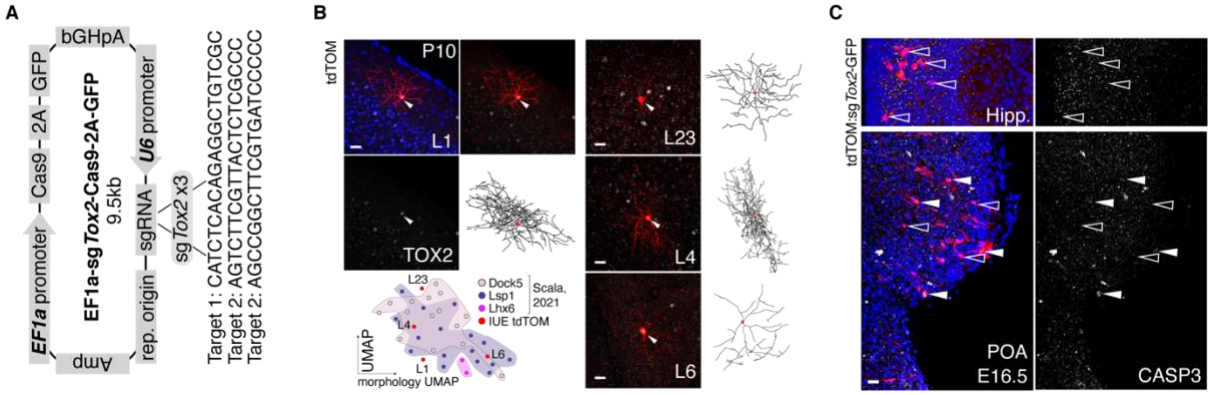

Results figure 12. Characterization of *in-utero* POA electroporation results. **A.** Schematic illustrating the design of the sg*Tox2*-GFP plasmid containing 3 single guidance sequences. **B.** Morphological reconstructions of control-electroporated (tdTOM) NGCs at P10 on different cortical layers (L1, L23, L4, L6), the expression of TOX2 (grey) is detailed on stack or split. Arrowhead indicates the localization of TOX2 in NGC nucleus. UMAP built on morphology feature extraction showing NGCs reconstructed from control electroporation experiments and NGCs from Scala et al., 2021. **C.** Low mag pictures of CASP3 expression on POA and hippocampus at E16.5, two days after sg*Tox2*GFP electroporation. Arrowheads indicate the presence of CASP3, while empty arrowheads mark its absence.

Scalebars: B 25um, C-E16.5 low mags 10um, B-E16.5 high mags 10um, B-P10 low mags 50um, B-P10 high mags 1-2 20um, B-P10 hemisphere 50um, C 25um. Abbreviations: Hipp, hippocampus.

Discussion and conclusions

Recent years witnessed an unprecedented revolution in the understanding of cell type diversity in the mature neocortex thanks to the advances made in single-cell transcriptomics (Tasic et al., 2018). However, despite this extensive progress, understanding IN diversity from a developmental point of view remains an open challenge. For example, when, where and how is each IN subtype is generated?

The lack of genetic fate-mapping tools for targeting specific IN populations is a significant constraint. Simultaneously, the vague comprehension of developmental IN emergence we count with prevents the design of genetic tools able to label early enough in maturation-specific IN subtypes or, at least, families. Recently developed single-cell lineage tracing techniques compatible with postnatal transcriptomic mapping started shedding light on the mysterious clonal relationships between interneurons, proving to be a complex puzzle where different adult cell types can originate from the same progenitor pool (Bandler et al., 2022).

Here, embracing the integrative conception of IN diversity emergence as a tale of space and time, we restricted the question to a specific cell type: NGCs. Why NGCs? Firstly, a genetic fate-mapping tool was recently described to follow these cells from their embryonic origins to their settlement in cortical microcircuits (Niquille et al., 2018). Secondly, they were described as POA born, a very restricted spatial location in the ventral telencephalon, which is thought not to generate other neocortical IN cell types.

Using genetic fate-mapping combined to single cell transcriptomics, we were able to demonstrate that the NGC type is indeed a family composed of three subtypes that are markedly different based on of their molecular architecture, electrophysiological profiles (function), laminar distribution, and morphology: two major ones populating mainly ULs (Dock5 and Lsp1) and a very scarce subtype in the neocortex that resides in DLs (Lhx6).

- Dock5 NGCs, which express the *Rxfp1* in a very specific manner, are enriched in *Ndnf* expression (although Lsp1 NGC cells express it faintly) and have a higher proportion

of genes involved in cell adhesion as well as glutamate ionotropic receptors (*Grik1, Grik2*, *Grin3a*, and *Grid1*). Functionally, they are non-late-spiking INs with a very shallow AHP (compared to Lsp1 NGCs) and a marked STDB. Several transcriptomic correlates were found to this electrophysiological profile, including *Grin3a*, *Grik1* and *Cnr1*. Layer positioning of Dock5 NGCs in L1 versus non-L1 subgroups revealed markedly different morphologies (horizontally elongated and oval, respectively) and subtle differences in specific electrophysiological parameters (e.g., rheobase). Late born compared to Lsp1s NGCs, Dock5 cells start to be produced in the POA around E13. During their precursor state, they express the receptor *Epha4* strongly in contrast to Lps1 NGCs, preparing them for the choice of a migratory route.

- Lsp1 NGCs, are enriched in *Npy* expression (compared to Dock5 cells) and display a higher proportion of GABA type A receptors (*Gabrd*, *Gabra5*). In addition, they are late-spiking cells displaying a wide AHP, electrophysiological features correlated with their molecular fingerprints: GABA receptors and *Ptprd*/*Slc32a2*, implicated in vesicular GABA processing. Contrary to Dock5 NGCs, Lsp1 cells are preferentially located outside L1 with a marked preference for L23 but they can be found along radial depth. As it is the case of Dock5 NGCs, Lsp1 electrophysiological patterns and morphology profiles varied greatly depending on their layer positioning: L1 Lsp1 cells were horizontal elongated (with an axonal arbor wider than the Dock5 one and located in the upper-most L1 portion, coinciding with Schuman description of Canopy cells, (Schuman et al., 2019)), and their latency to spike was closer to the one typical for a Dock5 cell. However, non-L1 Lsp1 displayed an oval morphology, and the deeper they were positioned in the cortex, the more pronounced was their AHP and late-spiking profile, and the bigger their cell body. Lsp1 NGCs start to be produced in the POA at least two embryonic days before Dock5 NGCs and were co-produced from the same progenitor pool from E13 on. At precursor stages, Lsp1 NGCs revealed an *Epha3* enrichment that contrasted with respect to the *Epha4* enrichment of Dock5 cells at the same maturation stage.

- Lhx6 NGCs, very scarcely present in the neocortex and typically populating the deepest layers, display an enriched expression of *Nos1* and is the only postnatal cell type in the cortex maintaining the expression of *Nkx2.1* until adulthood. At E14.5, Lhx6 NGC postmitotic cells can be found in the POA, in a spatial microdomain overlapping with

the generative niche for other NGC subtypes. Lhx6 NGC morphology is similar to Lsp1 morphology, but their axonal arborizations are less rich.

All NGC subtypes can be labeled using the *Hmx3*-Cre mouse line and performing *in-utero* electroporation at E14.5. These findings indicate that all NGC subtypes are born at the embryonic POA in, at least partially overlapping, spatio-temporal microdomains and thus likely originate from a shared progenitor pool.

NGC family (composed of the three aforementioned subtypes) can be distinguished clearly from CGE-derived cortical INs, further indicating that their molecular programs are highly divergent. In this regard, we found complementary orthogonal codes of TFs expressed in POA-born versus CGE-born cortical INs: NPAS family of TFs characterizes INs derived from the CGE while TOX family of TF are a signature feature from POA-derived INs. Furthermore, the three subtypes of NGCs express *Tox2* all along their maturation, from the progenitor stage to adulthood (at a relatively stable expression level as indicated by its conserved Z-Score).

To elucidate the importance of conserved codes of TF for IN fate specification and maintenance, we demonstrated through *in-utero*-electroporation that downregulating *Tox2* in POA progenitors at E14.5 leads to the failure of NGC cells to develop properly. This finding indicates that *Tox2* expression in NGCs is critical for their development.

The findings described here are of significant relevance for understanding how IN diversity is generated through development and for confirming the biological relevance of cell-type transcriptomic taxonomies. In line with previous efforts for deciphering IN diversity, here we dig deep into one of the most understudied IN types from the developmental point of view, and we combine different dimensions of IN characterization that provide a resolution into NGC diversification process never achieved before.

Previous literature eluded each NGC subtype treating them as fundamentally different cell types. However, their common *Hmx3* lineage and spatio-temporal origins demonstrate that NGC subtypes are members of the same family of INs. Specifically, Schuman et al., 2019 postulated the distinction of L1 Canopy cells and L1 NGCs, corresponding to Dock5 and Lsp1 NGC subtypes, respectively. Niquille et al., 2018, aware of the POA *Hmx3* lineage, described the existence of 1A and 1B NGCs, Lsp1s, and Dock5s, respectively. More recently, Valero et

al., 2021, reported the presence of a group of NGC cells populating deep neocortical layers expressing *Id2* and *Nkx2.1*, corresponding to the here-called Lhx6 NGC subtype. Furthermore, NGCs with a similar molecular profile to Lhx6 NGCs were previously described as a quite prominent IN population in the hippocampus (Ludovic Tricoire et al., 2010).

Recent literature expanded the study of cell diversity beyond the transcriptomic dimension by producing single cell atlases that cover methylome, chromatin accessibility, electrophysiological and morphological profiles.

Liu et al., 2021 analyzed adult cortical cell diversity using single-cell DNA methylation to document existent epigenomic profiles. They pointed to the existence of two Lamp5 subtypes (m-types) in which methylation signature genes significantly overlapped with the gene expression signatures here reconstructed with the Dock5-Lsp1 SVM model (Results figure 4B) (Liu et al., 2021): Lamp5 Dock5 and Lamp5 Grk5. Interestingly, the Lamp5 Grk5 methylome UMAP generated in this study contains a minor subgroup of cells (left-bottom most) with an mCH profile for *Nkx2.1* two-fold higher than the rest of the cells populating that cluster, suggestive of their belonging to the Lamp5 Lhx6 NGC subtype (http://neomorph.salk.edu/omb/gene?gene=Nkx2-1). This methylome atlas was successfully matched with the scATAC-seq atlas recently proposed by Li et al., 2021, which resolved Lamp5 interneurons in one single cluster named INH1 (Li et al., 2021). This dataset integration is highly relevant for the discovery of potential regulatory elements. In addition, they explored the gene and transcription factor motifs for each m-type finding many TFs that would hypothetically have a high impact on gene regulation. Even if not resolved at the subtype level, *Tox2* was highlighted in their supplemental extended data figure 7 as one of the TF candidates with a higher impact score for INs.

Scala et al., 2021, aimed at a multi-omics integrative atlas of adult cortical single cells, which combined single cell transcriptomics, electrophysiology and morphology assessment and resulted in a very insightful atlas of phenotypic cell types (Scala et al., 2021). Importantly, they were able to identify both discrete t-m-e (transcriptomic-morpho-electric) subtypes and also morpho-electric properties drawing gradients between subtypes (in line with what we found in the present study). (postnatal morphology examples presented here in Results figure 8F belong to Scala et al., 2021 dataset and match with NGC profiles in conformity with Tasic et al., 2018 nomenclature).

The present thesis also provides relevant insights into how IN diversity emerges at embryonic stages during neurogenesis. Importantly, we discovered that embryonic NGCs located in POA at E14.5, when maturation variation is moved to a second plane, have numerous molecular elements that allow to align them with postnatal NGCs, even at the subtype level. Combining STICR lineage information with transcriptomic profiling indicated that at E14.5, all NGC subtypes are simultaneously produced in the POA, a finding that goes in line with recent descriptions of graded generative time windows for *Sst* and *Pvalb* expressing cells born in the embryonic MGE (Lim et al., 2018). Furthermore, *in-utero* electroporation of the embryonic POA at E14.5 performed in the curse of the present thesis resulted in cortices harboring all NGC subtypes, confirming lineage tracing evidence (Bandler et al., 2022). This finding adds a key piece of evidence to the fate commitment debate (Bandler et al., 2022; Mayer et al., 2018; Telley & Jabaudon, 2018) for an IN family for which developmental emergence was never interrogated before at such resolution. Evidence here provided orients the balance towards an understanding of IN diversity generation that is regulated from the first moment of cell birth and fine-tuned as maturation progresses through increasingly diverging molecular programs that reach a plateau for maintenance during early postnatal stages.

A final cherry on the cake finding of the present study is the impact of the TF TOX2 on NGC development. *Tox2* TF stood out as a marker for all members of the NGC cell family. Its sustained expression throughout development and specificity (not expressed in other *Htr3a*-expressing subtypes nor the CGE) anticipated its potential role in regulating NGC fate-acquisition and maintenance. CRISPR mediated down-regulation of *Tox2* in NGC progenitors resulted in a severe disturbance of their maturation/specification, since no electroporated NGC was ever observed in the cortex. This finding is of crucial relevance since it acknowledges the role of TOX2 in NGC cell fate specification and maintenance. The putative selector gene *Tox2* is a characteristic type fingerprint inherited from the POA embryonic origin and is crucial for setting up and maintaining NGC identity.

The research work here presented is nevertheless not exempted of limitations and leaves many open doors for future interrogations. Although discovering that the disruption of TOX2 expression during NGC early maturation is crucial for their development, we ignore the details on the regulatory mechanisms that results in such a drastic outcome. However, evidence exists signaling TOX2 as a master regulator of cell fate specification in other model systems

(Aliahmad et al., 2011; Artegiani et al., 2015; W. Xu et al., 2019). Future exploratory work will be needed to elucidate the transcription regulation mechanisms of this TF as well as its potential chromatin accessibility controlling roles. In addition, it remains an open question whether overexpression of TOX2 in CGE progenitors (lacking its expression endogenously) would result in a fate re-specification of CGE INs, as previous work from the laboratory probed was the case with the MEIS2 transcription factor (Frazer et al., 2017).

Having provided a detailed molecular characterization of the two overarching NGC subtypes through development by using a pan-NGC mouse driver (*Hmx3*-Cre), the current study only gave an introduction on the very scarce Lhx6 NGCs. Extending this line of research is a logical step towards the understanding of how such functionally different subtypes are specified through development, for which a wider cell sampling with deep layers enrichment will be necessary. Furthermore, the design and fate-mapping exploration using enhancer AAV strategies or more restrained driver mouse lines using here identified subtype-specific molecular signatures would provide a final prove on the early specification of NGC subtypes.

This research leaves a wide window of NGC development unexplored: how do NGC subtypes migrate, integrate into cortical circuits and tune their very different activity profiles? Migration tracking and post-birth (P0-P5) NGC isolation probed a devious work in our hands but evidence here provided is highly suggestive of NGC subtypes taking divergent migratory routes that ultimately will drive their differential settlement into cortex and the beginning of the specification of their very different functions into cortical state modulation.

Altogether, this piece of work set the basis for deciphering the logic of IN subtype generation and indicates that space defines IN families while time likely regulates subtype generation. Fate specification appears to be tightly regulated during embryogenesis, creating proto-subtypes whose molecular signatures will be tuned through maturation until diverging into functionally distinct family members (subtypes).

References

Abboud, C., Brochoire, L., Drouet, A., Hossain, M. A., Hleihel, W., Gundlach, A. L., & Landry, M. (2021). Analgesic effect of central relaxin receptor activation on persistent inflammatory pain in mice: Behavioral and neurochemical data. *PAIN Reports*, *6*(2), e937. https://doi.org/10.1097/PR9.0000000000000937

Adnani, L., Han, S., Li, S., Mattar, P., & Schuurmans, C. (2018). Mechanisms of Cortical Differentiation. In *International Review of Cell and Molecular Biology* (Vol. 336, pp. 223–320). Elsevier. https://doi.org/10.1016/bs.ircmb.2017.07.005

Albert, M., Kalebic, N., Florio, M., Lakshmanaperumal, N., Haffner, C., Brandl, H., Henry, I., & Huttner, W. B. (2017). Epigenome profiling and editing of neocortical progenitor cells during development. *The EMBO Journal*, *36*(17), 2642–2658. https://doi.org/10.15252/embj.201796764

Aliahmad, P., Kadavallore, A., de la Torre, B., Kappes, D., & Kaye, J. (2011). TOX Is Required for Development of the CD4 T Cell Lineage Gene Program. *The Journal of Immunology*, *187*(11), 5931–5940. https://doi.org/10.4049/jimmunol.1101474

Allaway, K. C., Gabitto, M. I., Wapinski, O., Saldi, G., Wang, C.-Y., Bandler, R. C., Wu, S. J., Bonneau, R., & Fishell, G. (2021). Genetic and epigenetic coordination of cortical interneuron development. *Nature*, *597*(7878), 693–697. https://doi.org/10.1038/s41586-021-03933-1

Armstrong, C., Krook-Magnuson, E., & Soltesz, I. (2012). Neurogliaform and Ivy Cells: A Major Family of nNOS Expressing GABAergic Neurons. *Frontiers in Neural Circuits*, *6*. https://doi.org/10.3389/fncir.2012.00023

Artegiani, B., de Jesus Domingues, A. M., Bragado Alonso, S., Brandl, E., Massalini, S., Dahl, A., & Calegari, F. (2015). Tox: A multifunctional transcription factor and novel

regulator of mammalian corticogenesis. *The EMBO Journal*, *34*(7), 896–910. https://doi.org/10.15252/embj.201490061

Bacaj, T., Wu, D., Burré, J., Malenka, R. C., Liu, X., & Südhof, T. C. (2015). Synaptotagmin-1 and -7 Are Redundantly Essential for Maintaining the Capacity of the Readily-Releasable Pool of Synaptic Vesicles. *PLoS Biology*, *13*(10), e1002267. https://doi.org/10.1371/journal.pbio.1002267

Bandler, R. C., Mayer, C., & Fishell, G. (2017). Cortical interneuron specification: The juncture of genes, time and geometry. *Current Opinion in Neurobiology*, *42*, 17–24. https://doi.org/10.1016/j.conb.2016.10.003

Bandler, R. C., Vitali, I., Delgado, R. N., Ho, M. C., Dvoretskova, E., Ibarra Molinas, J. S., Frazel, P. W., Mohammadkhani, M., Machold, R., Maedler, S., Liddelow, S. A., Nowakowski, T. J., Fishell, G., & Mayer, C. (2022). Single-cell delineation of lineage and genetic identity in the mouse brain. *Nature*, *601*(7893), 404–409. https://doi.org/10.1038/s41586-021-04237-0

Basu, J., & Siegelbaum, S. A. (2015). The Corticohippocampal Circuit, Synaptic Plasticity, and Memory. *Cold Spring Harbor Perspectives in Biology*, *7*(11), a021733. https://doi.org/10.1101/cshperspect.a021733

Bennett, M. V. L., & Zukin, R. S. (2004). Electrical Coupling and Neuronal Synchronization in the Mammalian Brain. *Neuron*, *41*(4), 495–511. https://doi.org/10.1016/S0896-6273(04)00043-1

Bloem, B., Poorthuis, R. B., & Mansvelder, H. D. (2014). Cholinergic modulation of the medial prefrontal cortex: The role of nicotinic receptors in attention and regulation of neuronal activity. *Frontiers in Neural Circuits*, *8*. https://doi.org/10.3389/fncir.2014.00017

BRAIN Initiative Cell Census Network (BICCN), BRAIN Initiative Cell Census Network (BICCN) Corresponding authors, Callaway, E. M., Dong, H.-W., Ecker, J. R.,

Hawrylycz, M. J., Huang, Z. J., Lein, E. S., Ngai, J., Osten, P., Ren, B., Tolias, A. S., White, O., Zeng, H., Zhuang, X., BICCN contributing principal investigators, Ascoli, G. A., Behrens, M. M., Chun, J., … Sunkin, S. (2021). A multimodal cell census and atlas of the mammalian primary motor cortex. *Nature*, *598*(7879), 86–102. https://doi.org/10.1038/s41586-021-03950-0

Bugeon, S., Duffield, J., Dipoppa, M., Ritoux, A., Prankerd, I., Nicoloutsopoulos, D., Orme, D., Shinn, M., Peng, H., Forrest, H., Viduolyte, A., Reddy, C. B., Isogai, Y., Carandini, M., & Harris, K. D. (2022). A transcriptomic axis predicts state modulation of cortical interneurons. *Nature*, *607*(7918), 330–338. https://doi.org/10.1038/s41586-022-04915-7

Burney, M. J., Johnston, C., Wong, K.-Y., Teng, S.-W., Beglopoulos, V., Stanton, L. W., Williams, B. P., Bithell, A., & Buckley, N. J. (2013). An epigenetic signature of developmental potential in neural stem cells and early neurons. *Stem Cells*, *31*(9), 1868–1880. https://doi.org/10.1002/stem.1431

Capogna, M., & Pearce, R. A. (2011). GABA A,slow: Causes and consequences. *Trends in Neurosciences*, *34*(2), 101–112. https://doi.org/10.1016/j.tins.2010.10.005

Capone, F., Paolucci, M., Assenza, F., Brunelli, N., Ricci, L., Florio, L., & Di Lazzaro, V. (2016). Canonical cortical circuits: Current evidence and theoretical implications. *Neuroscience and Neuroeconomics*, 1. https://doi.org/10.2147/NAN.S70816

Chittajallu, R., Pelkey, K. A., & McBain, C. J. (2013). Neurogliaform cells dynamically regulate somatosensory integration via synapse-specific modulation. *Nature Neuroscience*, *16*(1), 13–15. https://doi.org/10.1038/nn.3284

Cohen-Kashi Malina, K., Tsivourakis, E., Kushinsky, D., Apelblat, D., Shtiglitz, S., Zohar, E., Sokoletsky, M., Tasaka, G., Mizrahi, A., Lampl, I., & Spiegel, I. (2021). NDNF interneurons in layer 1 gain-modulate whole cortical columns according to an animal's

behavioral state. *Neuron*, *109*(13), 2150-2164.e5. https://doi.org/10.1016/j.neuron.2021.05.001

Colonnese, M. T., Murata, Y., & Phillips, M. A. (2021). A new role for visual experience in top-down cortical development. *Neuron*, *109*(21), 3400–3401. https://doi.org/10.1016/j.neuron.2021.10.012

Connors, B. W., & Long, M. A. (2004). ELECTRICAL SYNAPSES IN THE MAMMALIAN BRAIN. *Annual Review of Neuroscience*, *27*(1), 393–418. https://doi.org/10.1146/annurev.neuro.26.041002.131128

Craig, M. T., & Witton, J. (2022). A cellular switchboard in memory circuits. *Science*, *377*(6603), 262–263. https://doi.org/10.1126/science.add2681

da Costa, N. M. (2010). Whose cortical column would that be? *Frontiers in Neuroanatomy*. https://doi.org/10.3389/fnana.2010.00016

D'amour, J. A., & Froemke, R. C. (2015). Inhibitory and excitatory spike-timing-dependent plasticity in the auditory cortex. *Neuron*, *86*(2), 514–528. https://doi.org/10.1016/j.neuron.2015.03.014

Dávid, C., Schleicher, A., Zuschratter, W., & Staiger, J. F. (2007). The innervation of parvalbumin-containing interneurons by VIP-immunopositive interneurons in the primary somatosensory cortex of the adult rat. *The European Journal of Neuroscience*, *25*(8), 2329–2340. https://doi.org/10.1111/j.1460-9568.2007.05496.x

Douglas, R. J. (1989). A canonical microcircuit for neocortex. *Neural Computation*, *1*(4).

Douglas, R. J., & Martin, K. A. C. (2004). Neuronal circuits of the neocortex. *Annual Review of Neuroscience*, *27*(1), 419–451. https://doi.org/10.1146/annurev.neuro.27.070203.144152

English, D. F., Ibanez-Sandoval, O., Stark, E., Tecuapetla, F., Buzsáki, G., Deisseroth, K., Tepper, J. M., & Koos, T. (2012). GABAergic circuits mediate the reinforcement-

related signals of striatal cholinergic interneurons. *Nature Neuroscience*, *15*(1), 123–130. https://doi.org/10.1038/nn.2984

Farhy-Tselnicker, I., & Allen, N. J. (2018). Astrocytes, neurons, synapses: A tripartite view on cortical circuit development. *Neural Development*, *13*(1), 7. https://doi.org/10.1186/s13064-018-0104-y

Feng, L., Zhao, T., & Kim, J. (2015). neuTube 1.0: A New Design for Efficient Neuron Reconstruction Software Based on the SWC Format. *ENeuro*, *2*(1), ENEURO.0049-14.2014. https://doi.org/10.1523/ENEURO.0049-14.2014

Frazer, S., Prados, J., Niquille, M., Cadilhac, C., Markopoulos, F., Gomez, L., Tomasello, U., Telley, L., Holtmaat, A., Jabaudon, D., & Dayer, A. (2017). Transcriptomic and anatomic parcellation of 5-HT3AR expressing cortical interneuron subtypes revealed by single-cell RNA sequencing. *Nature Communications*, *8*(1), 14219. https://doi.org/10.1038/ncomms14219

Freund, T. F., Katona, I., & Piomelli, D. (2003). Role of endogenous cannabinoids in synaptic signaling. *Physiological Reviews*, *83*(3), 1017–1066. https://doi.org/10.1152/physrev.00004.2003

Gelman, D. M., Martini, F. J., Nobrega-Pereira, S., Pierani, A., Kessaris, N., & Marin, O. (2009). The Embryonic Preoptic Area Is a Novel Source of Cortical GABAergic Interneurons. *Journal of Neuroscience*, *29*(29), 9380–9389. https://doi.org/10.1523/JNEUROSCI.0604-09.2009

Glickstein, S. B., Moore, H., Slowinska, B., Racchumi, J., Suh, M., Chuhma, N., & Ross, M. E. (2007). Selective cortical interneuron and GABA deficits in cyclin D2-null mice. *Development*, *134*(22), 4083–4093. https://doi.org/10.1242/dev.008524

Gouwens, N. W., Sorensen, S. A., Baftizadeh, F., Budzillo, A., Lee, B. R., Jarsky, T., Alfiler, L., Baker, K., Barkan, E., Berry, K., Bertagnolli, D., Bickley, K., Bomben, J., Braun,

T., Brouner, K., Casper, T., Crichton, K., Daigle, T. L., Dalley, R., … Zeng, H. (2020). Integrated Morphoelectric and Transcriptomic Classification of Cortical GABAergic Cells. *Cell*, *183*(4), 935-953.e19. https://doi.org/10.1016/j.cell.2020.09.057

Gundlach, A. L., Ma, S., Sang, Q., Shen, P.-J., Piccenna, L., Sedaghat, K., Smith, C. M., Bathgate, R. A. D., Lawrence, A. J., Tregear, G. W., Wade, J. D., Finkelstein, D. I., Bonaventure, P., Liu, C., Lovenberg, T. W., & Sutton, S. W. (2009). Relaxin family peptides and receptors in mammalian brain. *Annals of the New York Academy of Sciences*, *1160*, 226–235. https://doi.org/10.1111/j.1749-6632.2009.03956.x

Harding, S. D., Armstrong, J. F., Faccenda, E., Southan, C., Alexander, S. P. H., Davenport, A. P., Pawson, A. J., Spedding, M., Davies, J. A., & NC-IUPHAR. (2022). The IUPHAR/BPS guide to PHARMACOLOGY in 2022: Curating pharmacology for COVID-19, malaria and antibacterials. *Nucleic Acids Research*, *50*(D1), D1282–D1294. https://doi.org/10.1093/nar/gkab1010

Hay, Y. A., Deperrois, N., Fuchsberger, T., Quarrell, T. M., Koerling, A.-L., & Paulsen, O. (2021). Thalamus mediates neocortical Down state transition via GABAB-receptor-targeting interneurons. *Neuron*, *109*(17), 2682-2690.e5. https://doi.org/10.1016/j.neuron.2021.06.030

He, M., Tucciarone, J., Lee, S., Nigro, M. J., Kim, Y., Levine, J. M., Kelly, S. M., Krugikov, I., Wu, P., Chen, Y., Gong, L., Hou, Y., Osten, P., Rudy, B., & Huang, Z. J. (2016). Strategies and Tools for Combinatorial Targeting of GABAergic Neurons in Mouse Cerebral Cortex. *Neuron*, *91*(6), 1228–1243. https://doi.org/10.1016/j.neuron.2016.08.021

Hennequin, G., Agnes, E. J., & Vogels, T. P. (2017). Inhibitory Plasticity: Balance, Control, and Codependence. *Annual Review of Neuroscience*, *40*, 557–579. https://doi.org/10.1146/annurev-neuro-072116-031005

Hentschke, H., Benkwitz, C., Banks, M. I., Perkins, M. G., Homanics, G. E., & Pearce, R. A. (2009). Altered GABA $_{A,slow}$ Inhibition and Network Oscillations in Mice Lacking the GABA $_{A}$ Receptor β_{3} Subunit. *Journal of Neurophysiology*, *102*(6), 3643–3655. https://doi.org/10.1152/jn.00651.2009

Hou, W.-H., & Capogna, M. (2018). Dendritic Inhibition in Layer 1 Cortex Gates Associative Memory. *Neuron*, *100*(3), 516–519. https://doi.org/10.1016/j.neuron.2018.10.029

Hu, J. S., Vogt, D., Sandberg, M., & Rubenstein, J. L. (2017). Cortical interneuron development: A tale of time and space. *Development*, *144*(21), 3867–3878. https://doi.org/10.1242/dev.132852

Huang, Z. J., & Paul, A. (2019). The diversity of GABAergic neurons and neural communication elements. *Nature Reviews Neuroscience*, *20*(9), 563–572. https://doi.org/10.1038/s41583-019-0195-4

Ibrahim, L. A., Schuman, B., Bandler, R., Rudy, B., & Fishell, G. (2020). Mining the jewels of the cortex's crowning mystery. *Current Opinion in Neurobiology*, *63*, 154–161. https://doi.org/10.1016/j.conb.2020.04.005

Inan, M., Welagen, J., & Anderson, S. A. (2012). Spatial and Temporal Bias in the Mitotic Origins of Somatostatin- and Parvalbumin-Expressing Interneuron Subgroups and the Chandelier Subtype in the Medial Ganglionic Eminence. *Cerebral Cortex*, *22*(4), 820–827. https://doi.org/10.1093/cercor/bhr148

Isaacson, J. S., & Scanziani, M. (2011). How inhibition shapes cortical activity. *Neuron*, *72*(2), 231–243. https://doi.org/10.1016/j.neuron.2011.09.027

Jiang, X., Shen, S., Cadwell, C. R., Berens, P., Sinz, F., Ecker, A. S., Patel, S., & Tolias, A. S. (2015). Principles of connectivity among morphologically defined cell types in adult neocortex. *Science (New York, N.Y.)*, *350*(6264), aac9462. https://doi.org/10.1126/science.aac9462

Jiang, X., Wang, G., Lee, A. J., Stornetta, R. L., & Zhu, J. J. (2013). The organization of two new cortical interneuronal circuits. *Nature Neuroscience*, *16*(2), 210–218. https://doi.org/10.1038/nn.3305

Karayannis, T., Elfant, D., Huerta-Ocampo, I., Teki, S., Scott, R. S., Rusakov, D. A., Jones, M. V., & Capogna, M. (2010). Slow GABA transient and receptor desensitization shape synaptic responses evoked by hippocampal neurogliaform cells. *The Journal of Neuroscience: The Official Journal of the Society for Neuroscience*, *30*(29), 9898–9909. https://doi.org/10.1523/JNEUROSCI.5883-09.2010

Kelly, S. M., Raudales, R., He, M., Lee, J. H., Kim, Y., Gibb, L. G., Wu, P., Matho, K., Osten, P., Graybiel, A. M., & Huang, Z. J. (2018). Radial Glial Lineage Progression and Differential Intermediate Progenitor Amplification Underlie Striatal Compartments and Circuit Organization. *Neuron*, *99*(2), 345-361.e4. https://doi.org/10.1016/j.neuron.2018.06.021

Kirkcaldie, M. T. K. (2012). Neocortex. In *The Mouse Nervous System* (pp. 52–111). Elsevier. https://doi.org/10.1016/B978-0-12-369497-3.10004-4

Kopell, N., & Ermentrout, B. (2004). Chemical and electrical synapses perform complementary roles in the synchronization of interneuronal networks. *Proceedings of the National Academy of Sciences*, *101*(43), 15482–15487. https://doi.org/10.1073/pnas.0406343101

Kubota, Y. (2014). Untangling GABAergic wiring in the cortical microcircuit. *Current Opinion in Neurobiology*, *26*, 7–14. https://doi.org/10.1016/j.conb.2013.10.003

Larkum, M. E., Petro, L. S., Sachdev, R. N. S., & Muckli, L. (2018). A Perspective on Cortical Layering and Layer-Spanning Neuronal Elements. *Frontiers in Neuroanatomy*, *12*, 56. https://doi.org/10.3389/fnana.2018.00056

Lee, D. R., Rhodes, C., Mitra, A., Zhang, Y., Maric, D., Dale, R. K., & Petros, T. J. (2022). Transcriptional heterogeneity of ventricular zone cells in the ganglionic eminences of the mouse forebrain. *ELife*, *11*, e71864. https://doi.org/10.7554/eLife.71864

Letzkus, J. J., Wolff, S. B. E., & Lüthi, A. (2015). Disinhibition, a Circuit Mechanism for Associative Learning and Memory. *Neuron*, *88*(2), 264–276. https://doi.org/10.1016/j.neuron.2015.09.024

Letzkus, J. J., Wolff, S. B. E., Meyer, E. M. M., Tovote, P., Courtin, J., Herry, C., & Lüthi, A. (2011). A disinhibitory microcircuit for associative fear learning in the auditory cortex. *Nature*, *480*(7377), 331–335. https://doi.org/10.1038/nature10674

Li, Y. E., Preissl, S., Hou, X., Zhang, Z., Zhang, K., Qiu, Y., Poirion, O. B., Li, B., Chiou, J., Liu, H., Pinto-Duarte, A., Kubo, N., Yang, X., Fang, R., Wang, X., Han, J. Y., Lucero, J., Yan, Y., Miller, M., … Ren, B. (2021). An atlas of gene regulatory elements in adult mouse cerebrum. *Nature*, *598*(7879), 129–136. https://doi.org/10.1038/s41586-021-03604-1

Lim, L., Mi, D., Llorca, A., & Marín, O. (2018). Development and Functional Diversification of Cortical Interneurons. *Neuron*, *100*(2), 294–313. https://doi.org/10.1016/j.neuron.2018.10.009

Liu, H., Zhou, J., Tian, W., Luo, C., Bartlett, A., Aldridge, A., Lucero, J., Osteen, J. K., Nery, J. R., Chen, H., Rivkin, A., Castanon, R. G., Clock, B., Li, Y. E., Hou, X., Poirion, O. B., Preissl, S., Pinto-Duarte, A., O'Connor, C., … Ecker, J. R. (2021). DNA methylation atlas of the mouse brain at single-cell resolution. *Nature*, *598*(7879), 120–128. https://doi.org/10.1038/s41586-020-03182-8

Llorca, A., & Deogracias, R. (2022). Origin, Development, and Synaptogenesis of Cortical Interneurons. *Frontiers in Neuroscience*, *16*, 929469. https://doi.org/10.3389/fnins.2022.929469

Ludovic Tricoire, Pelkey, K. A., Daw, M. I., & Sousa, V. H. (2010). Common Origins of Hippocampal Ivy and Nitric Oxide Synthase Expressing Neurogliaform Cells. *The Journal of Neuroscience*, *30*(6), 2165–2176.

Mayer, C., Bandler, R. C., & Fishell, G. (2016). Lineage Is a Poor Predictor of Interneuron Positioning within the Forebrain. *Neuron*, *92*(1), 45–51. https://doi.org/10.1016/j.neuron.2016.09.035

Mayer, C., Hafemeister, C., Bandler, R. C., Machold, R., Batista Brito, R., Jaglin, X., Allaway, K., Butler, A., Fishell, G., & Satija, R. (2018). Developmental diversification of cortical inhibitory interneurons. *Nature*, *555*(7697), 457–462. https://doi.org/10.1038/nature25999

Mihaljević, B., Larrañaga, P., Benavides-Piccione, R., Hill, S., DeFelipe, J., & Bielza, C. (2018). Towards a supervised classification of neocortical interneuron morphologies. *BMC Bioinformatics*, *19*(1), 511. https://doi.org/10.1186/s12859-018-2470-1

Mimitou, E. P., Lareau, C. A., Chen, K. Y., Zorzetto-Fernandes, A. L., Hao, Y., Takeshima, Y., Luo, W., Huang, T.-S., Yeung, B. Z., Papalexi, E., Thakore, P. I., Kibayashi, T., Wing, J. B., Hata, M., Satija, R., Nazor, K. L., Sakaguchi, S., Ludwig, L. S., Sankaran, V. G., … Smibert, P. (2021). Scalable, multimodal profiling of chromatin accessibility, gene expression and protein levels in single cells. *Nature Biotechnology*, *39*(10), 1246–1258. https://doi.org/10.1038/s41587-021-00927-2

Minton, K. (2020). TOX2 helping hand for TFH cells. *Nature Reviews Immunology*, *20*(1), 4–5. https://doi.org/10.1038/s41577-019-0249-x

Miyoshi, G., Hjerling-Leffler, J., Karayannis, T., Sousa, V. H., Butt, S. J. B., Battiste, J., Johnson, J. E., Machold, R. P., & Fishell, G. (2010). Genetic fate mapping reveals that the caudal ganglionic eminence produces a large and diverse population of superficial cortical interneurons. *The Journal of Neuroscience: The Official Journal of the Society*

for Neuroscience, *30*(5), 1582–1594. https://doi.org/10.1523/JNEUROSCI.4515-09.2010

Moore, S., Meschkat, M., Ruhwedel, T., Trevisiol, A., Tzvetanova, I. D., Battefeld, A., Kusch, K., Kole, M. H. P., Strenzke, N., Möbius, W., de Hoz, L., & Nave, K.-A. (2020). A role of oligodendrocytes in information processing. *Nature Communications*, *11*(1), 5497. https://doi.org/10.1038/s41467-020-19152-7

Narayanan, R. T., Udvary, D., & Oberlaender, M. (2017). Cell Type-Specific Structural Organization of the Six Layers in Rat Barrel Cortex. *Frontiers in Neuroanatomy*, *11*, 91. https://doi.org/10.3389/fnana.2017.00091

Nasu, M., Esumi, S., Hatakeyama, J., Tamamaki, N., & Shimamura, K. (2021). Two-Phase Lineage Specification of Telencephalon Progenitors Generated From Mouse Embryonic Stem Cells. *Frontiers in Cell and Developmental Biology*, *9*, 632381. https://doi.org/10.3389/fcell.2021.632381

Nat, R., Apostolova, G., & Dechant, G. (2013). Telencephalic Neurogenesis Versus Telencephalic Differentiation of Pluripotent Stem Cells. In S. Wislet-Gendebien (Ed.), *Trends in Cell Signaling Pathways in Neuronal Fate Decision*. InTech. https://doi.org/10.5772/54251

Niquille, M., Limoni, G., Markopoulos, F., Cadilhac, C., Prados, J., Holtmaat, A., & Dayer, A. (2018). Neurogliaform cortical interneurons derive from cells in the preoptic area. *ELife*, *7*, e32017. https://doi.org/10.7554/eLife.32017

Nord, A. S., Pattabiraman, K., Visel, A., & Rubenstein, J. L. R. (2015). Genomic Perspectives of Transcriptional Regulation in Forebrain Development. *Neuron*, *85*(1), 27–47. https://doi.org/10.1016/j.neuron.2014.11.011

Nowakowski, T. J., Bhaduri, A., Pollen, A. A., Alvarado, B., Mostajo-Radji, M. A., Di Lullo, E., Haeussler, M., Sandoval-Espinosa, C., Liu, S. J., Velmeshev, D., Ounadjela, J. R.,

Shuga, J., Wang, X., Lim, D. A., West, J. A., Leyrat, A. A., Kent, W. J., & Kriegstein, A. R. (2017). Spatiotemporal gene expression trajectories reveal developmental hierarchies of the human cortex. *Science (New York, N.Y.)*, *358*(6368), 1318–1323. https://doi.org/10.1126/science.aap8809

Oláh, S., Füle, M., Komlósi, G., Varga, C., Báldi, R., Barzó, P., & Tamás, G. (2009). Regulation of cortical microcircuits by unitary GABA-mediated volume transmission. *Nature*, *461*(7268), 1278–1281. https://doi.org/10.1038/nature08503

Overstreet-Wadiche, L., & McBain, C. J. (2015). Neurogliaform cells in cortical circuits. *Nature Reviews Neuroscience*, *16*(8), 458–468. https://doi.org/10.1038/nrn3969

Palacios, J., Lidakanari, Zisis, E., MikeG, Benoit Coste, Asanin-Epfl, Vanherpe, L., Jdcourcol, Arnaudon, A., Berchet, A., Haleepfl, Getta, P., Povolotsky, A. V., A Sato, Alex4200, Bbpgithubaudit, Amsalem, O., & Tomdele. (2022). *BlueBrain/NeuroM: V3.2.0* (v3.2.0). Zenodo. https://doi.org/10.5281/ZENODO.6524037

Paterno, R., Casalia, M., & Baraban, S. C. (2020). Interneuron deficits in neurodevelopmental disorders: Implications for disease pathology and interneuron-based therapies. *European Journal of Paediatric Neurology: EJPN: Official Journal of the European Paediatric Neurology Society*, *24*, 81–88. https://doi.org/10.1016/j.ejpn.2019.12.015

Perkel, J. M. (2021). Single-cell analysis enters the multiomics age. *Nature*, *595*(7868), 614–616. https://doi.org/10.1038/d41586-021-01994-w

Petros, T. J., Bultje, R. S., Ross, M. E., Fishell, G., & Anderson, S. A. (2015). Apical versus Basal Neurogenesis Directs Cortical Interneuron Subclass Fate. *Cell Reports*, *13*(6), 1090–1095. https://doi.org/10.1016/j.celrep.2015.09.079

Pfeffer, C. K., Xue, M., He, M., Huang, Z. J., & Scanziani, M. (2013). Inhibition of inhibition in visual cortex: The logic of connections between molecularly distinct interneurons. *Nature Neuroscience*, *16*(8), 1068–1076. https://doi.org/10.1038/nn.3446

Pi, H.-J., Hangya, B., Kvitsiani, D., Sanders, J. I., Huang, Z. J., & Kepecs, A. (2013). Cortical interneurons that specialize in disinhibitory control. *Nature*, *503*(7477), 521–524. https://doi.org/10.1038/nature12676

Poorthuis, R. B., Muhammad, K., Wang, M., Verhoog, M. B., Junek, S., Wrana, A., Mansvelder, H. D., & Letzkus, J. J. (2018). Rapid Neuromodulation of Layer 1 Interneurons in Human Neocortex. *Cell Reports*, *23*(4), 951–958. https://doi.org/10.1016/j.celrep.2018.03.111

Pouchelon, G., Dwivedi, D., Bollmann, Y., Agba, C. K., Xu, Q., Mirow, A. M. C., Kim, S., Qiu, Y., Sevier, E., Ritola, K. D., Cossart, R., & Fishell, G. (2021). The organization and development of cortical interneuron presynaptic circuits are area specific. *Cell Reports*, *37*(6), 109993. https://doi.org/10.1016/j.celrep.2021.109993

Price, C. J., Scott, R., Rusakov, D. A., & Capogna, M. (2008). GABA(B) receptor modulation of feedforward inhibition through hippocampal neurogliaform cells. *The Journal of Neuroscience: The Official Journal of the Society for Neuroscience*, *28*(27), 6974–6982. https://doi.org/10.1523/JNEUROSCI.4673-07.2008

Qin, S., Ware, S. M., Waclaw, R. R., & Campbell, K. (2017). Septal contributions to olfactory bulb interneuron diversity in the embryonic mouse telencephalon: Role of the homeobox gene Gsx2. *Neural Development*, *12*(1), 13. https://doi.org/10.1186/s13064-017-0090-5

Ramadan, E., Fu, Z., Losi, G., Homanics, G. E., Neale, J. H., & Vicini, S. (2003). GABA A Receptor β3 Subunit Deletion Decreases α2/3 Subunits and IPSC Duration. *Journal of Neurophysiology*, *89*(1), 128–134. https://doi.org/10.1152/jn.00700.2002

Ramón y Cajal, S. (1923). *Recuerdos de mi vida: Historia de mi labor científica*. Alianza Editorial.

Roux, L., & Buzsáki, G. (2015). Tasks for inhibitory interneurons in intact brain circuits. *Neuropharmacology*, *88*, 10–23. https://doi.org/10.1016/j.neuropharm.2014.09.011

Rudolph, J., Zimmer, G., Steinecke, A., Barchmann, S., & Bolz, J. (2010). Ephrins guide migrating cortical interneurons in the basal telencephalon. *Cell Adhesion & Migration*, *4*(3), 400–408. https://doi.org/10.4161/cam.4.3.11640

Sakalar, E., Klausberger, T., & Lasztóczi, B. (2022). Neurogliaform cells dynamically decouple neuronal synchrony between brain areas. *Science*, *377*(6603), 324–328. https://doi.org/10.1126/science.abo3355

Salinas, E., & Thier, P. (2000). Gain modulation: A major computational principle of the central nervous system. *Neuron*, *27*(1), 15–21. https://doi.org/10.1016/s0896-6273(00)00004-0

Sandberg, M., Flandin, P., Silberberg, S., Su-Feher, L., Price, J. D., Hu, J. S., Kim, C., Visel, A., Nord, A. S., & Rubenstein, J. L. R. (2016). Transcriptional Networks Controlled by NKX2-1 in the Development of Forebrain GABAergic Neurons. *Neuron*, *91*(6), 1260–1275. https://doi.org/10.1016/j.neuron.2016.08.020

Scala, F., Kobak, D., Bernabucci, M., Bernaerts, Y., Cadwell, C. R., Castro, J. R., Hartmanis, L., Jiang, X., Laturnus, S., Miranda, E., Mulherkar, S., Tan, Z. H., Yao, Z., Zeng, H., Sandberg, R., Berens, P., & Tolias, A. S. (2021). Phenotypic variation of transcriptomic cell types in mouse motor cortex. *Nature*, *598*(7879), 144–150. https://doi.org/10.1038/s41586-020-2907-3

Scala, F., Kobak, D., Shan, S., Bernaerts, Y., Laturnus, S., Cadwell, C. R., Hartmanis, L., Froudarakis, E., Castro, J. R., Tan, Z. H., Papadopoulos, S., Patel, S. S., Sandberg, R., Berens, P., Jiang, X., & Tolias, A. S. (2019). Layer 4 of mouse neocortex differs in cell types and circuit organization between sensory areas. *Nature Communications*, *10*(1), 4174. https://doi.org/10.1038/s41467-019-12058-z

Schuman, B., Dellal, S., Prönneke, A., Machold, R., & Rudy, B. (2021). Neocortical Layer 1: An Elegant Solution to Top-Down and Bottom-Up Integration. *Annual Review of Neuroscience*, *44*(1), 221–252. https://doi.org/10.1146/annurev-neuro-100520-012117

Schuman, B., Machold, R. P., Hashikawa, Y., Fuzik, J., Fishell, G. J., & Rudy, B. (2019). Four Unique Interneuron Populations Reside in Neocortical Layer 1. *The Journal of Neuroscience: The Official Journal of the Society for Neuroscience*, *39*(1), 125–139. https://doi.org/10.1523/JNEUROSCI.1613-18.2018

Shepherd, G. M. G., & Yamawaki, N. (2021). Untangling the cortico-thalamo-cortical loop: Cellular pieces of a knotty circuit puzzle. *Nature Reviews Neuroscience*, *22*(7), 389–406. https://doi.org/10.1038/s41583-021-00459-3

Simon, A. (2005). Gap-Junctional Coupling between Neurogliaform Cells and Various Interneuron Types in the Neocortex. *Journal of Neuroscience*, *25*(27), 6278–6285. https://doi.org/10.1523/JNEUROSCI.1431-05.2005

Sotelo, C. (2020). The History of the Synapse. *The Anatomical Record*, *303*(5), 1252–1279. https://doi.org/10.1002/ar.24392

Speed, A., & Haider, B. (2021). Probing mechanisms of visual spatial attention in mice. *Trends in Neurosciences*, *44*(10), 822–836. https://doi.org/10.1016/j.tins.2021.07.009

Steinecke, A., Gampe, C., Zimmer, G., Rudolph, J., & Bolz, J. (2014). EphA/ephrin A reverse signaling promotes the migration of cortical interneurons from the medial ganglionic eminence. *Development*, *141*(2), 460–471. https://doi.org/10.1242/dev.101691

Sukenik, N., Vinogradov, O., Weinreb, E., Segal, M., Levina, A., & Moses, E. (2021). Neuronal circuits overcome imbalance in excitation and inhibition by adjusting connection numbers. *Proceedings of the National Academy of Sciences*, *118*(12), e2018459118. https://doi.org/10.1073/pnas.2018459118

Sultan, K. T., & Shi, S. (2018). Generation of diverse cortical inhibitory interneurons. *WIREs Developmental Biology*, *7*(2). https://doi.org/10.1002/wdev.306

Suzuki, N., Tantirigama, M. L., Aung, K. P., Huang, H. H., & Bekkers, J. M. (2022). Fast and slow feedforward inhibitory circuits for cortical odor processing. *ELife*, *11*, e73406. https://doi.org/10.7554/eLife.73406

Tasic, B., Yao, Z., Graybuck, L. T., Smith, K. A., Nguyen, T. N., Bertagnolli, D., Goldy, J., Garren, E., Economo, M. N., Viswanathan, S., Penn, O., Bakken, T., Menon, V., Miller, J., Fong, O., Hirokawa, K. E., Lathia, K., Rimorin, C., Tieu, M., … Zeng, H. (2018). Shared and distinct transcriptomic cell types across neocortical areas. *Nature*, *563*(7729), 72–78. https://doi.org/10.1038/s41586-018-0654-5

Telley, L., & Jabaudon, D. (2018). A mixed model of neuronal diversity. *Nature*, *555*(7697), 452–454. https://doi.org/10.1038/d41586-018-02539-4

Tole, S., & Hébert, J. (2020). Telencephalon patterning. In *Patterning and Cell Type Specification in the Developing CNS and PNS* (pp. 23–48). Elsevier. https://doi.org/10.1016/B978-0-12-814405-3.00002-3

Tremblay, R., Lee, S., & Rudy, B. (2016). GABAergic Interneurons in the Neocortex: From Cellular Properties to Circuits. *Neuron*, *91*(2), 260–292. https://doi.org/10.1016/j.neuron.2016.06.033

Turrero García, M., Mazzola, E., & Harwell, C. C. (2016). Lineage Relationships Do Not Drive MGE/PoA-Derived Interneuron Clustering in the Brain. *Neuron*, *92*(1), 52–58. https://doi.org/10.1016/j.neuron.2016.09.034

Uhl, G. R., & Martinez, M. J. (2019). PTPRD: Neurobiology, genetics, and initial pharmacology of a pleiotropic contributor to brain phenotypes. *Annals of the New York Academy of Sciences*, *1451*(1), 112–129. https://doi.org/10.1111/nyas.14002

Valero, M., Viney, T. J., Machold, R., Mederos, S., Zutshi, I., Schuman, B., Senzai, Y., Rudy, B., & Buzsáki, G. (2021). Sleep down state-active ID2/Nkx2.1 interneurons in the neocortex. *Nature Neuroscience*, *24*(3), 401–411. https://doi.org/10.1038/s41593-021-00797-6

Woodruff, A., Xu, Q., Anderson, S. A., & Yuste, R. (2009). Depolarizing effect of neocortical chandelier neurons. *Frontiers in Neural Circuits*, *3*, 15. https://doi.org/10.3389/neuro.04.015.2009

Xu, H., Jeong, H.-Y., Tremblay, R., & Rudy, B. (2013). Neocortical somatostatin-expressing GABAergic interneurons disinhibit the thalamorecipient layer 4. *Neuron*, *77*(1), 155–167. https://doi.org/10.1016/j.neuron.2012.11.004

Xu, W., Zhao, X., Wang, X., Feng, H., Gou, M., Jin, W., Wang, X., Liu, X., & Dong, C. (2019). The Transcription Factor Tox2 Drives T Follicular Helper Cell Development via Regulating Chromatin Accessibility. *Immunity*, *51*(5), 826-839.e5. https://doi.org/10.1016/j.immuni.2019.10.006

Yang, J., Yang, X., & Tang, K. (2022). Interneuron development and dysfunction. *The FEBS Journal*, *289*(8), 2318–2336. https://doi.org/10.1111/febs.15872

Yao, X.-H., Wang, M., He, X.-N., He, F., Zhang, S.-Q., Lu, W., Qiu, Z.-L., & Yu, Y.-C. (2016). Electrical coupling regulates layer 1 interneuron microcircuit formation in the neocortex. *Nature Communications*, *7*(1), 12229. https://doi.org/10.1038/ncomms12229

Zimmer, G., Rudolph, J., Landmann, J., Gerstmann, K., Steinecke, A., Gampe, C., & Bolz, J. (2011). Bidirectional EphrinB3/EphA4 Signaling Mediates the Segregation of Medial Ganglionic Eminence- and Preoptic Area-Derived Interneurons in the Deep and Superficial Migratory Stream. *Journal of Neuroscience*, *31*(50), 18364–18380. https://doi.org/10.1523/JNEUROSCI.4690-11.2011